Advances in **Optics** and **Photonics**

Electro-optic frequency combs

ALEXANDRE PARRIAUX,[1,*] **KAMAL HAMMANI,**[1]
AND **GUY MILLOT**[1,2]

[1]*Laboratoire Interdisciplinaire Carnot de Bourgogne (ICB), UMR 6303 CNRS – Université Bourgogne Franche-Comté, Dijon, France*
[2]*Institut Universitaire de France (IUF), 1 rue Descartes, Paris, France*
Corresponding author: alexandre.parriaux@u-bourgogne.fr

Frequency combs are optical spectra composed of a set of discrete equally spaced lines. Such spectra can be generated by diverse sources such as mode-locked lasers, resonators, or electro-optic modulators. This last possibility has shown a growing interest in the recent years for its advantageous features in providing high repetition rates, intrinsic mutual coherence, or high power per comb lines. Moreover, applications of electro-optic modulator-based combs have flourished in fundamental physics, spectroscopy, or instrumental calibrations. In this paper, we present the most recent progresses made on frequency combs generated by electro-optic modulators, along with the applications where these combs have shown a particular interest. © 2020 Optical Society of America

Electro-optic frequency combs

ALEXANDRE PARRIAUX, KAMAL HAMMANI, AND GUY MILLOT

1. INTRODUCTION

In 1960, Maiman launched the ruby laser, which became famous for its visible red light [1]. This invention was the beginning of a revolution in whole experimental physics. A few years later, in 1964, the first mode-locked laser (MLL) was developed by Hargrove *et al.*, and its temporal output showed the emission of pulses [2]. In the optical frequency domain, this laser presented a spectrum composed of a set of discrete lines that were equally spaced forming a comb picture. Therefore, such a spectrum is nowadays called an *optical frequency comb* (OFC).

Since 1964, the interest in generating OFCs has led to a tremendous activity, particularly in the context of laser spectroscopy. Thus, a frequency comb synthesizer that can be used as a ruler to measure optical frequencies with great precision has been developped at the end of the 90 s, leading in 2005 to the Nobel Prize in Physics for Hänsch and Hall [3,4]. Since then, many applications of OFCs have been developed starting from metrology [5], to spectrograph calibration for exoplanet detections [6], and passing by fundamental physics [7]. However, each application based upon a comb has a need for particular characteristics such as a given spectral power per line, spacing between the lines, and central wavelength. These requirements motivated the design of several very different setups for OFC generation such as ones based on femtosecond lasers, resonators or electro-optic modulators (EOMs).

In this paper, we will focus on the most recent progresses obtained in the generation of OFCs based on EOMs. First, we introduce the subject with generalities on OFCs and the common setups used for their generation. Then, we will focus on combs generated by the electro-optic modulation of a continuous wave (CW) laser, starting from the basic concepts up to the commonly used setups. This will lead us to the advantages and drawbacks of OFCs generated with such setups and further to the possible ways of bypassing the limitations. After that, we will present the applications of combs generated with EOMs, up to the state of the art in fundamental physics, spectroscopy, instrumental calibration, etc. We show that several domains are highly convenient for these comb sources since they possess numerous advantages. Finally, we will see the outlooks in the field based on recent published works, and to conclude, we will summarize the work presented in this paper.

2. GENERALITIES ON OPTICAL FREQUENCY COMBS

In this part, we introduce, in a nonexhaustive way, generalities behind OFC generation. We first theoretically present OFCs and the main characteristics of these particular spectra. Then, we present the most common experimental setups used to generate OFCs, which will provide a context for the current methods used.

2.1. Main Characteristics of Frequency Combs

2.1a. Theory of Frequency Comb Generation
Let us consider a pulsed laser emitting at a carrier frequency $\nu_c = \frac{\omega_c}{2\pi}$. All the pulses possess an envelope A cadenced at a repetition rate $\tau = \frac{2\pi}{\omega_r}$, where ω_r is the repetition frequency of the laser. We suppose that between two successive pulses, a phase difference φ can exist due to the difference of velocity between the carrier and the envelope.

Under these conditions and in the theoretical limit, where the laser emits for any time $t \in \mathbb{R}$ (neither beginning nor end), the pulse train f emitted by the laser can be written under the following form:

$$f(t) = \sum_{n=-\infty}^{\infty} (A(t) \cos(\omega_c t - n\varphi)) * \delta(t - n\tau), \tag{1}$$

where $n \in \mathbb{Z}$, δ is the Dirac distribution and $*$ is the convolution product. By taking the Fourier transform (FT) of f, we obtain the expression of the pulse train in the frequency domain, which is given by

$$\tilde{f}(\omega) = \mathrm{FT}(f(t)) = \int_{-\infty}^{\infty} f(t)e^{-i\omega t}\mathrm{d}t = \pi\omega_r \tilde{A}(\omega - \omega_c) \sum_{n=-\infty}^{\infty} \delta(\omega - \omega_0 - n\omega_r)$$

$$+ \pi\omega_r \tilde{A}(\omega + \omega_c) \sum_{n=-\infty}^{\infty} \delta(\omega + \omega_0 - n\omega_r), \tag{2}$$

where $\tilde{A}(\omega) = \mathrm{FT}(A(t))$ is the amplitude envelope of the spectrum and $\omega_0 = \frac{\omega_r}{2\pi}\varphi$ is the *carrier envelope offset frequency*.

Equation (2) shows two terms centered at $\pm\omega_c$. Since negative frequencies have no physical meaning, we focus on the first term centered at ω_c, which shows a sum of Dirac functions enveloped by $\tilde{A}$. Moreover, this term is different from zero only for particular frequencies defined by

$$\omega \equiv \omega_n = \omega_0 + n\omega_r. \tag{3}$$

This particular structure defined by Eq. (3) is very interesting since ω_r and ω_0 lie into the radio frequency (RF) domain. As shown in the next part, typical values of these frequencies are from the megahertz (MHz) to a few tens of gigahertz (GHz) depending on the laser source. Consequently, all comb lines are linked to RFs, which can be known with an extreme accuracy. Since optical frequencies cannot be measured directly due to the electronic limits, Eq. (3) allows us to know the optical frequencies of the comb with the same accuracy as is obtainable on ω_r and ω_0 [5].

To summarize, the spectrum of a pulsed source is composed of a set of discrete and equally spaced lines, which is called a frequency comb. Experimentally speaking, a pulsed laser has an emission with a finite coherence time. Hence, the spectrum is rigorously not a set of Dirac lines but more a set of Lorentzian lines that possess a width $\Delta\omega_l$ [8]. However, we usually have $\frac{\Delta\omega_l}{\omega_r} \ll 1$, which means that the approximation of an infinite coherence time is not aberrant. Even so, the finite linewidth of the comb lines must be kept in mind since it gives several points of information on the quality of the laser, as will be discussed in Subsection 4.2. An illustration of the temporal and spectral representation of a pulse train delivered by a pulsed source is presented in Fig. 1.

We considered above a pulsed laser that shows a phase difference φ between two successive pulses. This condition, which is due to the mode-locking of the laser, is important for the spectrum to present a comb structure. Indeed, without any phase relation between the pulses emitted by the laser, there would be no phase coherence between them, and, thus, they will not interfere. However, it is the interference of many coherent pulses that gives the spectrum its comb structure.

2.1b. Precision and Self-Referencing

Equation (3) shows that the optical frequencies of a comb are linked to two RFs ω_r and ω_0. Hence, to fully use an OFC, ω_r and ω_0 have to be known with an extreme accuracy. Since ω_r and ω_0 lie into the RF domain, these frequencies can be measured with precision [5,9]. The repetition frequency ω_r can simply be measured using a fast photodiode: the time spacing τ between two successive pulses is equal to the inverse of the repetition frequency. The carrier envelope offset frequency ω_0 is more difficult to measure since it is linked to the difference of phase φ between two successive pulses. Thus, one would need to measure φ, which means resolving the ultrafast oscillations of the carrier, which is impossible using standard electronics, especially for waves in the optical domain. This problem can be bypassed using a solution found independently by Jones *et al.* and Reichert *et al.* [10,11]. The solution consists in using nonlinear optics and especially second-harmonic generation, which will be used to frequency double an OFC to generate a second OFC of frequencies given by $2\omega_n = 2n\omega_r + 2\omega_0$. If the original comb spans over at least one *octave*, which means that the comb possesses a line of order p and its doubled order $2p$, then the line of frequency ω_{2p} from the original comb will interfere with the line of frequency $2\omega_p$ from the frequency doubled comb. The interference will lead to the generation of a signal at a frequency $2\omega_p - \omega_{2p} = 2p\omega_r + 2\omega_0 - 2p\omega_r - \omega_0 = \omega_0$ meaning that by detecting the beatnote, one can measure the carrier envelope offset frequency [10,11]. When both ω_r and ω_0 are measured, the comb is said to be fully *self-referenced*, and all comb lines can then be known using Eq. (3) with an accuracy equal to that obtained on ω_r and ω_0.

2.2. Frequency Comb Generation

Several experimental setups can be used to generate a mode-locked pulse train, i.e., an OFC. We now present the most common setups used to generate OFCs except those based on EOMs, which will be introduced in a more detailed way in the next part.

Figure 1
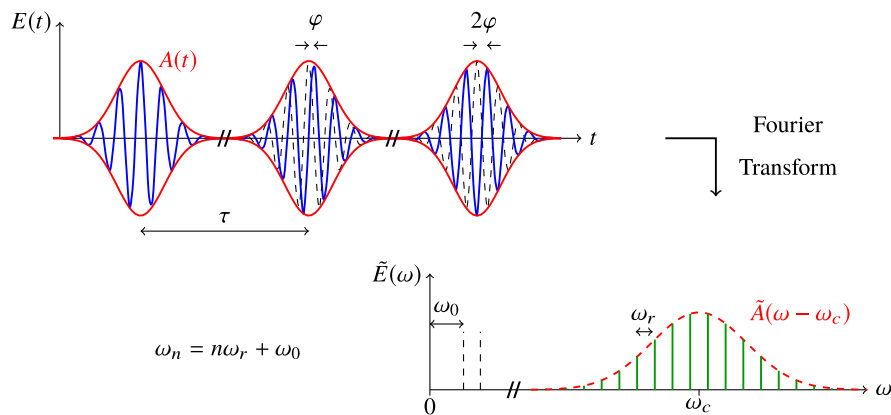
Representation of a pulse train delivered by a pulsed source in the temporal domain and in the frequency domain. In the temporal domain, a set of pulses of envelope A cadenced at a rate τ can be seen with a phase difference φ between two successive pulses due to the difference of velocity that can exist between the carrier and the envelope. In the spectral domain, a frequency comb of lines separated by the frequency $\omega_r = \frac{2\pi}{\tau}$ enveloped by $\tilde{A}$ centered at ω_c can be seen with an offset frequency $\omega_0 = \frac{\omega_r}{2\pi}\varphi$.

2.2a. Mode-Locked Lasers

Since their origin [2], most devices for generating combs still use MLLs. In MLLs, a cavity with a round trip time τ fixes the phase relationship between all the longitudinal modes and thus sets the repetition frequency of the laser, which can be from the MHz to a few GHz. Currently, the most common MLL is the Kerr-lens mode-locked titanium-sapphire laser (KLM Ti:sapphire). Figure 2 represents the typical structure of a KLM Ti:sapphire where the Ti:sapphire crystal, which allows self-focusing, is pumped with green light to provide gain [12,13]. Prisms are used to compensate the group velocity dispersion introduced by the crystal. To ensure the control and locking of ω_0 and ω_r, the output window and the rear mirror are on translating and rotating piezoelectric actuators, respectively. Therefore, such a laser can emit pulses up to a few tens of femtoseconds and thus a very broadband OFC. These lasers are usually centered around 800 nm and possess a repetition frequency from tens of MHz to several GHz. The KLM Ti:sapphire is the first component of the frequency comb generator or synthesizer that led in 2005 to the Nobel Prize in Physics.

Another example of common MLLs is the fibered laser with a typical structure shown in Fig. 3. Here, the mode-locking mechanism is the nonlinear polarization rotation that happens in a nonlinear optical fiber [14–16]. More precisely, the Kerr effect in the fiber leads to an intensity-dependent nonlinear phase shift, and, therefore, the polarization state is modified with the light intensity. Thus, a polarizer can be used as an effective saturable absorber. Obviously, several other configurations have been demonstrated based on true saturable absorbers, pulse shaping, etc. Compared to the KLM Ti:sapphire, such mode-locked fiber lasers are more compact and cheaper. More details on OFCs generated by MLLs can be found in Refs. [13,16–19].

2.2b. Optical Microresonators

More recently, another category of setups that is able to generate OFCs has emerged with microresonators [20]. Compared to MLLs, resonators are optical cavities built inside a material that is closed on itself. Several shapes of microresonators are available, such as a microtoroid, microsphere, microdisk, and microring, and a few of them are presented in Fig. 4. The coupling with light has to be made, employing evanescent waves by using, for instance, a tapered fiber or a prism. In microresonators, the round trip time is fixed by the length of the cavity, which is generally below 1 mm. So, the repetition frequencies achievable with these setups range from 10 GHz up to 1 THz.

The mechanism behind comb generation inside microresonators is based on nonlinear effects: a CW laser is usually injected in the resonator to seed a four-wave mixing

Figure 2
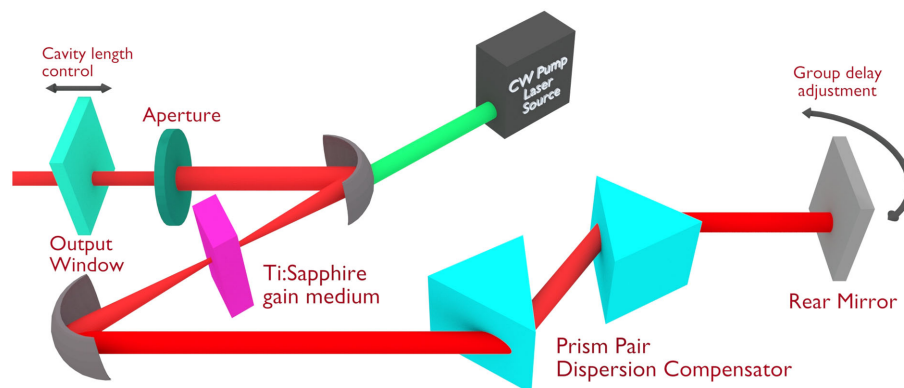
Schematic of a typical Ti:sapphire Kerr-lens laser cavity.

(FWM) phenomenon that leads to the generation of new frequencies. This corresponds to the creation of sidebands that are frequency detuned as the inverse of the round trip time of the cavity. Microresonators have reached a level of maturity, which is sufficient enough to generate coherent octave-spanning frequency combs using low input power and an ultrasmall footprint. More details on the subject can be found in Refs. [21–23].

2.2c. Other Architectures

Besides MLLs and microresonators, many other setups can be used to generate OFCs. A first example is the use of nonlinear effects in optical fibers such as Brillouin scattering and FWM [24]. When exploited in a cavity, it is possible to produce an OFC that spans over several tens of nanometers [25]. Still using nonlinear effects and especially FWM, a dual wavelength pump can produce an OFC in nonlinear fibers [26,27]. Finally, the use of acousto-optic modulators in cavities has been demonstrated for OFC generation. By using the ability of shifting frequencies of a certain amount, it is possible to generate an OFC by cascading the acousto-optic effect on the frequencies circulating in the loop [28,29].

Figure 3
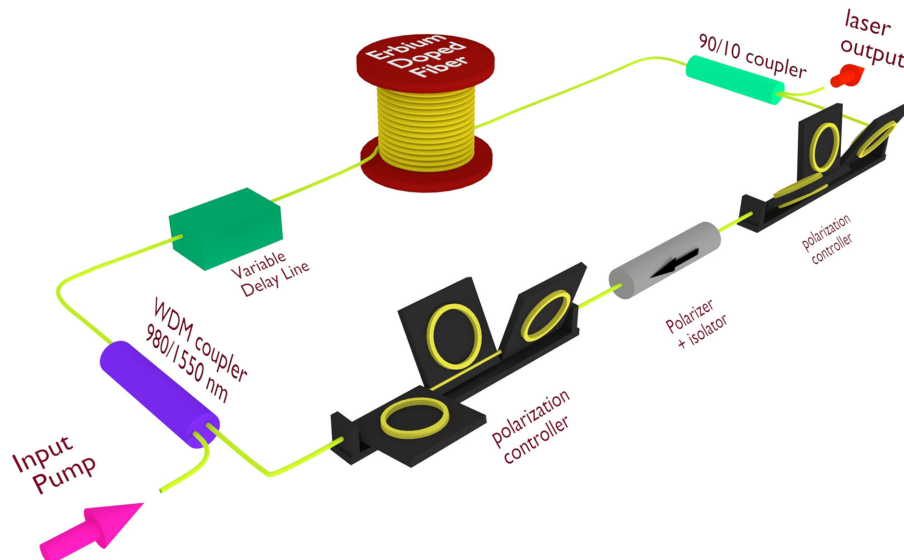
Schematic of a typical self-starting fibered laser.

Figure 4

Schematic of typical shapes of microresonators going from the toroid (left) to the integrated ring resonator (right) but also the sphere (center).

3. ELECTRO-OPTIC MODULATION

In the previous part, we showed that several setups are available for OFC generation. However, we did not introduce the particular example of setups based on EOMs, which is one of the main points of this paper. Hence, we now focus on OFCs that are generated with EOMs, which we will call from now on EOM-based combs or more simply *electro-optic combs* (EOCs). We start with a brief reminder on the electro-optic effect and its well-known characteristics. Then, we will present the different existing components for EOC generation from the basic ones up to the most recent ones. Finally, we will show the advantages of this particular way of generating OFCs compared to common sources.

3.1. Pockels Effect and Modulators

The electro-optic effect is a nonlinear phenomenon that includes several effects. Generally speaking, an electro-optic effect is a phenomenon that modifies the refractive index of a material by applying a static electrical field. The modification in the refractive index imposes a phase of an electromagnetic field propagating inside the material. The electro-optic effect can be seen as a wave mixing effect between an electromagnetic field and the static field [30]. Several phenomena can be defined as an electro-optic effect, but here we will focus only on the two major ones. The first one is the *Pockels effect*, which shows that the refractive index of a material can linearly change with the electrical field applied. Named after Pockels who investigated the effect [31], the phenomenon was discovered independently by Kundt and Röntgen [32,33]. The Pockels effect is also known as the *linear electro-optic effect* and can appear only in noncentrosymmetric materials since it is a second-order nonlinear process.

The second electro-optic effect is the *Kerr effect*, which shows a change in the refractive index of a material proportionally to the square of the electrical field [34]. This effect can appear in any material, and since it is a third-order nonlinear effect, it is much weaker that the Pockels effect. From now on, we will thus focus only on the Pockels effect because it is used in most existing EOMs. Knowing all this, from now, the use of the adjective "electro-optic" will refer to the Pockels effect that we will start to describe.

3.1a. Physical Process

Let us consider a noncentrosymmetric, anisotropic, nonoptically active, and lossless material. The constitutive relation $\mathbf{D} = \varepsilon_0 \varepsilon \mathbf{E}$, when components are explicited, can be written in the following form:

$$D_i = \varepsilon_0 \sum_j \varepsilon_{ij} E_j \Leftrightarrow E_i = \frac{1}{\varepsilon_0} \sum_j \eta_{ij} D_j, \tag{4}$$

where ε_0 is the vacuum permittivity, ε is the permittivity tensor, and η is the inverse tensor of ε. In any coordinates system x_i with $i = \{1, 2, 3\}$, the index ellipsoid can be written as

$$\sum_{i=1}^{3} \sum_{j=1}^{3} \left(\frac{1}{n^2} \right)_{ij} x_i x_j = 1. \tag{5}$$

The constants $\left(\frac{1}{n^2} \right)_{ij}$ describe the refractive index in the x_i coordinate system, and they are symmetric in ij since the permittivity tensor is symmetric due to the particular material considered here. In the crystallographic coordinate system, we can find that $\left(\frac{1}{n^2} \right)_{ij} = \eta_{ij}$. Moreover, when assumed that η can be Taylor expanded in relation to the

components of the applied electrical field **E**, when restricted to the linear order, we obtain

$$\eta_{ij} = \eta_{ij}^{(0)} + \sum_k r_{ijk} E_k + o(E_k), \tag{6}$$

where r is the tensor describing the linear electro-optic effect. Since η is real and symmetric, r is symmetric in its two first indices. For convenience, the $3 \times 3 \times 3$ tensor r_{ijk} can then be contracted in a 3×6 tensor r_{hk} using the following indices sorting $h = 1 \to ij = 11$, $h = 2 \to ij = 22$, $h = 3 \to ij = 33$, $h = 4 \to ij = 23/32$, $h = 5 \to ij = 13/31$, and $h = 6 \to ij = 12/21$. Thus, the variations in the refractive index can be expressed as

$$\Delta \left(\frac{1}{n^2} \right)_h = \sum_j r_{hj} E_j. \tag{7}$$

The r_{hj} coefficients are the electro-optic coefficients that give the variation of the refractive index in relation with the changes in the applied electrical field.

3.1b. Elementary Modulators

Using the concepts seen above, we now present three basic EOMs capable of modulating a particular property of an input light. This will allow us to conceptualize several fundamental characteristics and properties of modulators. Note that every type of EOM is based on the application of a phase on the incident light using the electro-optic effect, but used within a particular setup, this phase modulation can lead to the modulation of another light parameter.

Phase modulator. Let us consider a uniaxial crystal such as a potassium dihydrogen phosphate (KDP) of crystal axes (x, y, z) for which the r_{hj} tensor is different from zero only for r_{41}, r_{52}, and r_{63}. A longitudinal electrical field E_z, commonly called the *RF signal*, is applied on the crystal along the z direction leading to a modification of the principal axis system to (x', y', z). The index ellipsoid is thus modified, and the refractive indices are given by

$$n_{x'} = n_o - \frac{1}{2} n_o^3 r_{63} E_z, \quad n_{y'} = n_o + \frac{1}{2} n_o^3 r_{63} E_z, \tag{8}$$

where n_o is the ordinary refractive index. When considering a wave that is propagating in the z direction and that is linearly polarized on either the x' or the y' axis, a phase $\Delta\varphi$ is induced by the electro-optic effect and given, for a polarization of the light on the y' axis, by

$$\Delta\varphi = (n_{y'} - n_o) \frac{2\pi L}{\lambda} = \frac{\pi n_o^3 r_{63} V}{\lambda}, \tag{9}$$

where L is the crystal length and $V = E_z L$ is the voltage associated to the applied RF signal. A phase $\Delta\varphi$ is then printed on the incident light, which gives a phase modulator (PM). It is useful to introduce the quantity V_π, which is the voltage needed to induce a π phase. $\Delta\varphi$ is then given by

$$\Delta\varphi = \pi \frac{V}{V_\pi} \quad \text{with} \quad V_\pi = \frac{\lambda}{n_o^3 r_{63}}. \tag{10}$$

The modulator constant $K = \frac{\pi}{V_\pi}$ is named the *modulation index*. With KDP, we have $r_{63} = 10.5 \ \text{pm} \cdot \text{V}^{-1}$ and $n_o = 1.514$ at 546.1 nm, so at this wavelength, a numerical application gives a value of $V_\pi = 15 \ \text{kV}$ [30].

Polarization modulator. The basic PM seen above can be slightly modified using one or two polarizer(s) to obtain a polarization modulator. In the case of the PM, light is injected on one of the principal axes x' or y', so the polarization state is unchanged at the output. However, if an input polarizer injects a linearly polarized light at 45° from the principal axes, a retardation $\Delta\varphi$ between the two components will arise such that

$$\Delta\varphi = \Delta n \frac{2\pi L}{\lambda} = (n_{y'} - n_{x'})\frac{2\pi L}{\lambda} = \frac{2\pi n_o^3 r_{63} V}{\lambda} = \pi \frac{V}{V_\pi} \quad \text{with} \quad V_\pi = \frac{\lambda}{2n_o^3 r_{63}}. \quad \text{(11)}$$

Here, the V_π voltage presents the more profound physical signification that at this particular voltage, the modulator rotates the polarization of $\frac{\pi}{2}$ and thus is equivalent to a half-wave plate. Note that a PM is the particular case of a polarization modulator where the rotation of polarization is null. At the output of the crystal, a second polarizer with the same orientation as the first one is generally used to project the two components of the electrical field on the same axis.

Intensity modulator. Finally, an intensity modulator (IM) can be created when adding a quarter-wave plate after a polarization modulator with this set is placed between two crossed polarizers. The schematic of such a setup is shown in Fig. 5.

The initial polarizer is implemented to obtain a given linearly polarized light at the input of the crystal, which is practically also the case for a phase and a polarization modulator. After passing through the crystal and the quarter-wave plate, the incident light propagating in the z direction will see its components acquiring a phase difference $\Delta\varphi$ given by

$$\Delta\varphi = \Delta n \frac{2\pi L}{\lambda} + \frac{\pi}{2} = \frac{2\pi n_o^3 r_{63} V}{\lambda} + \frac{\pi}{2} = \frac{\pi V}{2 V_\pi} + \frac{\pi}{2} \quad \text{with} \quad V_\pi = \frac{\lambda}{4n_o^3 r_{63}}. \quad \text{(12)}$$

This shows the utility of putting a quarter-wave plate at the output: the voltage V_π is reduced by a factor of 2 compared to the polarization modulator and by 4 compared to the PM, and the numerical application gives us here $V_\pi = 3.75$ kV.

The transmission T (also called the transfer function) after the output polarizer is given by

Figure 5
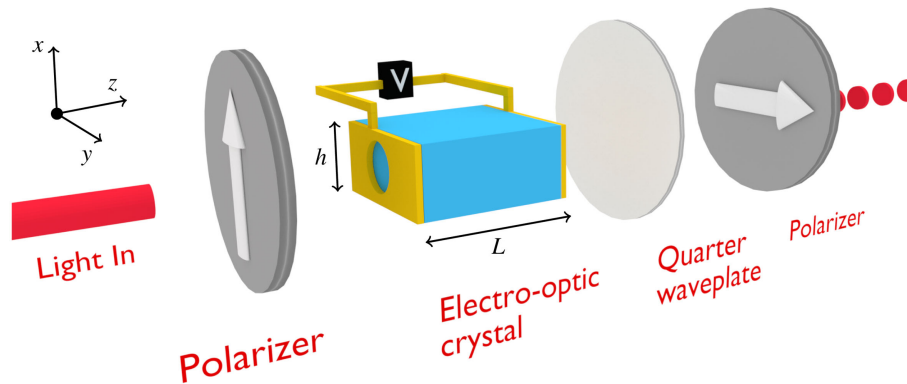
Schematic showing the setup of a basic intensity modulator based on the electro-optic effect with a longitudinal electrical field applied on a crystal of length L and height h. Experimentally speaking, an aperture is generally cut out of the electrodes (in yellow), or transparent electrodes are used for the incident light to propagate through the crystal.

$$T = \frac{|\mathbf{E}_{\text{out}}|^2}{|\mathbf{E}_{\text{in}}|^2} = \sin^2\left(\frac{1}{2}\Delta\varphi\right) = \sin^2\left(\frac{\pi V}{4 V_\pi} + \frac{\pi}{4}\right). \tag{13}$$

If V is static, T is fixed, but an IM is obtained when considering a time-dependent voltage V. The $\frac{\pi}{2}$ phase shift induced by the quarter-wave plate is also justified here by the form of the transfer function. Indeed, this supplementary phase shift sets the operating point of the modulator, which is named, in this case, the *quadrature point*. This gives a transfer function that is linear in the vicinity of the quadrature point, which avoids distortions of the optical signal obtained relative to the RF signal fed to the modulator. To illustrate this, let us consider a time-dependent RF signal V of peak voltage V_0. If $\frac{\pi V_0}{4 V_\pi} \ll 1$, then we have

$$T = \sin^2\left(\frac{\pi V}{4 V_\pi} + \frac{\pi}{4}\right) = \frac{1}{2}\left(\cos\left(\frac{\pi V}{4 V_\pi}\right) + \sin\left(\frac{\pi V}{4 V_\pi}\right)\right)^2 = \frac{1}{2} + \frac{\pi V}{4 V_\pi} + o\left(V_0^2\right). \tag{14}$$

Hence, in the vicinity of the quadrature point, T is approximatively linear. The transfer function T of Eq. (13) is plotted in Fig. 6 along with the linear approximation around the quadrature point.

Three different EOMs have been described above according to which physical characteristic of the input light is modulated. This classification will be kept all throughout this paper. Note again that all of these EOMs rely on the same physical principle, which is the phase modulation of an input light.

3.1c. High-Performance Modulators

The EOMs described above allowed us to introduce some general characteristics useful for this paper. Note, however, that such basic architectures are almost never used in standard available EOMs because of their poor performance. One of the main drawbacks is that the V_π voltage can reach several kilovolts, which is not convenient for embedded systems, for instance. Thus, it makes sense to look for materials having the lowest possible V_π voltage, i.e., with the highest electro-optic coefficient. To the same purpose, it is much more interesting to use a transverse static electrical field instead of a longitudinal one as shown in Fig. 5 for the basic IM. First, this avoids the need for using transparent electrodes with respect to the incident light, or to cut an aperture out of the electrodes. Second, using a transverse static electrical field leads

Figure 6
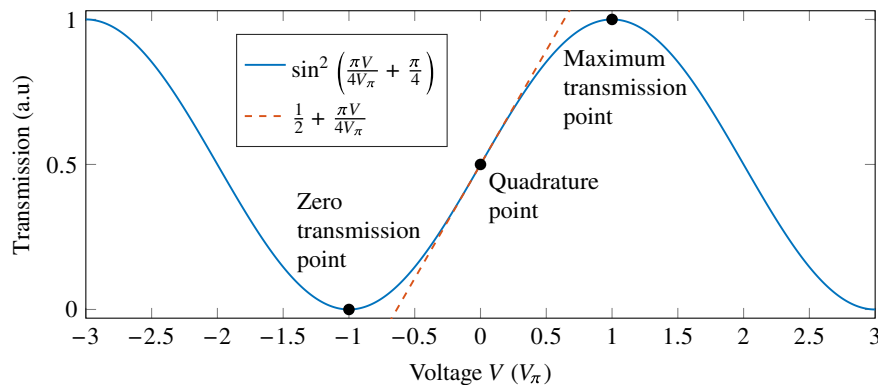
Graph showing the transfer function of a basic intensity modulator set at its quadrature point along with several other characteristic points and the approximated linear function around the quadrature point.

to a voltage $V = E_x h$, where $h < L$ is the height of the crystal. In this case, the V_π voltage is proportional to $\frac{h}{L}$, which can lead to a V_π value of the order of tens of volts when the crystal is properly designed.

A second main drawback of basic EOMs is their very simple architectures that are easily subject to parasite effects, decreasing their efficiency (see Subsection 4.1). In particular for IMs, adding polarizers or quarter-wave plates causes the performance of the EOM to rely on the characteristics of these components. Thus, other architectures have been studied, and it was found that relying on an interferometer could allow improvements of the EOM characteristics. The idea is to introduce an electro-optic material within an interferometer, usually a Mach–Zehnder interferometer [35,36]. This particular design allows us to replace the output polarizer by an interference effect leading to a lower required driving voltage [37]. Such an EOM is then often called a Mach–Zehnder modulator (MZM), and two main designs are commonly available as presented in Fig. 7.

Other architectures have also been studied, but they usually deliver less convenient highly chirped outputs. In the following, we will thus focus only on the operation principles of the two MZMs shown in Fig. 7. First, waveguides are printed on an electro-optic material that is designed with an adequate cutting along its crystallographic axes. At the input, the waveguide starts with a 50/50 splitter that is made with a Y-junction to create two arms. Then, both arms are covered with a set of electrodes that will be used to independently apply a RF signal and a static voltage. Both voltages induce an electro-optic effect and thus add a phase on the input light. The novel static voltage specific to MZMs is called the *bias voltage* and is added to select a particular operating point of modulation of the EOM. For instance, a bias voltage of $\frac{V_\pi}{2}$ induces a $\frac{\pi}{2}$ phase shift, which mimics the quarter-wave plate used in the basic IM seen above and, thus, sets the modulator to the quadrature point.

Depending on the fact that the arms are subjected to the same or not the same set of electrodes, the MZM is then respectively qualified as a single-drive MZM or a dual-drive MZM (DDMZM). At the output, both arms are then recombined with a second Y-junction leading to an interference effect. For a single-drive MZM, the phases applied on both arms can be exactly the same or can have opposite signs depending on how the electrodes are set. In the first case, the MZM is said to be in a *push–push* mode and will be equal to a pure PM. In the case of opposite phase signs, the MZM is said to be in a *push–pull* mode and will be equal to a pure IM. For a DDMZM, in the

Figure 7
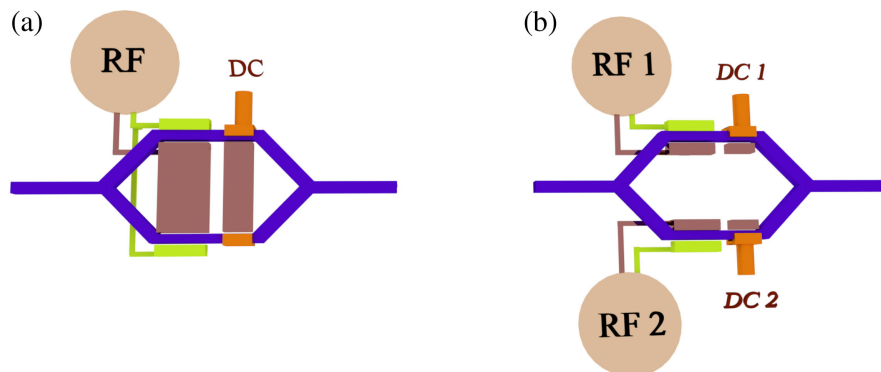
Schematic showing the two most common electro-optic modulators based on a Mach–Zehnder interferometer. (a) Single-drive Mach–Zehnder modulator. (b) Dual-drive Mach–Zehnder modulator.

general case of different voltages applied, the modulator is both a PM and an IM, as described in the following.

3.2. Comb Generation with Electro-Optic Modulators

We now introduce the experimental setups, to generate OFCs, based on EOMs. To understand the different characteristics of these setups, it is first necessary to understand the theory behind the generation of comb structures with EOMs. As presented in the previous part, each EOM is based on the phase modulation of an input CW laser and, depending on the components added around (polarizers, quarter-wave plates, interferometer, etc.), the modulator acquires other functionalities. It is then useful to know the characteristics of the combs that can be generated with the different EOMs available.

3.2a. Principles of Electro-Optic Combs

In this part, we come up to the theory behind the generation of EOCs. We will see, when possible, the form of the spectral output delivered by the different existing EOMs. Moreover, several characteristics of these EOMs will be presented such as the number of lines that can be generated or, when relevant, the obtained shape of the comb under particular conditions.

Phase modulator. Let us consider a PM of modulation index K that is fed by a CW laser at a carrier frequency ω_c and of amplitude A_0. The modulator is driven by an electrical sinusoidal waveform generator at a modulation frequency ω_m. Thus, the electrical field is given by $V(t) = V_0 \sin(\omega_m t)$, where V_0 is the peak voltage. At the output of the modulator, the initial optical field acquires a phase $\Delta \varphi = K V(t)$, and thus the output optical field A can be expressed as

$$A(t) = A_0 e^{i\omega_c t} e^{i\Delta\varphi} = A_0 e^{i\omega_c t} e^{iKV_0 \sin(\omega_m t)}. \tag{15}$$

In the frequency domain, the amplitude spectrum is obtained by FT, and we have

$$\tilde{A}(\omega) = \mathrm{FT}(A(t)) = A_0 \delta(\omega - \omega_c) * \left(\int_{-\infty}^{\infty} e^{iKV_0 \sin(\omega_m t)} e^{-i\omega t} \mathrm{d}t \right). \tag{16}$$

Using the Jacobi–Anger expansion, i.e., by expanding plane waves in series of cylindrical waves [38], we obtain

$$\tilde{A}(\omega) = A_0 \delta(\omega - \omega_c) * \left(\int_{-\infty}^{\infty} \sum_{n=-\infty}^{\infty} J_n(KV_0) e^{it(n\omega_m - \omega)} \mathrm{d}t \right)$$

$$= A_0 \sum_{n=-\infty}^{\infty} J_n(KV_0) \delta(\omega - n\omega_m - \omega_c), \tag{17}$$

where J_n are the Bessel functions of the first kind. The last equation shows that the optical spectrum is an OFC where all the frequencies of the comb are defined by

$$\omega \equiv \omega_n = n\omega_m + \omega_c \quad \text{with} \quad n \in \mathbb{Z}. \tag{18}$$

If ω_c is decomposed such that $\omega_c = p\omega_m + \omega_0$, where $p \in \mathbb{N}$ and ω_0 is the carrier envelope offset frequency, then Eq. (18) is given by $\omega_n = (n + p)\omega_m + \omega_0$, which is equivalent to Eq. (3) when renumbering the index of frequencies. However, when dealing with EOCs, the Eq. (18) is much more practical and natural to use since it shows the frequency of the input CW laser, which is usually known compared to ω_0,

which has to be measured. Expressed this way, the integer n gives the line number in relation with the CW component sets at $n = 0$.

Equation (17) also shows that the amplitude of the EOC lines follows the Bessel functions of the first kind J_n, which are presented in Fig. 8(a) for the first four. This characteristic is particularly important since we can see that the modulation index K and the peak voltage V_0 are the only parameters that fix the amplitude, the flatness, and the number of lines of the comb. Figure 8(b) presents an example of simulated EOC that can be generated with a PM. It shows that a comb generated by a PM presents two maximums around the wings of the spectrum, with this feature arising directly from the sinusoidal form of the voltage V, which is commonly used but independent of the peak voltage V_0 and the modulation index K. However, the positions of these maximums depend on V_0 and K. Thus, this feature can be used to arbitrarily define the number of exploitable lines N of the comb as the number of lines existing between the maximums of the spectrum. This definition leads to N being twice the order of the Bessel function associated to the lines of maximum amplitudes. A numerical simulation presented in Fig. 9(a) shows that N closely follows a linear function defined by

$$N = 2\lfloor K V_0 \rfloor, \tag{19}$$

where $\lfloor \cdot \rfloor$ is the floor function [39,40]. We can see from Fig. 9(a) that for high $K V_0$ values, an overestimation appears, but since this definition of N does not take into account the comb lines on the wings of the spectrum, this overestimation can be seen as closer to the real number of comb lines generated by the PM. However, for low $K V_0$ values, the number of comb lines N as defined above is far from the actual number of lines generated by the PM, simply because of the predominance of the lines on the wings. For a more accurate definition of the number of lines generated, N should be then defined relative to an intensity limit. With such a definition, numerical simulations show that Eq. (19) is no more valid, but N can still be approximated by simple nonlinear functions that are empirical to find. Figure 9(b) shows the graphs of N defined by different intensity limits and their least squares fit of simple nonlinear functions. Nevertheless, Eq. (19) is still a good approximation since high values of $K V_0$ are generally considered and the exploited lines are generally on the top of the spectrum. Note that for a single PM, $K V_0$ rarely exceeds a value of 15, but higher

Figure 8
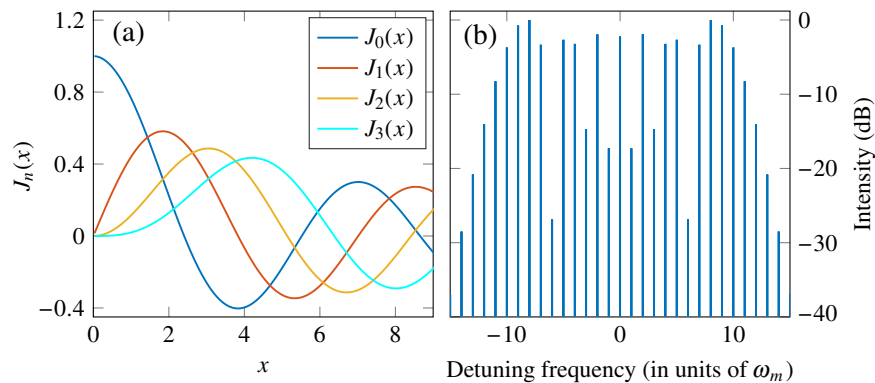
(a) Graph showing the first four Bessel functions of the first kind. The amplitude of the lines of an EOC generated by phase modulation is directly related to these functions. (b) Simulated EOC generated with a phase modulator with $K V_0 = 10$.

values can be obtained when cascading modulators, which is why Fig. 9 displays $K V_0$ values up to 45.

Mach–Zehnder modulator. Now, let us consider combs generated with MZMs starting with the general case of a DDMZM where, on one arm of the EOM, a voltage $V_1(t) = V_{0,1} \sin(\omega_m t)$ is applied, whereas a voltage $V_2(t) = V_{0,2} \sin(\omega_m t)$ is applied on the second arm. The temporal output of this modulator is then given by

$$A(t) = \frac{A_0}{2} e^{i\omega_c t} \left(e^{i K_1 (V_1(t) + V_{b,1})} + e^{i K_2 (V_2(t) + V_{b,2})} \right), \quad (20)$$

where K_1 and K_2 are, respectively, the modulation indices of arms 1 and 2 and $V_{b,1}$ and $V_{b,2}$ are the bias voltages applied on arms 1 and 2. The optical spectrum is thus given by

$$\tilde{A}(\omega) = \frac{A_0}{2} \sum_{n=-\infty}^{\infty} \left(J_n(K_1 V_{0,1}) e^{i K_1 V_{b,1}} + J_n(K_2 V_{0,2}) e^{i K_2 V_{b,2}} \right) \delta(\omega - n\omega_m - \omega_c). \quad (21)$$

Compared to a PM, the bias voltages add a degree of freedom, which will be particularly useful for spectrum flattening. Although the number of comb lines generated with a DDMZM, when the RF signals and the bias voltages are different, is similar to the number of comb lines generated with a PM, the shape of the comb generated can be drastically different; therefore, only a definition based on an intensity limit should be used in this case.

As already mentioned, a DDMZM is a PM and an IM. Equation (20) allowed us to simply investigate the spectral domain by FT, but the temporal domain can also be studied by writing the output temporal envelope A in the following form:

$$A(t) = A_0 e^{i\omega_c t} e^{i\frac{1}{2} K_1 (V_1(t) + V_{b,1})} e^{i\frac{1}{2} K_2 (V_2(t) + V_{b,2})}$$

$$\times \cos\left(\frac{1}{2} (K_1 (V_1(t) + V_{b,1}) - K_2 (V_2(t) + V_{b,2})) \right), \quad (22)$$

Figure 9
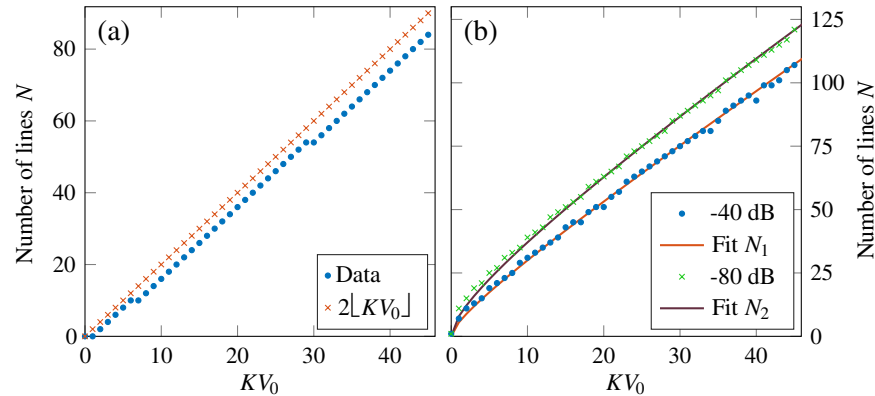
Graphs showing the number of comb lines N generated by a phase modulator driven by a sinusoidal waveform of peak voltage V_0 when (a) N is defined by twice the order of the Bessel function leading to the line of maximum intensity, which is close to $2\lfloor K V_0 \rfloor$, and (b) N is defined by an intensity limit that can be fitted by $N_1(x) = 3.657\sqrt{x} + 1.84x$ at -40 dB and by $N_2(x) = 6.106\sqrt{x} + 1.774x$ at -80 dB.

and thus the transfer function of the DDMZM is given by

$$T = \frac{|\mathbf{E}_{\text{out}}|^2}{|\mathbf{E}_{\text{in}}|^2} = \cos^2\left(\frac{1}{2}(K_1(V_1(t) + V_{b,1}) - K_2(V_2(t) + V_{b,2}))\right). \tag{23}$$

This last equation shows that the phase modulation is accompanied by an intensity modulation.

The above study of the DDMZM can be restricted to a single-drive MZM in the push–push mode (and thus a pure PM) by setting $K_1 = K_2 = K$, $V_{0,1} = V_{0,2} = V_0$, and $V_{b,1} = V_{b,2} = V_b$. In this case, the optical spectrum is given by

$$\tilde{A}(\omega) = A_0 e^{iKV_b} \sum_{n=-\infty}^{\infty} J_n(KV_0)\delta(\omega - n\omega_m - \omega_c), \tag{24}$$

which is almost the same as Eq. (17) apart from an additional phase term associated to the bias voltage. On the contrary, a single-drive MZM in the push–pull mode can be obtained (and thus a pure IM) by setting $K_1 = K_2 = K$, $V_{0,1} = -V_{0,2} = V_0$, and $V_{b,1} = -V_{b,2} = V_b$. In this case, the transfer function of this EOM is given by

$$T = \frac{|\mathbf{E}_{\text{out}}|^2}{|\mathbf{E}_{\text{in}}|^2} = \cos^2(KV(t) + KV_b). \tag{25}$$

By applying a bias voltage $V_b = -\frac{V_\pi}{4}$, meaning that $KV_b = -\frac{\pi}{4}$, the MZM can be set to the quadrature point where the transfer function is almost linear, as shown for the basic IM (see Fig. 6). Regarding the optical spectrum, we have

$$\tilde{A}(\omega) = \frac{A_0}{2} \sum_{n=-\infty}^{\infty} \left(J_n(KV_0)e^{iKV_b} + J_n(-KV_0)e^{-iKV_b}\right)\delta(\omega - n\omega_m - \omega_c)$$

$$= \frac{A_0}{2} \sum_{n=-\infty}^{\infty} J_n(KV_0)\left(e^{iKV_b} + (-1)^n e^{-iKV_b}\right)\delta(\omega - n\omega_m - \omega_c), \tag{26}$$

where we used the fact that the Bessel functions of the first kind are symmetric for n even and antisymmetric for n odd. Here, a sinusoidal RF signal was used to drive the MZM. Note, however, that an analytical expression for any other RF signal is difficult to obtain. Note also that usually, single-drive MZMs exhibit a single input for the RF signal and one input for the bias voltage V_b, which simplifies the setup, and the choice between the push–push or the push–pull mode is made by setting the electrodes accordingly.

Polarization modulator. Finally, polarization modulators are in-between a MZM in the push–pull mode and a DDMZM with the same RF voltage applied on both arms but with opposite signs. A bias voltage V_b can be available in some of these EOMs depending on the architecture, and a polarization modulator is usually used with an injection at 45° from the principal axes **x** and **y**. When using a RF signal $V(t) = V_0 \sin(\omega_m t)$, the amplitude output of the polarization modulator is given in the temporal domain by

$$\mathbf{A}(t) = A_0 e^{i\omega_c t}\left(e^{iKV_0\sin(\omega_m t)}e^{iKV_b}\mathbf{x} + e^{-iKV_0\sin(\omega_m t)}e^{-iKV_b}\mathbf{y}\right). \tag{27}$$

At the output of the modulator, the field goes through a polarizer making an α angle relative to the principal axes of the crystal. The output field is thus

$$A(t) = A_0 e^{i\omega_c t}\left(e^{iKV_0\sin(\omega_m t)}e^{iKV_b}\cos(\alpha) + e^{-iKV_0\sin(\omega_m t)}e^{-iKV_b}\sin(\alpha)\right), \tag{28}$$

which gives in the spectral domain

$$\tilde{A}(\omega) = A_0 \sum_{n=-\infty}^{\infty} (J_n(KV_0)e^{iKV_b}\cos(\alpha) + J_n(-KV_0)e^{-iKV_b}\sin(\alpha))\delta(\omega - n\omega_m - \omega_c).$$

(29)

Still using the parity of the Bessel functions with respect to n, the last equation can be simplified such as

$$\tilde{A}(\omega) = A_0 \sum_{n=-\infty}^{\infty} J_n(KV_0)\left(e^{iKV_b}\cos(\alpha) + (-1)^n e^{-iKV_b}\sin(\alpha)\right)\delta(\omega - n\omega_m - \omega_c).$$

(30)

The number of lines generated with a polarization modulator is similar to that of a DDMZM. Compared to the other EOMs, here the output polarizer adds an additional degree of freedom to shape the comb structure.

3.2b. Common Setups

Now that we have introduced the different types of existing modulators and the structure of the comb they can generate, we present the most common setups used to generate EOCs. Figure 10 shows an illustration of several setups that we will describe in detail.

Single modulators. EOC generation can be rather straightforward when using only one EOM, keeping the setup very simple. Three main setups are possible, as presented in Figs. 10(a)–10(c), and the theory behind each of these setups has been developed in the theoretical part. Experimentally speaking, these setups are limited by their electro-optic bandwidth that fixes the maximum linespacing. Nowadays, commercial EOMs show a common bandwidth around 40 GHz, but some EOMs are also available up to 70 GHz. Note also that EOMs, which are currently in development, can present an electro-optic bandwidth larger than 100 GHz, which we will discuss in the outlooks at Section 6. Regarding DDMZMs, several setups have been proposed due to the high flexibility of these EOMs [41–47], and these setups are generally designed to produce a flat comb.

Association of a phase modulator with an intensity modulator. Except when using DDMZMs, setups with only one modulator are rather rare, especially when high repetition rates are required. As shown before, for the generation of combs with

Figure 10
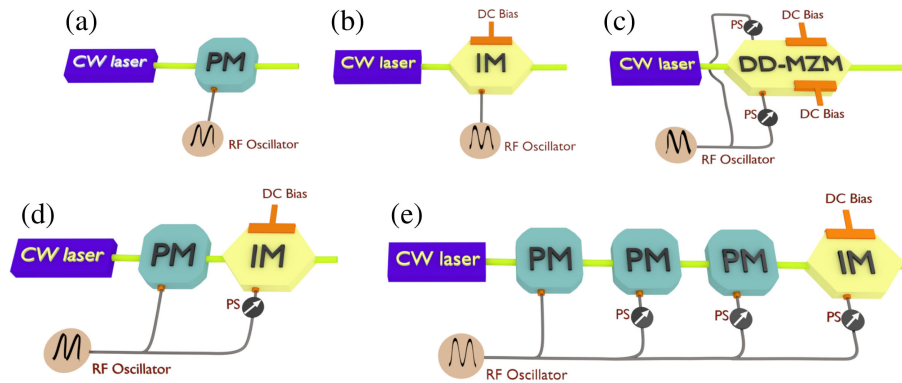
Schematic showing different setups based on electro-optic modulators for frequency comb generation. PM, phase modulator; IM, intensity modulator; PS, phase shifter; MZM, Mach–Zehnder modulator; DDMZM, dual-drive Mach–Zehnder modulator.

PMs, and especially in the Fig. 8(b), the comb structure is not monotonic since comb lines inside the spectrum can have a very low intensity due to the zeros of the Bessel functions. This problem can be overcome by flattening the comb when using an IM after the PM, leading to the setup presented in Fig. 10(d) [48]. Indeed, modulating the intensity with the same RF signal as the one used for phase modulation allows us to suppress some instantaneous frequencies [48]. By shifting the RF signal fed to the IM using electronics components, it is possible to keep only the linear chirped part of the phase modulated light, which results in a flattened spectrum. Several setups using the association of a PM with an IM have been reported to produce a flat EOC [48–52].

Cascade of modulators. For generating a wide EOC at high repetition rates, using only one EOM is generally not enough. Since an EOM can be damaged if too high of a RF voltage is applied, this limit being generally below 40 dBm for the most efficient commercial EOMs, the maximum number of lines generated by an EOM is limited. This problem can be managed by cascading in series several EOMs, which increases the number of lines generated by a factor equal to the number of EOMs, leading to the setup presented in Fig. 10(e). The number of PMs used is typically between two and four, and an IM is added at the output for flattening the spectrum. Once again, particular attention must be taken to the relative phase between the EOMs, which has to be aligned through the use of electrical phase shifters [53]. The number of lines generated with N EOMs at a driving voltage V_0 is equivalent to the number of lines generated by a theoretical single EOM driven at a voltage NV_0. Here, the number of lines can be determined using the equations and the graphs presented in Fig. 9. Numerous setups have been proposed using a cascade of EOMs for short pulse generation or wide EOCs with an external spectral broadening [54–59].

Polarization modulators. EOC generation using polarization modulators is less common than using PMs or IMs, but some studies have shown the possibility of using these particular EOMs. Indeed, although a polarization modulator within a two polarizer configuration can be equivalent to an IM, modifying the polarizer orientations allows an additional degree of freedom, which can be seen as an advantage to optimize the flatness or the stability. Moreover, polarization modulators can be used without a bias voltage, which can show advantages. However, there is no real common setup used with polarization modulators, and several architectures can be found with one modulator [60], two modulators [61–63], one modulator plus a PM [64], one modulator plus an IM [65], two modulators plus an IM [66], or several modulators in parallel [67,68]. This last configuration, also called a dual-parallel polarization modulator, requires lower voltage than the two cascaded configuration, and it allows us to reach higher modulation frequencies.

Electro-optic cavities. A last category of common setups used for EOC generation can be defined by setups based on an electro-optic effect exploited in a cavity. This can regroup either EOMs placed within a cavity or a cavity itself subjected to an electro-optic effect. For the sake of simplicity, we choose to name such a setup an *electro-optic cavity*. Several common electro-optic cavities have been designed through the years, and these setups are presented in Fig. 11.

A natural setup that can be used to increase the potential of a PM is to place the EOM within a Fabry–Perot cavity, as illustrated in Fig. 11(a) [69–71]. Such setups require particular conditions in the design since the traveling time of the cavity has to match the repetition rate of the RF signal. Hence, these setups are generally enslaved to counterbalance drifts, which would place the setup outside the resonance. Although these setups do not seem to be easy to implement, they possess interesting characteristics due to the filtering features of the cavity. Indeed, the architecture of the setup avoids the increasing of the phase noise of each comb line at high frequency detunings [72], which can be advantageous. Note that since the cavity is based upon mirrors,

these setups are free space, but they can be fibered, and they are commercially available.

A second kind of electro-optic cavity, presented in Fig. 11(b), is based on the incorporation of an EOM inside a fibered cavity that is enslaved [73–78]. Indeed, for the same reasons as with the Fabry–Perot cavity, there is a need to keep the setup in a resonant configuration, which is done by actively enslaving the cavity. These setups present particular advantages for on chip EOMs [79–82]. Differences with the electro-optic cavity based on a Fabry–Perot cavity are that this cavity is unidirectional and fibered and that no mirrors are required.

Finally, whispering gallery mode resonators subjected to an electro-optic effect can produce an EOC with a setup presented in Fig. 11(c) [83,84]. Compared to the previous setups where it was only the optical wave that was resonating, in these setups the RF signal is also resonating, which enhances the electro-optic effect and leads to a V_π voltage of an order of magnitude below conventional EOMs. Although high advantages are reported, the complexity of designing such setups makes them uncommon for the moment.

3.3. Advantages Compared to Usual Comb Sources

Now that the common setups for EOC generation have been presented, we will introduce the advantages of generating combs with EOMs as compared to the other common comb sources, described in Subsection 2.2.

3.3a. Tunability

One of the first advantages of EOCs is that they originate from a CW laser that is often chosen tunable in frequency. This way, the comb produced by the electro-optic setup is also frequency tunable since EOMs generally have a large working frequency bandwidth. For example, commercial EOMs designed for operations near 1.55 µm can easily be used between 1.53 and 1.60 µm, which sometimes depends more on the manufacturer. Moreover, the repetition rate of EOCs is also easily tunable since it is provided by an electrical waveform generator. Hence, the repetition rate can be easily tuned just by acting directly on the purely electronic devices. However, as already mentioned, this feature is restricted for setups that are not based on a cavity. Note that these two tunable features can be very interesting in several applications. Such a large flexibility in tunability cannot be offered by MLLs and even less by microresonators where the tunability is almost not possible.

3.3b. Repetition Frequency

We have seen that the repetition frequency of EOCs can be easily tuned, but another advantage of EOCs regarding the repetition frequency is their flexibility without

Figure 11

(a)   (b)   (c)

Fabry–Perot Cavity   Fibered Cavity   WGM resonator in Resonant Cavity
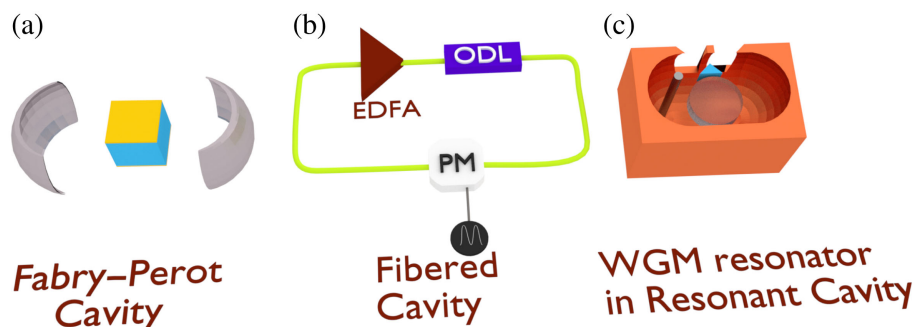
Schematic showing different setups based on an electro-optic cavity.

modifying the setup. Indeed, EOMs can generate an EOC with a linespacing that is almost equal to their electro-optic bandwidth, typically around 40 GHz for conventional and commercial EOMs. Thus, EOCs cover almost all repetition frequencies provided by other comb sources at the exception of microresonators that can go well beyond 100 GHz. Although limited by the electro-optic bandwidth, it is possible to increase the linespacing of EOCs. More precisely, with MZMs and polarization modulators driven by a sinusoidal RF voltage, by setting the proper working point of the EOM, only the odd-order or even-order modes of the comb can be generated, which increases the repetition frequency by a factor of 2. Up to now, we used the bias voltage to set the IM to its half-transmission point (the quadrature point), but setting the IM to another working point such as the zero transmission point can also be useful [85,86]. Indeed, by setting the bias voltage to $V_b = \frac{V_\pi}{2}$, using Eq. (26), the optical spectrum is given by

$$\tilde{A}(\omega) = A_0 \sum_{n=-\infty}^{\infty} J_{2n+1}(KV_0)\delta(\omega - (2n+1)\omega_m - \omega_c). \tag{31}$$

Consequently, the EOC generated with a MZM set at its zero transmission point has a repetition frequency of $2\omega_m$, and only the comb lines associated to the odd-order modes are generated. The same feature can be obtained at the maximum transmission point of the EOM: under the condition of a null bias voltage, still using Eq. (26), the optical spectrum is given by

$$\tilde{A}(\omega) = A_0 \sum_{n=-\infty}^{\infty} J_{2n}(KV_0)\delta(\omega - 2n\omega_m - \omega_c). \tag{32}$$

Hence, at its maximum transmission point, the MZM also generates a comb with a repetition frequency of $2\omega_m$, but here, only the even-order modes are generated. When setting the EOM at the zero or the maximum transmission point, one should be careful of the theoretical number of comb lines generated, which has to be divided by 2 when compared to the quadrature point, for instance. An example of EOCs, generated by a MZM in a push–pull mode at these particular transmission points, is presented in Fig. 12. Note that a theoretical study has generalized this approach with a setup based on $M \in \mathbb{N}^*$ PMs in parallel, with the MZM being the case where $M = 2$. Under proper conditions, an EOC has the potential to be generated with a repetition frequency up to M times the frequency fed to the PMs [87].

Figure 12
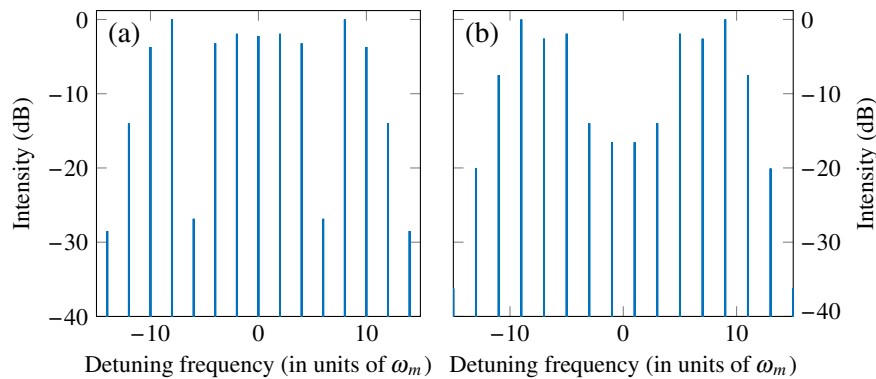
Simulated EOCs generated with a Mach–Zehnder modulator in a push–pull mode with $KV_0 = 10$. (a) For a null bias voltage only the even-order modes are generated, whereas (b) for a bias voltage set at $\frac{V_\pi}{2}$ only the odd-order modes are generated.

Nonlinear effects in optical fibers can also be used to increase the repetition frequency by amplifying only even harmonics of an initial EOC using modulation instability, as demonstrated theoretically and experimentally in Ref. [88]. These last experiments showed the generation of EOCs with a repetition frequency up to 80 GHz. Another example of the use of nonlinear effects for this aim is the Talbot effect combined with cross-phase modulation, which was experimentally demonstrated in Ref. [89] to be able to generate an EOC at 5 times the initial repetition frequency of 10 GHz.

3.3c. Spectral Flattening

Compared to other comb sources, EOMs have several degrees of freedom to shape the comb generated (shape of the RF signal, bias voltage, input polarization state, etc.), which can be used to obtain a comb with low intensity variations between the lines, and the theoretical ideal shape would be a pure flat-topped comb. This feature can find applications in spectroscopy or in the calibration of instruments (see Subsection 5.3). Two main possibilities are available to produce a flat-topped EOC. The first one is the use of a set of particular conditions that are fed to the EOMs, as described below. Whereas, the second way relies on the spectral broadening of the comb, which reshapes the spectrum. Here we will focus on the first possibility, and the second one will be described later after introducing the corresponding spectral broadening phenomenon. Note that further details on the spectral flattening of EOCs can be found in the review article [53], where some points on the subject have already been addressed.

Cascade of modulators. As already described in Subsection 3.2b, a common technique used to obtained a flat-topped EOC is the use of one or several PM(s) followed by an IM [48,52,90,91]. This technique is particularly interesting since it is independent of the repetition frequency, and it does not require any other optical components. However, as it can be observed in Fig. 13(a), which shows a numerical simulation of an EOC obtained in this configuration, the power fluctuation obtained by only cascading EOMs is of several dB. The flatness is still better than the comb presented in Fig. 8(b), where no IM was used. Similar results can be obtained only with PMs associated with a dispersive medium between two PMs [92,93]. In this case, the dispersive medium acts as a time-lens, and pulses are generated in the same way as when using an IM. This approach is a particular case of time-to-frequency conversion of flat-topped pulses [94]. Adding a dispersive medium between a PM and an IM can also lead to an increase of the flatness of an EOC [95]. Here, an optical fiber acts as a

Figure 13
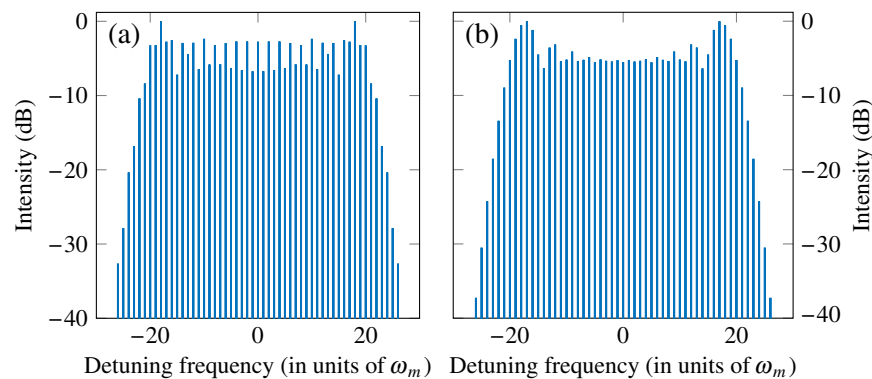
Numerical simulations of an EOC generation obtained when (a) an intensity modulator follows a phase modulator with $KV_0 = 20$ and (b) a DDMZM is used with the particular conditions $K_1 V_{0,1} - K_2 V_{0,2} = \frac{\pi}{2}$ and $K_1 V_{b,1} - K_2 V_{b,2} = \frac{\pi}{2}$ [42].

chirp stretcher, which transforms the phase profile towards a quasi-parabolic profile instead of a sinusoidal one within the time region where the IM will carve out pulses. Using this technique, a flatness with a power fluctuation of less than 1 dB can be achieved over the whole bandwidth of the comb [95].

Use of Mach–Zehnder modulators. Another approach for generating flat-topped EOCs is to use DDMZMs. Indeed, knowing the additional degrees of freedom available compared to other EOMs, it is possible to find a particular set of parameters regarding the amplitude of the RF voltages and the bias voltages, so that when both arms are combined, they become complementary in the intensity of each comb lines, and the output is a flat-topped EOC [41,42]. Figure 13(b) shows a numerical simulation of an EOC obtained with a DDMZM with $K_1 V_{0,1} - K_2 V_{0,2} = \frac{\pi}{2}$ and $K_1 V_{b,1} - K_2 V_{b,2} = \frac{\pi}{2}$ [42]. Other studies using several input CW lasers feeding a single DDMZM showed that a flat-topped EOC can be produced [45]. Note that the approach presented above can also be used for generating flat-topped combs when using MZMs in parallels [96–100].

Optimization of the RF signal. Another approach to produce a flat-topped EOC is to use a RF signal that is not purely sinusoidal. Since electronic components can easily allow the generation and shaping of RF waveforms, this solution shows a certain ease of doing compared to pure optical methods. In general, the used RF signals are not highly different from pure sinusoidal signals, and only small changes are made. The combination of a sinusoidal signal with its second harmonic is one of the main approaches. It can be applied either on a particular EOM in the setup [51,101], or to the different arms of a DDMZM [44]. This approach is motivated by the fact that under proper amplitudes and phase shifts, the phase applied by electro-optic modulation is quadratic, leading to a linear chirp and thus to a flat-topped spectrum. Studies on high-order harmonics have also been performed [102,103].

In what concerns the optimization of the RF signal, it has been demonstrated that a small frequency offset applied to a particular EOM could flatten the spectrum [104]. Finally, it was demonstrated that ultra-flat-topped EOCs can be generated using an optimized bit sequence on an EOM [105,106].

Generation of Nyquist pulses. Flat-topped EOCs can be obtained by generating Nyquist pulses using EOMs, and especially cardinal sine pulses. Indeed, the FT of such pulses is a rectangular function, which gives a natural approach to generate flat-topped EOCs. Most of the methods for cardinal sine pulses generation are based on MZMs driven with particular RF signals, which mix several aspects introduced above. One of the common ways is to use two MZMs in series [107–110], and the rectangular-shaped spectrum is obtained by applying particular RF signals and bias voltages, sometimes together with an optical treatment between the MZMs [109,110]. All required parameters highly depend on the setup used, but some theoretical studies can be found regarding this point (see in particular the Methods section of Ref. [107]). Besides two MZMs in series, other setups have been proposed based on a dual-parallel MZM [111] or a single DDMZM [112], for instance.

4. ELECTRO-OPTIC MODULATOR LIMITATIONS AND BYPASSING METHODS

In the previous part, we presented the generation of EOCs and their advantages when compared to other comb sources. However, we relatively stayed in the theoretical surroundings, and most of the experimental reality of EOMs has not been discussed. Indeed, some characteristics related to EOMs are not as perfect as they could be in theory due to limitations in their conception, for instance. Here, the main limits of

generating EOCs will be presented starting by several intrinsic characteristics of EOMs. The next part will deal with a pure experimental limitation in EOC generation, which is the accumulation of the phase noise and how this problem can be managed. Finally, several ways will be proposed to improve one of the main drawback of EOCs, namely their limited spectral bandwidth.

4.1. Modulator Intrinsic Characteristics

As mentioned above, the experimental reality of EOMs makes EOCs slightly different from what can be expected from theory. In particular, several characteristics of EOMs need to be taken into account for a more accurate description of EOCs. These characteristics, which generally lead to limitations, will be introduced here starting with the drawbacks associated to the conception of EOMs. After that, we will discuss the limitations due to the operating wavelength of EOMs.

4.1a. Drawbacks Due to Imperfections

Extinction ratio. One of the main drawbacks regarding nonperfect MZMs is the finite extinction ratio (ER), which can affect the quality of IMs. The ER is related to the residual power coming from the CW laser that is not modulated. This characteristic is due to the fact that a MZM always has imbalances between its arms and even the smallest asymmetry leads to a finite ER. For instance, the Y-junctions of the MZM are not perfectly 50/50 dividers, which creates asymmetries. In the temporal domain, a finite ER leads to a CW background that can be detrimental. If P_p is the maximum peak power of the pulse modulated and P_b the power of the CW residual background, then one can define the ER τ_{ER}, such as

$$\tau_{\mathrm{ER}} = \frac{P_p + P_b}{P_b}. \qquad \textbf{(33)}$$

Standard IMs possess a typical ER of 20 dB. A value of 30 to 40 dB is achievable, but the EOM needs a bias voltage that is well controlled. Indeed, the bias voltage, apart from setting the EOM to a given point of modulation, also helps to reach a balance of the MZM by inducing a phase that compensates the asymmetries. Consequently, any drift of the bias voltage from its optimum point due, for example, to temperature variations, will cause the ER to decrease.

Regarding the EOC generation, a finite ER leads to the presence of a powerful central component. A low finite ER is especially detrimental for spectral broadening as it will be shown in Subsection 4.3a. Moreover, a low ER has the drawback of lowering the energy in the generated pulse and thus its peak power. Note that the CW background can be reduced by cascading two or more IMs, which increases the overall ER of the setup.

Residual amplitude modulation. Residual amplitude modulation is a limitation of imperfect PMs due to an unwanted amplitude modulation of the laser [113,114]. Residual amplitude modulation can arise from several physical effects such as an electro-optic crystal that is inappropriately designed or an optical injection of the laser that is not optimized [115,116]. Regarding the shape of the EOC, residual amplitude modulation induces an imbalance in the amplitude of the lines [115], but also a noise that can be detrimental, as it will be seen later [116–118].

4.1b. Operating Wavelengths

Nowadays, commercially available EOMs are mainly based on $LiNbO_3$, which has a transparency window from the visible to around 5 μm. However, for efficient electro-optic modulation, modulators have to be optimized in their design (waveguides, cutting, etc.), which restricts their operating wavelength to a given spectral region.

Although a given EOM could operate outside its assigned spectral range, it will not be optimized for this operating region, and its efficiency will decrease (a higher V_π voltage could be needed, the ER could be lower, etc). This drawback means that for generating an EOC at a given wavelength, the EOM must be designed accordingly. Commercially available EOMs do not possess a full range of operating central wavelengths, and since EOMs were at first a design for telecommunication applications, the available central wavelengths are indexed on optical telecommunication bands and especially in the near-infrared (NIR). Therefore, one can find EOMs in the first telecommunication window around 900 nm, in the O-band around 1300 nm, in the $C + L$ band around 1550 nm, and around 2000 nm.

As we have discussed above, the electro-optic effect decreases according to the inverse of the wavelength λ; thus, it is more difficult to obtain efficient EOMs working at high wavelengths such as in the mid-infrared (MIR). However, studies based on other materials than $LiNbO_3$ have been reported for MIR operating EOMs such as using Si-on-$LiNbO_3$ [119], or black phosphorus [120]. Note that wavelengths for which EOMs are not especially designed can be reached by nonlinear frequency conversion of an EOC after its generation. For instance, crystals or waveguides can be used for harmonic generation, which can lead to EOCs operating in the visible domain [121–124]. Wave mixing phenomena can generate instead EOCs in the 2 μm region [125], or in the MIR [126–128]. The nonlinear frequency conversion processes of EOCs will be further investigated in Subsection 4.3b.

4.2. Noise Sources

In all physical setups, different sources of noise can be detrimental for the stability of the system but also for the feasibility of potential applications. This is especially true for OFC generation that requires a low phase noise. Indeed, since a comb is the result of the interference between a set of pulses, if the pulses possess too large random phase contribution, i.e., a high phase noise, then the spectrum cannot reveal the shape of a comb. To be more precise, any source of noise will restrain the comb from acquiring an ideal set of Dirac structure: the more important the noise is, the more the lines of the comb will be broadened [8,19].

To observe this in a mathematical context, let us take Eq. (1), where we considered an ideal pulse train without any source of noise. The form of the pulse train in this equation can be modified to take into account several sources of noise that are time-dependent such as amplitude noise ΔA_0, phase noise ψ, or noise in the repetition rate $\Delta \tau$ (also called timing jitter). By performing the changes in Eq. (1), the form of the pulse train becomes

$$f(t) = \sum_{n=-\infty}^{\infty} ((A_0 + \Delta A_0(t))a(t)\cos(\omega_c t - n\varphi)) * \delta(t + n\tau + \Delta\tau(t)))e^{i\psi(t)}, \quad \textbf{(34)}$$

where a is the normalized pulse envelope function defined without amplitude noise such as $A(t) = A_0 a(t)$. In conventional MLLs, all these sources of noise have to be taken into account [8,19]. In EOC generation, noises have different origins compared to MLLs, and the phase noise is particularly the main issue. As a matter of fact, although studies were performed also on the timing jitter of EOCs [129,130], in the following, we will only deal with the phase noise. Generalities on noises related to OFCs can be found in Ref. [19].

When only the phase noise is taken into account, the previous equation can be simplified to

$$f(t) = \sum_{n=-\infty}^{\infty} ((A(t)\cos(\omega_c t - n\varphi)) * \delta(t + n\tau))e^{i\psi(t)}. \tag{35}$$

In this case, we can obtain the optical power spectrum S such as demonstrated in Ref. [8],

$$S(\omega) = \frac{|\tilde{A}(\omega - \omega_c)|^2}{\tau^2} \sum_{n=-\infty}^{\infty} \frac{2\Delta\omega_l}{(\omega - \omega_n)^2 + \Delta\omega_l}, \tag{36}$$

where $\Delta\omega_l$ is the width of a line of the comb related to ψ and $\omega_n = n\omega_r + \omega_0$ as previously defined. Consequently, the comb deviates from a pure Dirac structure, and it shows a set of Lorentzian lines. This feature can be particularly detrimental if spectral broadening of the comb is considered since the new generated comb lines will see their linewidth increased with respect to the index line number [131]. If the broadening of the lines becomes too important, i.e., if there is too much phase noise accumulated on the new generated comb lines, then the comb will lose its structure. In the present part, this phenomenon will be investigated in the particular case of EOCs. This will lead to the methods that can be used to avoid the phase noise accumulation problem.

4.2a. Phase Noise Origin

To bring to light how the phase noise influences the structure of an EOC, let us take again a PM that is fed by a voltage $V(t) = V_0 \sin(\omega_m t + \psi)$, where ψ is a static phase noise coming from the RF oscillator. Using Eq. (15), the output spectrum of the EOM is now given by

$$\tilde{A}(\omega) = A_0 \sum_{n=-\infty}^{\infty} J_n(KV_0)e^{in\psi}\delta(\omega - n\omega_m - \omega_c). \tag{37}$$

This last equation shows that the nth line has a $n\psi$ phase. Such a simple example shows the main problem of the phase noise coming from the RF oscillator, which is the accumulation of the noise on the generated lines: it increases linearly with the index line number. We considered above a static phase noise, but if we consider instead a low amplitude time-dependent phase noise ψ, which allows us to approximate $e^{in\psi(t)} \approx (1 + in\psi(t))$, the output spectrum can be written as

$$\tilde{A}(\omega) = A_0 \sum_{n=-\infty}^{\infty} J_n(KV_0)(\delta(\omega) + in\tilde{\psi}(\omega)) * \delta(\omega - n\omega_m - \omega_c), \tag{38}$$

where $\tilde{\psi}(\omega) = \mathrm{FT}(\psi(t))$. Similarly to the case of a static noise, this last equation shows that the phase of a comb line increases linearly with the index line number and proportionally to the spectrum of the phase noise of the RF oscillator. Moreover, by taking into account higher-order terms in the expansion of $e^{in\psi(t)}$, one can note that the amplitude of the comb lines can also be affected by the phase noise. As already mentioned in the introduction, the accumulation of the phase noise can be problematic, especially if the integrated phase noise of each spectral line exceeds π radian. In this case, the first-order coherence of the comb will degrade as n^2, and the comb will loose its structure [132,133]. Figure 14 illustrates the problem of the phase noise accumulation.

The problem of the phase noise accumulation for EOC generation has been put into light theoretically by Ishizawa *et al.*, and measurements of the integrated phase noise

have been performed to observe this phenomenon [134]. The experiments clearly showed that different RF oscillators lead to a different linear accumulation of the phase noise with respect to the line number. Other studies, where the phase of the comb lines has been directly recorded, were performed to put in evidence the phase noise accumulation, and the results are coherent with the previous ones [135].

The particular characteristic of phase noise accumulation can be detrimental if spectral broadening of the comb is considered. Indeed, EOCs possess a much smaller bandwidth compared to OFCs obtained with conventional sources, so spectral broadening EOCs might be required (this will be further discussed in Subsection 4.3a). However, for an efficient spectral broadening, the phase noise has to be considered and managed so that its accumulation on the new created lines does not deteriorate the coherence of the pulse train and, thus, the structure of the comb. Figure 15 shows an example of spectral broadening in a highly nonlinear fiber (HNLF) of an OFC generated with an IM driven by a RF oscillator possessing either a high or a low RF noise. We can observe that with a high RF noise [Figs. 15(a) and 15(c)], the comb structure is not uniform over the whole optical bandwidth, whereas with a low RF noise [Figs. 15(b) and 15(d)], lines can be observed over the whole spectrum. From this simple experiment, it is clear that the phase noise plays an important role for spectral broadening. Consequently, controlling and reducing the phase noise of an EOC is a real issue that we will now investigate to see which techniques can be used to handle it.

4.2b. Phase Noise Reduction

Reduction of the phase noise over the whole bandwidth of an EOC can be performed using different techniques. As shown in Fig. 15, the first and the most intuitive way is to use RF components that have an ultralow phase noise. This approach can be enough for several applications, and it has the advantage of keeping the setup simple. Note, however, that even the most perfect RF components have a noise that can be detrimental [132]. With the same idea, using a CW laser with an ultrahigh coherence (i.e., with the lowest spectral linewidth possible) will make the generated EOC with a low phase noise. But, as for the RF components, even the most perfect CW laser has a phase noise that can be detrimental.

The next step towards phase noise reduction is generally the use of a feedback technique on the EOC generation. Watts *et al.* were able to reduce the noise of a 16-line

Figure 14
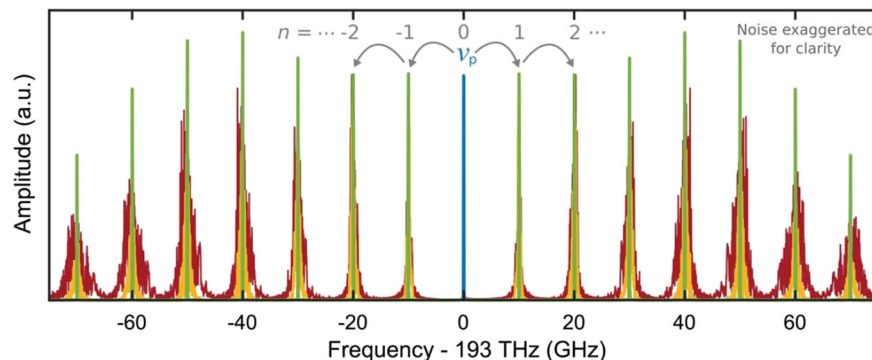
Schematic showing the phase noise accumulation on high-order sidebands of an EOC (red) compared to a filtered comb (yellow) but also to an ideal stabilized comb (green). From Carlson *et al.*, Science **361**, 1358–1363 (2018) [133]. Reprinted with permission from AAAS.

EOC allowing them to decrease their linewidth from around 20 MHz to almost below 100 kHz for the entire comb [136]. The idea behind this particular feedback technique is to measure the phase noise of a single line and to apply over the entire comb a signal that is the inverse of the previous measurement, which compensates the original noise. With the same idea, another feedback approach was used in Ref. [137]. Ishizawa *et al.* used a MLL whose output comb is referenced to a frequency standard providing narrow lines compared to an EOC. When the MLL is combined with the EOC, interference signals are recorded, compared to a reference, and fed back to the self-adjusted RF generator of the EOC, thus compensating the increasing of the phase noise with the line number. A similar approach of phase locking between several lines of an EOC and a MLL is demonstrated in Ref. [138].

Further phase noise reduction can be investigated using a Fabry–Perot cavity as a comb line filter. We mentioned earlier that electro-optic cavities based on a Fabry–Perot configuration could help with avoiding some accumulation of the phase noise [72]. This is due to the transfer function of the cavity, which has a comb shape with Lorentzian lines of a few MHz linewidth (also called an Airy distribution [139]). Thus, by matching the free spectral range of the cavity and the repetition rate of the EOM, the cavity can be used as a powerful line-by-line filter. A Fabry–Perot cavity, when not exploited in an electro-optic cavity, is usually used after a spectral broadening stage and thus after the EOC generation [58,132,133]. The aim is to provide a comb with a reduced phase noise [see Fig. 14 (yellow comb)] that can be spectrally broadened a second time without loosing the comb structure. Note that a Fabry–Perot cavity can also be used to stabilize the CW laser using a Pound–Drever–Hall locking scheme, which reduces its linewidth and thus increases its coherence [91,140].

Figure 15
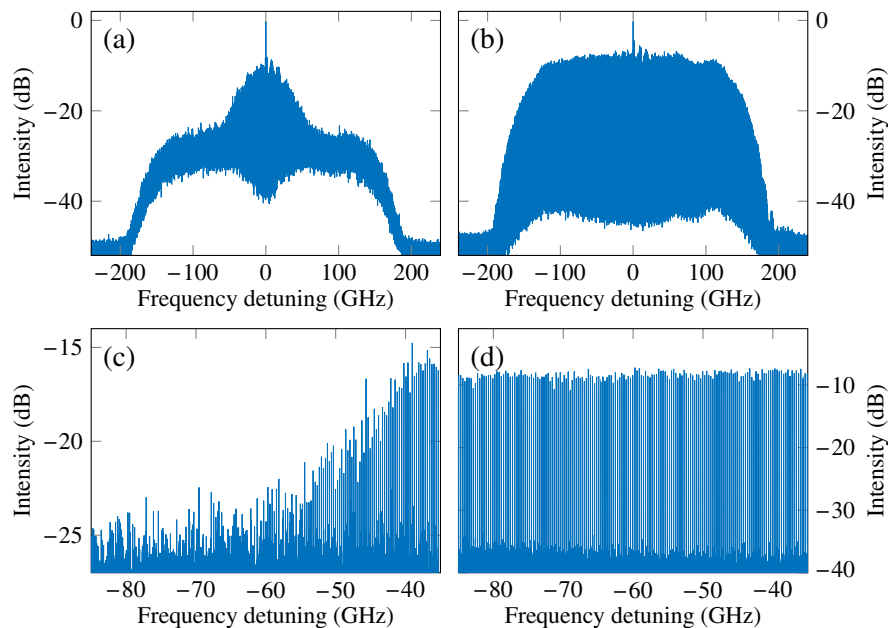
Optical spectrum recorded with a resolution of 5 MHz showing the spectral broadening of an input comb generated by an intensity modulator with (a) a high and (b) a low RF noise source. (c) and (d) are, respectively, zooms of (a) and (b) showing the output comb structure and its limitations. The powerful central component observable in (a) and (b) is the result of using an intensity modulator with a finite extinction ratio of 35 dB.

4.3. Spectral Properties

Compared to MLLs, EOMs can produce at maximum only a few hundreds of GHz wide optical spectra, which is one of the main drawbacks of these combs. Though it is possible to increase the bandwidth of EOCs by implementing EOMs within a cavity, disadvantages can arise from the required enslavements and from the repetition rate fixed by the design. Lots of studies have been performed to increase the bandwidth of EOCs without cavities. As already seen, another possibility is to cascade EOMs and more particularly several PMs plus an IM, with the IM being used to flatten the spectrum by keeping the linearly chirped part of the modulated light. Even though the widths available are still very narrow compared to common comb sources, since the pulses are linearly chirped, they can be second-order dispersion compensated using fibers, gratings, or spectral shaping [141]. This can lead to short pulse generation well below the capabilities of EOMs, which is also favorable to a possible further spectral broadening [142].

4.3a. Spectral Broadening

Cascading EOMs to increase the bandwidth of EOCs is a solution that is not convenient for obtaining large spectra since it would require too many EOMs, thus increasing the cost and the complexity of the setup. A different approach used for the same goal is to broaden the EOC in nonlinear materials. In the following, we will see the ways of broadening EOCs with and without taking care of the phase noise accumulation problem.

Direct broadening. The most common way of broadening EOCs is by using nonlinear effects in optical fibers or waveguides [24]. Here we take advantage of the all-fibered feature of EOMs, which avoids the complexity of spatial alignment and injection in the nonlinear material. Regarding the fibers, HNLFs operating in the normal dispersion regime are generally used in order to avoid detrimental effects such as modulation instability that could dramatically decrease the coherence of the pulse train [143]. Indeed, in the anomalous dispersion regime, modulation instability is known to exponentially amplify noises in a bandwidth close to the pump source [24]. Thus, operating in the normal dispersion regime can avoid this effect. Depending on the soliton number N, the broadening can be made by self-phase modulation or dispersive shock waves when the dispersion coefficient is relatively high [24]. Let us recall that the soliton number N is defined as $N^2 = \gamma P_0 |\beta_2|^{-1} \delta_0^2$, where γ is the Kerr coefficient, β_2 is the second-order dispersion parameter, P_0 is the input peak power, and δ_0 is the e^{-1} temporal half-width at half-maximum in intensity. Consequently, to obtain a large spectral broadening, pulses have to be generated to obtain a high peak power. Thus, the common setup used to generate an EOC is several PMs plus an IM. The output is then second-order dispersion compensated to obtain short pulses (below 1 ps) that can be amplified.

A number of studies have been reported on EOC spectral broadening in nonlinear fibers [49,54,85,144–148], and some works even present the use of several HNLFs [149,150]. The results lead to very diverse outputs from a few tens of nanometers to almost an octave spanning EOC, especially when using an ultralow noise generator and referencing the different elements of the setup to a frequency standard. In this case, EOCs can be broadened up to several hundreds of nanometers, and an example of used setup is presented in Fig. 16 [151]. Further broadening becomes very close to supercontinuum generation and is harder to generate without loosing the comb structure. Scrambling of the comb structure can only be avoided by limiting the phase noise accumulation.

Direct spectral broadening can also be performed using the features of nonlinear optical loop mirrors (NOLM) and/or nonlinear amplified loop mirrors (NALM) [152,153]. A schematic of such devices is illustrated in Fig. 17. Commonly used in telecommunications, NOLMs and NALMs are nonlinear devices that can shape the temporal and spectral profile of pulses using particular HNLF characteristics, amplifier gain, coupler ratio, etc. For example, NOLMs can help to reduce the power of the CW background or parasite lobes of pulses, which can be particularly interesting for EOC generation [154,155]. Moreover, spectral broadening occurs within the loop, and the shape of the spectrum can be tuned using the same degree of freedom, as listed above. Compared to a direct injection into a HNLF, the additional degrees of freedom of NOLMs and NALMs facilitate the spectral shaping of EOCs but at the expense of a greater complexity of the devices. Moreover, NOLMs and NALMs are known to be highly polarization-dependent, which makes the setup highly sensitive to the environment [154].

Noise compensation. As shown previously, phase noise compensation becomes essential for large and efficient spectral broadening. Setups that take into account the phase noise accumulation limitation have already been presented in Subsection 4.2b, and thus here, we will only focus on the part associated to the broadening of EOCs.

Phase noise compensation for EOC spectral broadening is generally used to obtain a comb that spans over an octave enabling self-referencing. Due to the complex setups needed, only a few demonstrations of such broadenings have been performed.

Figure 16
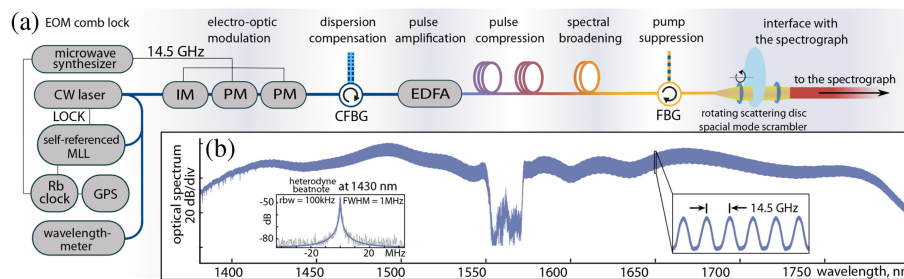
MLL, mode-locked laser; IM, intensity modulator; PM, phase modulator; CFBG, chirped fiber-Bragg grating; EDFA, erbium-doped fiber amplifier; FBG, fiber Bragg grating. Figure showing (a) an example of setup used for spectral broadening an electro-optic comb over several hundreds of nanometers and (b) the spectrum obtained. Reprinted with permission from Obrzud *et al.*, Opt. Express **26**, 34830–34841 (2018) [151]. Copyright 2018 Optical Society of America.

Figure 17
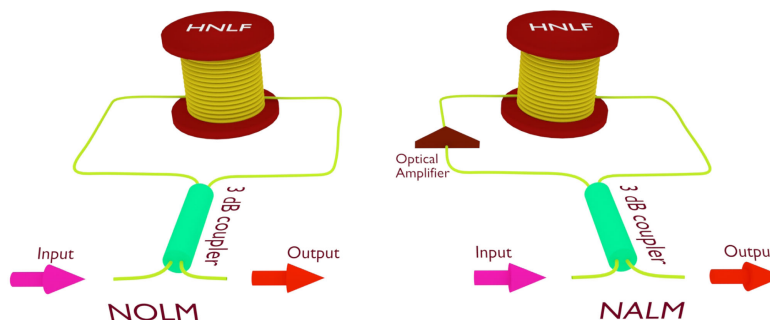
Schematic showing a nonlinear optical loop mirror and a nonlinear amplified loop mirror.

These broadenings are generally made in a two stage mechanism: the first stage is a standard nonlinear broadening in a HNLF with low dispersion, thus resulting in a pure self-phase modulated spectrum that spans over a few tens of nanometers. In the second stage, phase noise accumulated in the first stage is removed using a Fabry–Perot cavity, as already seen above. Note that a Fabry–Perot cavity can be used before the first nonlinear broadening stage [156]. Pulses are then chirp compensated to produce powerful short pulses. The second stage of nonlinear broadening can be made in a set of optical fibers with particular characteristics [58,132], or in a waveguide [133,157,158]. Figure 18 shows an example of spectral broadening that can be obtained in a silicon-nitride waveguide for an EOC of 30 GHz linespacing. Note that other type of architectures can be found based on an optical-pulse-synthesizer with a spectral broadening made on a single stage but with a succession of HNLFs [59].

4.3b. Spectral Extension

Phase noise accumulation is problematic to obtain a large spectral broadening, and a complex setup is needed to solve the problem [133]. However, extending the comb working range can also be performed by parametric conversion for targeting a particular spectral window. In this case, the comb is not broadened, but it acquires an extension in a spectral region well distinct from the original comb bandwidth. To avoid ambiguities, we choose to name these techniques *spectral extension* techniques. Spectral extension can be particularly suitable for generating combs in a spectral region with a far frequency detuning from the initial comb. Indeed, far frequency detunings would have to be obtained with a broadening close to supercontinuum generation, and the initial comb would thus need an extremely low noise to keep the comb structure [133]. To avoid these kinds of complexities, several studies have been realized to extend the working range of electro-optic setups by converting the bandwidth of the comb into the desired working range using parametric conversion. Several nonlinear effects can be used for spectral extension, which will be discussed in the following.

Harmonic generation. The first approach to extend an EOC is to use harmonic generation in a crystal. This is a frequency upconversion technique mostly used to reach the visible domain. For instance, second-harmonic generation, which is a $\chi^{(2)}$ nonlinear effect, can be performed using a standard crystal such as a beta-barium borate

Figure 18
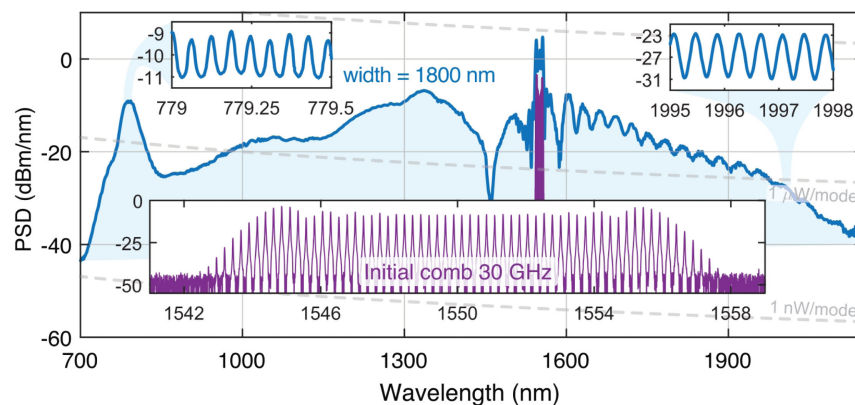
Example of spectral broadening obtained in a $w = 1800$ nm wide silicon nitride waveguide of a 30 GHz comb with a compensated phase noise. The above insets show that a comb structure is observable over the whole bandwidth of the spectrum. From Carlson *et al.*, Science **361**, 1358–1363 (2018) [133]. Reprinted with permission from AAAS.

[123], or a periodic poled lithium niobate (PPLN) crystal [121,122]. In the second case, only a quasi-phase-matching is available, and thus the intensity of the second harmonic increases linearly with the length of the crystal. If a sufficient power is available and if the crystal is well-designed, high-order harmonics might be generated using high-order nonlinear effects such as $\chi^{(3)}$ or $\chi^{(4)}$, which was experimentally demonstrated up to the fourth harmonic [121]. When the nth harmonic is generated, the comb will possess a bandwidth that is n times the bandwidth of the initial comb. Note that waveguides can also be used for harmonic generation such as the third harmonic [124]. In either case, an efficient spatial coupling is required, and the all-fibered characteristic of the setup is generally lost. Figure 19(a) shows the principle of spectral extension by harmonic generation.

Difference frequency generation. Other $\chi^{(2)}$ nonlinear effects can be used for spectral extension of EOCs such as difference frequency generation (DFG). A CW laser of frequency ν_p acts as a pump, and an EOC of central frequency ν_i acts as an idler. By DFG, a signal at frequency ν_s can be created according to the relation $\nu_p - \nu_i \rightarrow \nu_s$. Figure 19(b) shows the principle of spectral extension by DFG. DFG can be performed using standard crystals, but a certain flexibility is obtained when using PPLN crystals. In this case, signals can be generated up to 5 μm (the limit of the transparency window of $LiNbO_3$), but the main drawback is the need of using a powerful and often costly CW pump laser.

DFG used for spectral extension of EOCs with PPLN crystals has been reported especially for reaching the MIR. An EOC generated around 1550 nm combined with a powerful CW laser at 1064 nm can lead to a spectral extension around 3.3 μm [126,127]. The 3 μm spectral region can also be reached by DFG with an EOC generated around 1050 nm combined with a CW laser around 800 nm [128]. These works will be further discussed in the application part of the paper in Section 5.

Four-wave mixing in optical fibers. As mentioned above, the use of crystals for parametric conversion generally leads to the loss of the all-fibered characteristic of the setup. However, it is possible to use a $\chi^{(3)}$ nonlinear effect in an optical fiber to

Figure 19
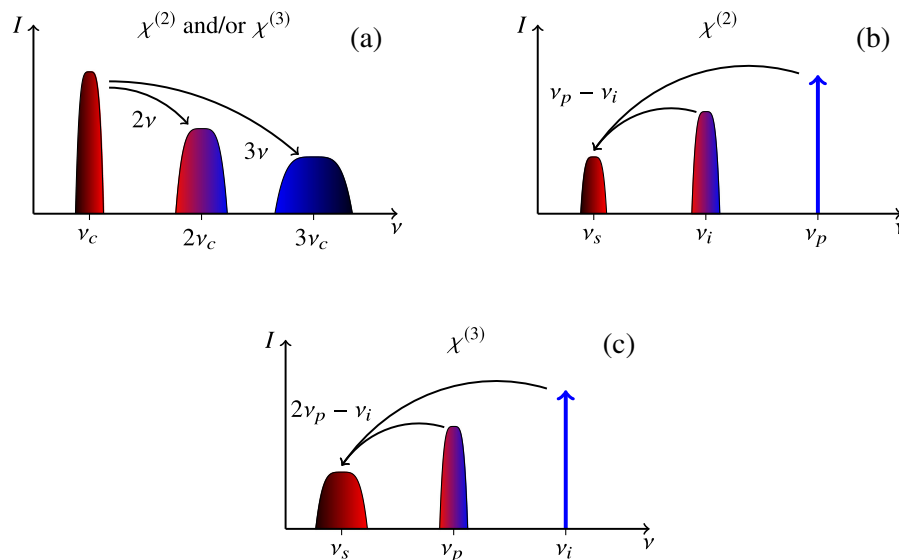
Schematic showing the different possibilities to spectrally extend the bandwidth of a comb using nonlinear effects. (a) Harmonic generation, (b) difference frequency generation, and (c) degenerate four-wave mixing.

spectrally extend the bandwidth of EOCs, which bypasses the problem. Here the parametric conversion is usually done with a degenerate FWM phenomenon, which is also called modulation instability [24], where an EOC of central frequency ν_p acts as a pump and a CW laser of frequency ν_i acts as an idler wave. When pump and idler waves are mixed with the proper phase matching conditions especially given by the fiber parameters, a signal of frequency ν_s can be created satisfying the relation $2\nu_p - \nu_i \rightarrow \nu_s$. In this case and compared to DFG, the signal created by degenerate FWM will possess a bandwidth that is twice the initial bandwidth of the comb. Figure 19(c) shows the principle of spectral extension by FWM. Note that the idler wave can also be a second EOC and that the generated comb can also be extended [159,160]. Note also that FWM for the spectral extension of an EOC was demonstrated in a waveguide [161]. Finally, it was recently experimentally demonstrated that the spectral extension of an EOC can be performed over a large frequency detuning of 40 THz starting with an EOC around 1550 nm and a CW laser around 1310 nm to create a signal around 2000 nm [125]. However, with such spectral extension, the fiber has to be carefully engineered to provide an exploitable comb without the need of amplifying the signal.

4.3c. Spectral Flattening

Spectral broadening of a comb can be accompanied with a spectral flattening of the comb, which can be a desired feature, as described in Subsection 3.3c. Here, we point out the effects that lead to the flattening of the spectrum by spectral broadening. Note that spectral extension can also be accompanied by a spectral flattening feature [159]. Since Ref. [53] has already presented some of the following results, we will be succinct on these points.

Dispersive shock waves. As already seen in the previous part, spectral broadening is more efficient in the normal dispersion regime and can be made by dispersive shock waves [24]. Besides avoiding certain detrimental effects such as modulation instability, this method has the advantage of flattening the spectrum [55,162–165]. This feature can be observed in Figs. 15(b) and 15(d), where the spectral broadening of an input cardinal sine spectrum was made by dispersive shock waves leading to a flat-topped output comb. Note that the flattening has the advantage of being independent of the shape of the input pulses [165].

Nonlinear loop mirrors. In the previous part, we have seen that spectral broadening can be performed using NOLMs/NALMs. These nonlinear devices can also be used to shape the spectrum, which can be particularly interesting for spectral flattening. Several experimental demonstrations have been made for this particular application, and highly flat EOCs can be obtained over a few nanometers up to more than a hundred of nanometers [146,155,166,167]. Here, loop mirrors are used as a nonlinear pulse shaper to obtain flat-topped pulses with a quadratic phase (and so a linear chirp) giving a flat-topped EOC. This can be achieved with a setup that is well-designed using optical fibers with particular parameters. However, the setup used is dependent of the repetition frequency, which limits its use [155].

Although EOCs possess some limitations, several ways to overcome those issues have been presented in this part, which explains why the EOC topic has exponentially grown in the recent years.

5. APPLICATIONS OF ELECTRO-OPTIC FREQUENCY COMBS

OFCs first revealed their potential in frequency metrology [5], but lots of other applications have been developed afterwards. In this part, we present the applications

where EOCs have shown particular interests. We start with the spectroscopic applications since some concepts often used in this field can be applied in other fields. This will lead us to other interferometric applications that are based on two mutually coherent EOCs such as distance measurements or optical imaging. After that, spectroscopic applications will be discussed again, but through the calibration of spectrographs using EOCs. This will introduce the more fundamental applications of EOCs that we will extend to the spectral shaping of EOCs for arbitrary waveform generation. Finally, the applications for RF photonics and telecommunications will be discussed.

5.1. Spectroscopy

OFCs can be very appealing for use in spectroscopy since all the frequencies of the comb can be known with an extreme accuracy. For instance, in the case of absorption spectroscopy, the central wavelength of an absorption line can be measured with a resolution that is equal to the linespacing of the comb. Given that EOMs can provide low repetition frequencies, high resolution spectroscopy can be considered with EOCs. On the contrary, high repetition frequencies can also be achieved, which is well-adapted to liquid phase spectroscopy instead. In this part, we present the use of EOCs for spectroscopic applications. One can split these studies in two distinct parts: a spectroscopy made using a single comb and spectroscopy made using two mutually coherent combs, which is a powerful and smart technique. With both techniques, heterodyne measurements have to be performed since resolving the comb lines with a spectrometer or an optical spectrum analyzer is generally very difficult. Indeed, this equipment rarely possesses a resolution sufficient enough to resolve the lines of the comb, which prohibits the direct use of the comb structure.

5.1a. Single Comb Spectroscopy

Using a single comb for spectroscopic applications is the easiest solution, especially for linear spectroscopy, which we will consider here. The choice of EOCs for single comb spectroscopy relies on the possibility of easily getting a low linespacing (kHz or MHz) and thus a very high resolution. Although MLLs can provide such repetition rates, they are more bulky and usually free space, and they are not easily tunable regarding their repetition frequency and their central wavelength, which can be disadvantageous. Indeed, single comb spectroscopy has a need for a particular line of the comb to be resonant with the atomic transition investigated. Thus, EOCs possess certain advantages here, and a low repetition frequency can be used to probe fine and hyperfine atomic transitions, which are associated to low frequency differences between energy levels.

Several works showed the use of EOCs for atomic spectroscopy [168–172]. In these studies, a CW is split in two arms, where one of them feeds a PM driven by an arbitrary/pseudorandom waveform generator. The result is an EOC that spans over a few GHz with a linespacing that can be of a few thousands of kHz [170,171], or a few MHz [168,169,172]. In these setups, either the EOC or the second arm of the initial CW laser is frequency shifted using an acousto-optic modulator. In both cases, the CW laser will be used as a local oscillator for heterodyne measurements, and in parallel, the EOC is directed towards a gas cell, and the output is combined with the local oscillator. The beatnote between each line of the comb and the local oscillator gives rise to a signal in the RF domain, which possesses the information on the absorption of the gas. Note that in this configuration, the bandwidth of the comb has to be smaller than the bandwidth of the detector to resolve all the beatnotes in the RF domain. Moreover, since the width of the comb is of a few GHz, this technique is generally restricted to the study of a few transitions that have to be rather narrow.
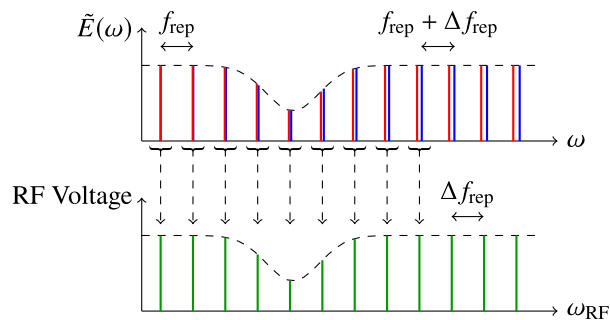
5.1b. *Dual-Comb Spectroscopy*

More recently, another approach has emerged to perform spectroscopy: the so-called *dual-comb spectroscopy* (DCS) technique [173,174]. DCS is also a heterodyne technique but with the use of a second comb instead of a CW laser, as it is in the case of single comb spectroscopy. Indeed, heterodyne measurements with a CW laser cannot be performed if the comb source is too wide since detectors and analyzers rarely possess a bandwidth exceeding 100 GHz. Thus, other techniques have to be investigated for spectroscopy on wider scales such as DCS.

The principle is the following: two mutually coherent OFCs with a slightly different repetition frequency Δf_{rep} can interfere and produce a third comb in the RF domain with a Δf_{rep} linespacing. If at least one comb is partially absorbed by a sample before interfering, then the absorption lines are also visible in the RF domain. Moreover, the dispersion spectrum can also be retrieved if only one comb experiences the absorption. The combination of the absorption and the dispersion spectrum is called the *complex spectrum*. Figure 20 presents a schematic showing the principles of the DCS technique.

The dual-comb technique is very popular since it allows real-time measurements and lets all the advantages of OFCs enter the spectroscopic field: it overcomes the fact that combs with a low repetition frequency cannot be resolved when using a spectrometer or an optical spectrum analyzer by transposing the combs in a domain much easier to analyze. However, the technique is usually known as complex to implement since there is a need of mutual coherence between two combs. When the combs are generated by two different laser sources, the mutual coherence has to be obtained by enslavement of the lasers, which can be cumbersome [175,176].

The dual-comb technique becomes more simple when using EOCs: since an EOC originates from the modulation of a CW laser, two mutually coherent OFCs can easily be generated by splitting in two arms the initial CW laser and by placing equivalent EOMs in both arms. The only difference between the combs must be the repetition frequency that has to be Δf_{rep} slightly different. This can easily be done since the repetition rate is set by a waveform generator, which allows a precise tuning of the repetition frequency by simply dialing a knob. When designed this way, the mutual coherence is intrinsic to the setup, and no operation of enslavement is required. The setup is therefore qualified as being in a *free-running mode* since the combs are

Figure 20

Principles of dual-comb spectroscopy: two mutually coherent optical frequency combs (red and blue) with a slightly different repetition rate can interfere, which creates a third comb (green) in the radio frequency domain. If at least one comb experiences an absorption (dashed lines), the radio frequency comb will also present this signature.

generally not referenced, except if the frequency of the initial CW laser is measured [174].

Several setups based on EOMs have been demonstrated for DCS, and a typical example of a dual-comb setup based on EOMs is presented in Fig. 21. In the following, we describe them according to their overall design complexity.

Using two modulators. The most simple setup for DCS with EOMs is realized when only one EOM is placed in each arm of the spectrometer. The setup has to be designed in relation with the sample under study. For instance, a gas at ambient temperature and pressure presents absorption lines of the order of 10 GHz full width at half-maximum, whereas a liquid presents wider absorption lines. Thus, the linespacing of the combs has to be chosen according to the experiment.

The first demonstration of DCS using only two EOMs was made by Long *et al.* using DDMZMs [177]. The authors succeeded in recording the complex spectrum of a particular line of CO_2 at a repetition frequency of 200 MHz. Further works using DDMZMs have shown possibilities to improve the precision of the setup [178,179]. In parallel, pure PMs were used in setups for absorption spectroscopy [180–182] or dispersion spectroscopy [183] with a bandwidth around a few tens of GHz and repetition frequencies ranging from 100 MHz to 500 MHz. Spectroscopy with a resolution of 20 MHz was also demonstrated by driving the PMs with optimized pseudo-random binary sequences [184]. Since the comb bandwidth generated by these setups is relatively small, single gas spectroscopy is generally limited to the probing of one particular absorption line. However, a mix of gases such as air, due to the relatively low partial pressures of each gas in the mixture, can present several molecular signatures when using an adequate absorption length [181].

Finally, setups using IMs for DCS have also been demonstrated by Millot *et al.* [163]. Spectral broadening in a HNLF using a counterpropagative configuration allowed us to maintain the intrinsic mutual coherence of the combs resulting in several-nanometer-wide, flat-topped EOCs at a 300 MHz repetition frequency. CO_2 absorption spectroscopy was carried out in a 50 m hollow core fiber filled with the gas, and an example of absorption spectrum recorded in the RF domain and transposed back in the optical domain is presented in Fig. 22. The simplicity of implementation of DCS with EOCs has further stimulated its extension to the 2 µm spectral region, which is much more suitable for gas sensing using standard cells [186].

Using several modulators. As already seen, setups based on the cascading of several EOMs can be advantageous for flat-topped broadband combs with a linespacing larger than 10 GHz. This feature can be particularly interesting for liquid phase spectroscopy since liquids show larger absorption lines compared to gases. Several experimental demonstrations of such setups have been performed, either for liquid

Figure 21
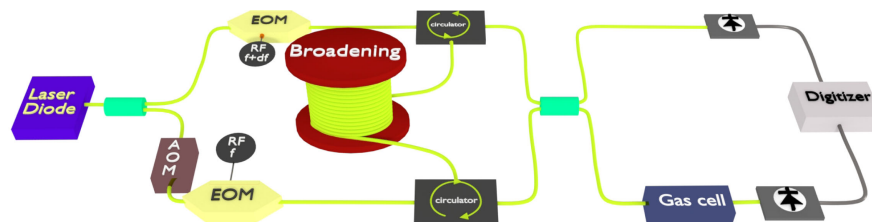
General example of a dual-comb setup based on electro-optic modulators. Depending on the setup and the experiment, some parts such as the broadening stage can be avoided.

[187] or gas spectroscopy [157,188,189]. In the case of gases, the results showed that these setups are not particularly efficient since their resolution is too low. Increasing the resolution can be made by tuning the CW laser and overlapping several spectra but at the expense of postprocessing data treatments [188,189]. However, even with a low resolution, these setups can be sufficient for gas detection over large spectral bandwidths.

On the contrary, setups using several EOMs show all their potential for dispersion spectroscopy over large bandwidths at high repetition frequencies. Experimental demonstrations hold particular promises towards the measurements of small phase variations such as dispersion induced by waveguides, which is rather complex to detect due to the small lengths of the waveguides [164,190]. An example of such spectral phase measurements using a dual-comb setup based on several EOMs is presented in Fig. 23 [164].

Finally, several modulators can be used as a two stage mechanism for EOC generation [191,192]. This way, it is possible to produce an EOC with a high resolution starting from a low resolution EOC.

Using hybrid techniques. Setups for DCS can be developed with hybridizations of sources or components in combination with EOMs. The motivations of hybridization can be purely due to experimental constraints [191], or they can come from the advantages offered by the other components or sources. An example can be the use of a spectrally filtered MLL as a source rather than a CW laser [193]. This method provides directly an arm of the dual-comb setup with the characteristics of the MLL such as a large bandwidth at low repetition rates and a low phase noise. In the same time, the second arm of the setup can be created using an EOM that provides higher repetition rates, flattening possibilities, etc. Thus, these setups usually possess high differences in the repetition rates of the generated combs, and DCS is made possible by using the quasi-integer ratio technique, which shows shorter recording time but at the cost of numerical data processing [194].

Another example of hybrid setup is the use of different EOMs such as an IM and an electro-optic cavity [195]. Here, the different features between the two EOCs generated are exploited, which can lead to highly dense EOCs recordable in a very short time thanks to the quasi-integer ratio technique.

Figure 22
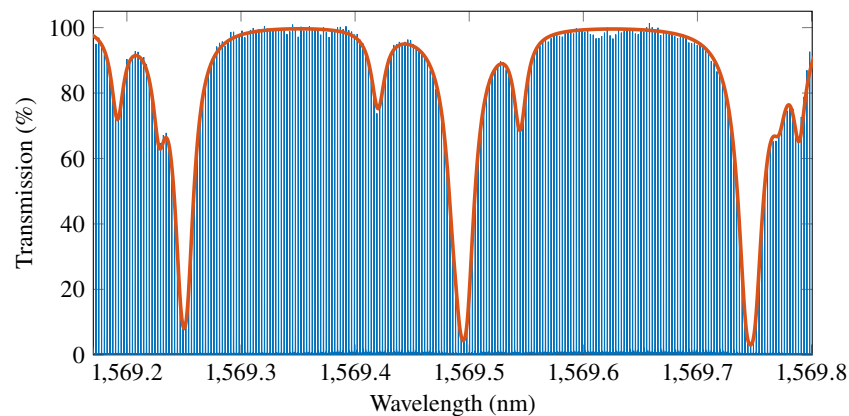
Example of absorption spectrum of a mix of 90% $^{12}CO_2$ and 10% $^{13}CO_2$ obtained in the radio frequency domain and transposed back in the optical domain using a dual-comb setup based on intensity modulators. The solid line in red corresponds to a calculated spectrum using data coming from the HITRAN database [185].

Exotic architectures. DCS can be performed using other kinds of architectures that are particularly suitable for EOMs. As already seen, due to the absence of a cavity, EOCs have the advantage of being agile in repetition rate. Thus, several setups have been developed to exploit this agility for dual-comb applications [196,197], and experimental absorption spectra of HCN are reported. Using a single EOC divided in two arms, a delay can be placed in one arm so that when the repetition rate of the EOC is rapidly switched, the device output is similar to that obtained with two slightly different repetition rate combs. The device is then equivalent to a dual-comb setup with two mutually coherent frequency combs originating from the same source. An example of such setup is presented in Fig. 24.

However, some drawbacks can be found in this type of architecture. First, the delay line, which is often a fiber, induces a phase modification in one arm and not in the other, which can impact the mutual coherence. This can be overcome by putting a

Figure 23
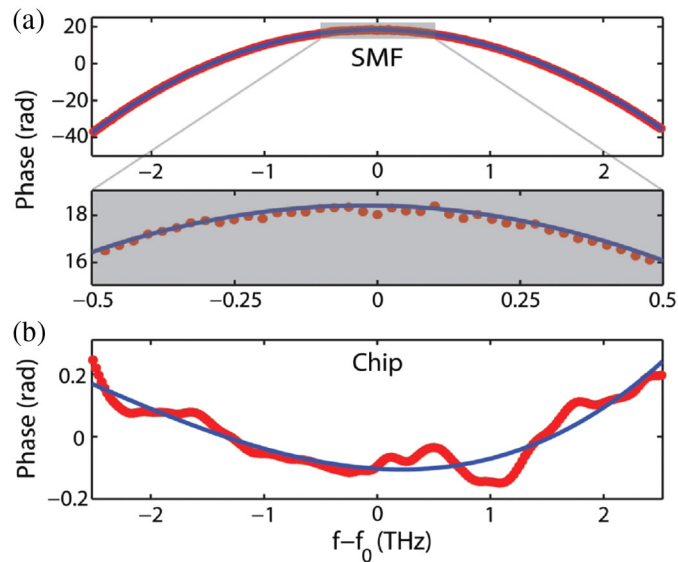
Examples of spectral phase measurements using a dual-comb setup based on several modulators. (a) shows the phase induced by the dispersion of 20 m of single-mode fiber, whereas (b) is for a silicon nitride waveguide. Reprinted with permission from Durán *et al.*, Opt. Lett. **41**, 4190–4193 (2016) [164]. Copyright 2016 Optical Society of America.

Figure 24
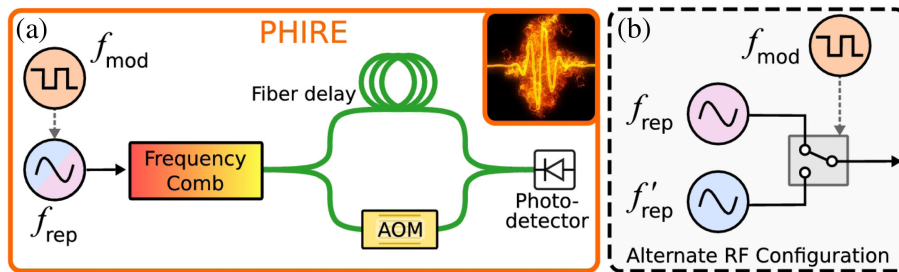
Example of exotic dual-comb setup based on a delay line and on the modulation of the repetition frequency of the modulator with two different configurations. Reprinted with permission from Carlson *et al.*, Opt. Lett. **43**, 3614–3617 (2018) [197]. Copyright 2018 Optical Society of America.

phase compensator after the delay line [197]. Second, the acquisition speed is limited by the tuning speed of the RF oscillator whereas in a conventional dual-comb setup, it is the bandwidth of the detector that limits the acquisition speed [196]. However, this approach reduces significantly the cost of an electro-optic dual-comb setup since the components needed are divided by 2.

Finally, emerging setups based on microrings can be used for DCS. A recent work showed the possibility of recording the absorption spectrum of acetylene with a 10 GHz linespacing [198].

5.1c. Wavelength Extension

Almost all dual-comb setups seen above are developed in the NIR since most EOMs are operating in this domain, as seen in Subsection 4.1b. Obviously DCS would be more interesting at higher wavelengths, starting at 2 μm and up to the MIR, where gases show stronger absorption lines. Even though EOMs have been reported operating in the MIR [119,120], some limitations arise for designing dual-comb setups in this region, especially due to the lack of amplifiers in these regions and the difficulty to spectrally broaden the combs. Thus, direct electro-optic modulation for DCS in a spectral region outside the NIR is more difficult to obtain.

As shown earlier, it is possible to extend the spectrum of an EOC using nonlinear effects, which could be an alternative for dual-comb operations at higher wavelengths from the NIR. Spectral broadening could also be a solution, but this seems difficult to implement for reaching the MIR due to the phase noise accumulation issue that has to be managed, as already described in Subsections 4.2 and 4.3a. Although complex, designing such setups is possible, and a few works have been reported [157]. However, these studies have only reached the 2 μm region where dual-comb setups based on the direct modulation of a CW laser can still be designed [186], and the used repetition rates do not allow high precision spectroscopy. Spectral broadening to reach the MIR is not the best solution, while spectral translation techniques are instead more interesting. For dual-comb applications, the main point is that spectral extension has to be performed in exactly the same way for each comb to avoid a degradation of the mutual coherence.

A few works have been reported for converting EOCs via DFG by using PPLN crystals. The first one by Yan *et al.* has led to the generation of combs at 3.3 μm [126]. The NIR dual-comb setup at 1560 nm presented in Ref. [163] was converted with two distinct PPLN crystals using a 3 W CW ytterbium laser at 1064 nm. No degradation of the mutual coherence was observed, and absorption spectra of methane and ethylene were reported. Note that the conversion of a NIR dual-comb setup can be realized using only one PPLN crystal, as demonstrated in Ref. [127]. In this work, a 1.5 W CW laser at 1064 nm and an electro-optic dual-comb setup at 1538 nm were used for the conversion of the EOCs around 3.45 μm, where methane absorption spectroscopy was performed. Finally, the 3 μm region can also be reached by converting a 1050 nm dual-comb setup with a 1.5 W CW laser operating around 800 nm, and nitrous oxide, ammonia, and acetylene complex spectra are demonstrated in Ref. [128].

Another approach reported for the spectral extension of a dual-comb setup is the use of FWM in an optical fiber. Parriaux *et al.* reported the use of this technique for converting the NIR dual-comb setup presented in Ref. [163] to around 2 μm [125]. Compared to the use of PPLN crystals, the all-fibered characteristic of the setup is kept, and using a counterpropagative configuration with a single HNLF helps to maintain the initial mutual coherence. Note that even if the 2 μm region can be probed with a dual-comb setup designed at this wavelength [186], the spectral extension

technique presented in Ref. [125] can be used to probe other spectral regions within the transparency window of the fiber.

Finally, a recent work by Jerez *et al.* showed the possibility of converting a dual-comb setup based on EOMs in the terahertz (THz) domain [199]. Although no spectroscopic measurement was performed, a demonstration of the setup was made by recording the transmission of a microwave filter in the W-band.

5.2. Dual-Comb Interferometry

Dual-comb setups are not limited for spectroscopic applications. Indeed, interferometers based on two mutually coherent combs can also be used for lots of other applications. In this part, we present some of them, which are based on EOCs including optical imaging and distance measurements.

5.2a. Optical Imaging

In the previous part, we introduced different spectroscopic applications that could be used in the medical domain for analyzing the concentration of certain gases. For medical analyses, imaging techniques are also highly required to observe the localization of substances, which can be done using light in the optical domain. Here, lasers can be highly suitable sources for these applications, especially an OFC, which is a coherent source. Moreover, dual-comb interferometry can be used for its capacity of high speed recording, which can be very useful for imaging applications.

A first example of an imaging technique is optical coherence tomography, which is a three-dimensional imaging technique mostly used in ophthalmology. The first use of an electro-optic dual-comb setup for optical coherence tomography imaging was actually the first dual-comb setup ever reported by Lee *et al.* [200]. However, all the analyses were performed in the temporal domain, and thus the potential of the setup was not fully exploited.

The second demonstration of optical coherence tomography using EOCs was made by Kang *et al.* [166]. Using a setup based on several EOMs and nonlinear loop mirrors, the authors succeeded in generating two mutually coherent ultraflat EOCs with a linespacing of 8.1 GHz over 7 nm, as presented in Fig. 25(a). Tomography was illustrated by analyzing the interferogram obtained by the retro-reflection of one comb on

Figure 25
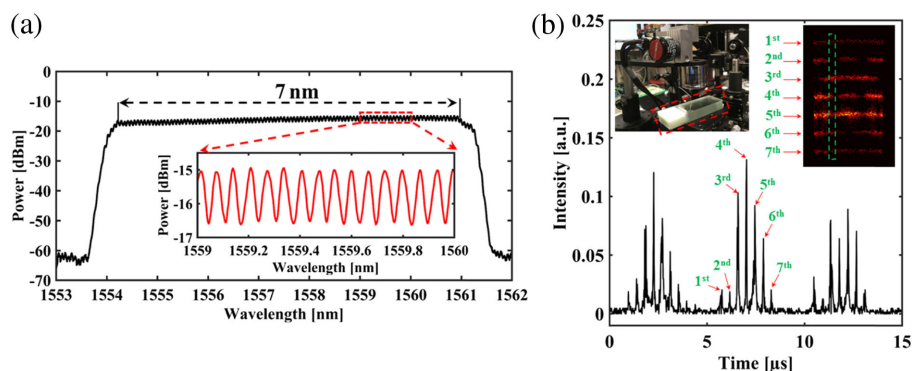
(a) Electro-optic comb generated using nonlinear loop mirrors for tomography imaging. (b) On the top left, photography of the setup showing six slices of glass under study. On the bottom, example of interferogram obtained by the dual-comb setup, which, after data treatment, gives the imaging placed on the top right. Reprinted with permission from Kang *et al.*, Opt. Express **26**, 24928–24939 (2018) [166]. Copyright 2018 Optical Society of America.

several objects such as a mirror, a slice of glass and several piled up slices of glass. Figure 25(b) shows a photo of the setup and an example of interferogram obtained when analyzing six slices of glass. Moreover, the figure shows the imaging obtained from the interferogram. The setup can also operate in a video-mode with a depth imaging available up to 1 cm.

The second example of optical imaging technique is microscopy. Based on EOCs and a dual-comb interferometer, a single study has been reported so far [167]. The used setup is highly similar to the one presented in Ref. [166] to perform tomography imaging but here adapted for the current application. Figure 26 shows an example of image obtained with this setup on beads and onion epithelial cells.

5.2b. *Distance Measurements*

Distance measurement is one domain where lasers are the most used, which has led to the creation of a whole branch of detection methods named *LIDAR* (light detection and ranging). In this domain, dual-comb interferometers have also found their place using a technique very similar to dispersion spectroscopy but without the sample to analyze. The idea is to measure the phase $\Delta\varphi$ induced by the propagation of a comb over a distance L, which is proportional to this distance. With a dual-comb system, this measurement can be easily done in the RF domain by recording the complex spectrum and extracting the phase, as seen before. The advantages of using a dual-comb setup for distance measurements is the acquisition speed that is available at high repetition rates. More details can be found in Ref. [201] while here we will focus on the particular setups based on EOCs.

The first use of an electro-optic dual-comb setup for distance measurements was made by Lay *et al.* [202]. Although the generated combs had only two sidebands obtained by phase modulation within a 80 GHz bandwidth, the technique allowed us to measure distances up to 1 m with a sub-micrometer standard deviation, paving the way for further research developments in this domain. The architecture was next improved by using PMs within a Fabry–Perot cavity, which allowed the generation of 300 GHz wide combs and distance measurements up to 10 m with an agreement within 15 μm, when compared to real measurements [203].

Electro-optic dual-comb setups have also been designed for the detection of vibrations by distance measurements, i.e., for vibrometry. The main difference with the previous studies is that the target is no more static, which requires high speed measurements and thus high repetition rates, which are characteristics well suited for EOCs. Vibrometry can be performed indirectly by interrogating a Bragg grating that works as a sensor [204]. In this case, it is only the absorption spectrum that is under study and more precisely the variation of the comb lines' intensity. Vibrometry can also be done directly by fully exploiting the phase coherence between the combs, as

Figure 26

5 μm   100 μm

On the left, image of beads, and on the right, image of onion epithelial cells. Both images were obtained using a dual-comb setup. Reprinted with permission from Feng *et al.*, Opt. Lett. **44**, 2919–2922 (2019) [167]. Copyright 2019 Optical Society of America.

demonstrated by Teleanu *et al.* [205]. In their study, the setup presented in Ref. [190] was used and slightly modified to incorporate a circulator in one arm that is linked to the vibration source, thus performing dynamic dispersion spectroscopy. This setup is presented in Fig. 27. In combination with time of flight measurements, small delays of 1 ps could be recovered, and for static measurements, sub-nanometer precision can be reached.

The idea of time of flight measurements combined with the dual-comb technique was enhanced for long distance measurements. Several studies have shown accurate measurements from tens of meters [206,207] up to the kilometer with a sub-millimeter accuracy [208].

Note that in the same goal as for spectroscopic applications, exotic electro-optic dual-comb setups can be used for distance measurements, especially the ones based on the switching of the repetition rate of an EOM [209]. The results are similar to other setups: distance measurements up to several hundreds of meters with an accuracy better than 10 μm. Vibrometry was also demonstrated with a similar exotic dual-comb setup [197], which has already been presented in Fig. 24. The setup showed the ability to recover the audio being played by a speaker 1 m below a window placed at 4.5 m from the setup. Note that other setups can be designed such as the one presented in Ref. [210], which is based on three EOCs: the results showed an accuracy of 750 nm over measurements of several tens of meters. Finally, a dual-comb setup based on two different central wavelengths can also be used for distance measurements with particular advantages for compensating fiber drifts [211]. The results showed standard deviations below 2 μm, and, in addition, with the use of a coordinate measuring machine, topographic measurements of several objects were demonstrated.

5.2c. Other Dual-Comb Applications

The characteristics of the dual-comb technique such as sampling without moving parts in the setup can also be exploited for arbitrary waveform characterization. Using an EOC that is characterized beforehand, the electric field from an unknown second mutually coherent comb with a slightly different repetition rate can be measured [212]. However, this technique can only be used to characterize a comb source since its concept relies on a dual-comb setup.

Optical thickness measurement can also be measured using a dual-comb setup. By recovering the transmission of the Fabry–Perot cavity induced by a sample, one can extract the free spectral range that is directly linked to the thickness of the sample [213].

Figure 27
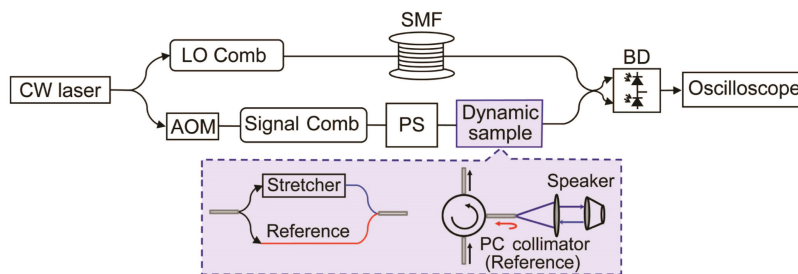
Experimental dual-comb setup used for vibrometry. In one arm of the spectrometer, a circulator is placed to orient the comb toward a dynamic sample. AOM, acousto-optic modulator; PS, pulse shaper; BD, balanced detector. Reprinted with permission from Teleanu *et al.*, Opt. Express **25**, 16427–16436 (2017) [205]. Copyright 2017 Optical Society of America.
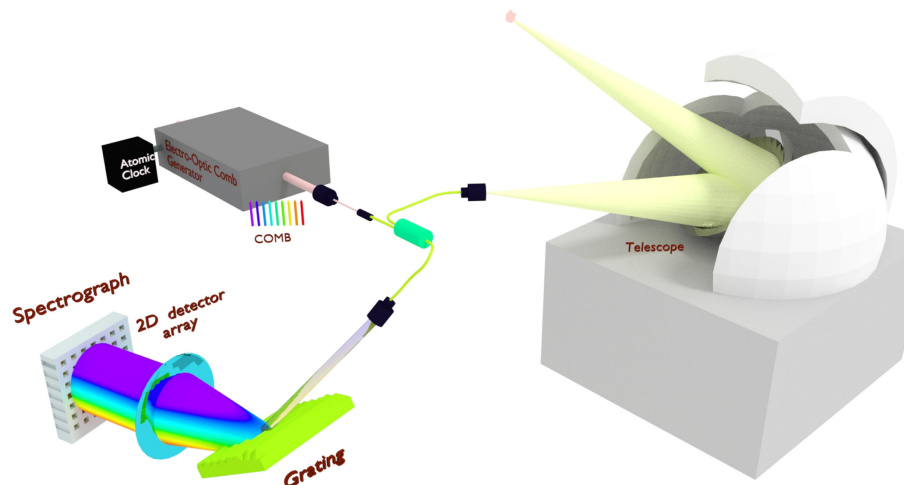
5.3. Calibration of Spectrographs

In all the applications considered until now, the combs were used as the light source to analyze samples. This configuration cannot be used for some spectroscopic applications such as in astronomy, where it is impossible to interrogate the sample under study (stars, exoplanets, etc.). Nevertheless, other configurations can be exploited to perform spectroscopic applications in this field: combs can be used as frequency rulers to calibrate spectrographs to provide an extremely stable frequency reference, so that measurements can be made with the greatest accuracy [214,215]. OFCs used for the calibration of spectrographs are called *astrocombs*. After a brief reminder of the concept behind these particular combs, the interest of EOCs in this field will be presented followed by the experimental demonstrations of electro-optic astrocombs.

5.3a. Astrocomb Principles

In various applications, spectrographs need highly precise radial velocity (RV) measurements of celestial objects. For example, exoplanets can be detected by measuring the Doppler shift of spectral lines emitted by their stars since their presence modifies the RV of the star, thus inducing a spectral shift [216]. Note that the first exoplanet detection, which has used this technique, led in 2019 to the Nobel Prize in Physics for Mayor and Queloz. However, the effect is relatively small, in particular for Earth-mass exoplanets detection, which requires a precision below $10 \text{ cm} \cdot \text{s}^{-1}$ [6,214,217]. Variations of fundamental constants can also be studied by astronomical observations, but the precision needed to observe changes would be greater than for exoplanets detection, below $1\text{cm} \cdot \text{s}^{-1}$ [214,215,217], thus requiring calibration techniques. Here, as shown in Subsection 2.1b, OFCs can provide extremely accurate references, and moreover, as listed in Table 1 of Ref. [214], they possess features close to the ideal needed calibration source, which is the main motivation for generating astrocombs. Figure 28 shows the principle of OFCs for spectrograph calibrations.

Several astrocombs have been experimentally reported and tested with different setups, generally based on femtosecond lasers [218]. However, these sources present low repetition rates, typically below 1 GHz, which is not suitable for this application

Figure 28

Schematic showing the principle of frequency combs for spectrograph calibration. Light received by an astronomical object is coupled with a frequency comb and decomposed by a spectrograph. The comb, previously referenced to a frequency standard, provides an extremely accurate ruler used to calibrate the spectrograph.

[214]. Thus, Fabry–Perot cavities have to be used to increase the repetition frequency, which can be difficult to implement knowing the large optical bandwidth of the source. Another drawback regarding these laser sources is that their central wavelength is most of the time in the visible domain. For astrocombs designed towards the detection of exoplanets, the central wavelength is of a huge importance since it restrains the class of stars under study. Indeed, Sun-like stars (G-class stars) can be investigated with visible light, but since they are highly massive compared to Earth-like planets, these exoplanets are difficult to detect knowing the high precision required in the RV measurements. In this context, it is easier to detect Earth-like planets orbiting smaller stars such as red dwarfs (M-class stars). Moreover, M-class stars are predominant in our galaxy, and they more likely seem to be the home to low mass telluric exoplanets rather than giants gaseous exoplanets [219]. All these characteristics make them unique candidates of investigation, but these stars have an emission spectrum that is mostly located in the NIR, which is not adapted to most of astrocombs based on femtosecond lasers. Even if some setups were designed in the NIR and produced results, they still remain less popular [217,218].

5.3b. Electro-Optic Astrocombs

Several attempts have been made to generate astrocombs based on EOMs [151,158,220]. The main motivations are that EOCs can provide high repetition frequencies with a large availability in the NIR region: they are low cost, they can be all-fibered, etc., which make them particularly suitable for spectrograph calibrations. The main disadvantage of EOCs for this application is their low spectral bandwidth, which requires spectral broadening, as shown in Subsection 4.3a, and, thus, a particular attention to the phase noise accumulation. A particularity of electro-optic astrocombs is that the main uncertainty is given by the carrier envelope offset frequency determination. Thus, the initial CW laser and the RF oscillator that fix the repetition rate must be carefully referenced to provide a long-term stability, prevent wavelength shifts, etc., all of this reducing the uncertainties in the RV measurements [220].

Regarding electro-optic astrocomb setups themselves, a main advantage compared to other astrocombs is their short up-and-running time, and capabilities to be easily piloted from outside [151,158]. Moreover, these setups are generally all-fibered, which provides a plug-and-play feature and a higher stability when polarization maintaining components are used. Indeed, by fixing the polarization state of the comb along the setup, unwanted effects due to mechanical vibrations, temperature fluctuations, and polarization random fluctuations can be avoided [151].

5.3c. Experimental Demonstrations

The first demonstration of an electro-optic astrocomb was made by Yi *et al.* and implemented on the Keck observatory [220]. The setup used was based on a 1560 nm CW laser modulated by two synchronized PMs plus one IM. The EOC with a 12 GHz linespacing is then phase compensated, amplified, and broadened in a HNLF to obtain a more than 100 nm exploitable spectrum that showed an excellent stability over 5 days.

A second demonstration made by Obrzud *et al.* succeeded in implemention at the Roque de los Muchachos observatory a 400 nm wide electro-optic astrocomb centered at 1560 nm with a linespacing of 14.5 GHz [151]. Compared to the previous work of Yi *et al.*, where the CW laser was referenced to a gas molecular resonance and the RF oscillator to an atomic clock [220]; here, Obrzud *et al.* referenced all of their setup to an atomic clock providing a higher and absolute accuracy. The EOC generation setup is relatively similar to the one of Yi *et al.*, but a larger spectrum was

obtained by using a nonlinear pulse compression configuration in optimized fibers before spectral broadening in a HNLF. Moreover, the HNLF was chosen with a very low dispersion slope to produce a flat spectrum over its entire bandwidth. This results in a relatively simple setup without complex components such as filters or equalizers. The schematic of the setup and an example of a generated EOC have already been presented in Fig. 16. Further studies showed that this setup could acquire an extension in the visible domain by using third-harmonic generation in a silicon nitride waveguide [124].

The last reported demonstration of an electro-optic astrocomb was made by Metcalf *et al.* at the McDonald observatory [158]. In the previous studies, limits are close to be reached in the wavelength span obtained since a wider spectrum would require phase noise cancellation. Thus, the setup presented by Obrzud *et al.* in Ref. [151] can be slightly modified to incorporate a Fabry–Perot cavity after the EOC generation, resulting in a comb spanning around 600 nm after nonlinear broadening [156]. In the same goal, Metcalf *et al.* used the results obtained in Refs. [132,133] to manage the phase noise accumulation issue, for astrocomb generation [158]. The setup is more complex than what was presented in previous works since a Fabry–Perot cavity, a second spectral broadening configuration in a silicon nitride chip, filters, and a programmable flattener have to be used. However, a remarkable ultraflat 500 nm wide EOC centered at 1064 nm and at a repetition frequency of 30 GHz was obtained. A recent work showed that a similar setup as the one presented in Ref. [158] could acquire an extension in the visible domain by using second-harmonic generation in a beta-barium borate crystal [123].

5.4. Arbitrary Waveform Generation by Spectral Shaping

OFCs can provide powerful sources for more fundamental applications. Still using the ability of EOCs to possess high linespacing, such combs can then be spectrally shaped line-by-line in phase and amplitude to produce a well-defined structure. This reshaped EOC can find applications in lots of domains as will be now discussed, starting with the basics on OFC shaping.

5.4a. Basic Concepts

We have already seen that an EOC can be shaped at its generation stage by using well-defined sets of parameters [bias voltage(s), RF voltage(s), etc.] or by cascading EOMs, which can lead to flat-topped spectra. These techniques can also be used for particular temporal waveform generation such as Gaussian or triangular pulses, and lots of studies have been performed. For instance, the use of a DDMZM and a dispersive fiber was theoretically and experimentally investigated in Ref. [221] for various waveform generation. Although these techniques use EOMs, they focus mainly on the influence of the parameters applied to the EOMs and their neighboring optical components. As a result, they rarely exploit the performance of the combs generated by the EOMs, which falls behind the scope of this paper.

However, waveform generation can also be performed with other techniques that can be more versatile, especially the ones based on the spectral shaping of an OFC. Indeed, by modifying the phase and amplitude of each comb line, various outputs can be obtained. Thus, a single setup is needed, and the control is only made relative to the setup shaping element. To shape an OFC, the common technique is to use a 4f-system schematically presented in Fig. 29(a). The idea behind this setup is the following: an input light that is incident on a spectral disperser such as a grating will see its frequency components spatially separated. Then, an optical element such as a lens focuses the frequency components on a modulator. This modulator can be electronically programmable if an acousto-optic crystal, a set of liquid crystals, a deformable

mirror, etc., are used, which enables the control of the amplitude and the phase of the frequency components. At the output, the shaped frequency components are put back together using various optical components and a dispersive device. More details on the pulse shaping technique can be found in Ref. [222].

5.4b. Spectral Shaping

Although spectral shaping can be performed on any coherent sources, a particular flexibility is obtained when dealing with EOCs. Indeed, the modulator inside the shaper has a finite spectral resolution, which is linked to the number of pixels available. Consequently, a source with a limited number of frequency components is more suitable for spectral shaping, and a full shaping can be performed only if each spectral component is individually shaped. Nowadays, shapers with a resolution below 1 GHz are challenging to obtain, which means that for full comb shaping, a comb with a linespacing at least superior to 1 GHz is required [223]. This particular characteristic is well-suited for EOCs. Moreover, since EOMs are most of the time fibered components, the spectral shaping can be performed using a reflective geometry, as schematized in Fig. 29(b). Using a circulator at the shaper input and a mirror behind the modulator, the experimental setup is then a back and forth shaper, which is easy to use. A review on the subject can be found in Refs. [53,224].

A number of studies have been reported for spectral shaping an EOC. The most common technique used is a spectral shaper in reflective geometry based on liquid crystal modulators [86,225–229]. Jang *et al.* showed the possibility of shaping a 5 GHz EOC over more than 100 comb lines for complex waveform generation and repetition frequency doubling [226]. Note that even if possible, the spectral shaping of a high number of comb lines might not be necessary for every waveform generation, and controlling only a few lines can be enough, as demonstrated in Refs. [86,229]. Other architectures are available for spectral shaping such as arrayed waveguide gratings, which are on-chip structures with an IM array and a PM array [230,231]. Each waveguide is defined as a channel that is the equivalent of a pixel. One of the first demonstrations of this technique showed the spectral shaping of a 10 GHz EOC for arbitrary waveform generation [230]. A more recent study presented a spectral shaper with 32 channels designed for 25 GHz EOCs and showed the possibility of repetition frequency doubling but also as a RF filter [231]. Note that spectral shaping can also be used to reduce the amplified spontaneous emission coming from amplifiers, to induce a quadratic phase for chirp compensation of pulses, which avoids the use of long fibers, but also to shape the temporal domain towards a particular form [164,190,205]. Spectral flattening is also a feature that can be obtained by attenuating each line of the

Figure 29
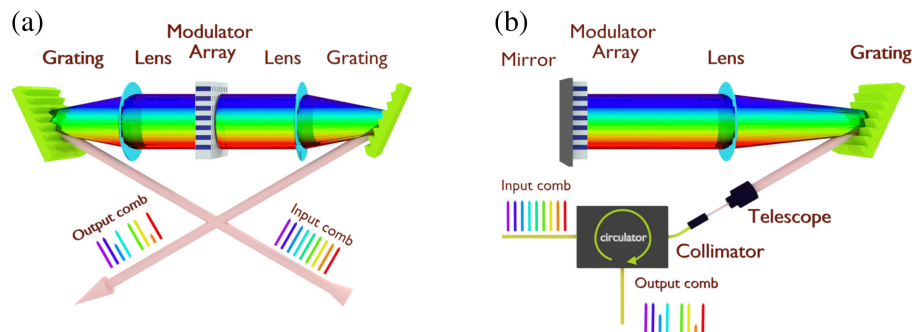
Schematic showing (a) a general setup for spectral shaping with a 4f-system and (b) a spectral shaper using a reflective geometry, which is highly suitable for fibered setups.

EOC towards a no intensity fluctuating comb [220]. However, this method greatly reduces the flexibility of EOCs, as compared to other flattening possibilities.

Regarding the more fundamental applications of spectral shaping of an EOC, besides arbitrary waveform generation, the linear sculpturing of comb lines can be used to synthesize an initial condition that, when propagated in an optical fiber with particular parameters, can lead to the formation of well-defined structures and to the study of their evolutions such as breathers [232–234], rogue waves [235,236], and Peregrine solitons [237–239]. Note that the initial condition to inject is obtained by using the inverse scattering method [24]. Although some of these structures can be generated without spectral shaping [240–242], the EOC shaping methods are easy and convenient to use, especially when studying the evolution of the analyzed structure, which avoids fiber cut-back experiments.

5.5. Other Applications

In this part, we report the applications of EOCs that have been less studied compared to the previous ones, or applications that have already been treated in previous review articles in the literature. In this last case, we will only provide a short summary, and the reader can refer to the cited review articles for more details.

5.5a. RF Photonics

Due to the capacity of EOMs to nonlinearly mix an optical signal and a RF signal, RF processing techniques have been developed by controlling the light in the optical domain and then going back to the RF domain. These applications can, for instance, be oriented towards microwave filtering. A review on the subject can be found in Ref. [53].

5.5b. Telecommunications

As previously seen, EOMs have the ability to rapidly generate a coherent set of lines with a large linespacing. These features can find applications in the telecommunication domain, especially for wavelength division multiplexing, where each comb line can be used as a channel for data processing. A review on the subject can be found in Ref. [243].

5.5c. Metrology

Metrology, which is one of the origin points of OFCs, can also be performed using EOCs, especially for measuring RF and THz frequencies. In the same way as for RF photonic applications, an unknown signal is set as the RF signal of an EOM to modulate a CW laser. All information carried by the RF signal is then transposed on the optical signal, which can be treated and then analyzed either in the optical or in the electrical domain. Several techniques and setups based on EOCs can be used for these measurements, and a review on the subject can be found in Ref. [244]. Note that a recent work has shown the precise measurement of THz radiations by heterodyne detection using a filtered EOC [245].

5.5d. Cloaking

Finally, applications towards cloaking, i.e., hiding an event by avoiding the detection of this event, can be performed using EOCs. Cloaking can be used for securing communications, and the idea is to shape the temporal and/or spectral profile of a probe beam (which is considered as the illumination source) so that an event cannot print information on it. After passing the event, the probe beam is shaped again so that it comes back to its original form. This last step aims to leave no trace that a cloaking was performed. Since telecommunications use high repetition rates, cloaking has to be performed in agreement with these rates, which can be challenging. However,

the utilization of EOCs can be a suitable approach to this aim since EOMs have been designed and efficiently improved for telecommunication applications.

The first use of an EOC for temporal cloaking was made by Lukens *et al.* [246]. Here the aim is to create pulses in a probe beam so that any detection exterior to these pulses is null. The authors demonstrated that, for a CW laser as an illumination source, the required temporal modification for cloaking informations at a high repetition rate is equivalent to the generation of flat EOCs. In addition to the use of a temporal Talbot effect, a CW probe beam can be cloaked at a ratio around 50% at a repetition frequency of 12 GHz. The experimental setup is composed of several PMs in addition with gratings and fibers to create short pulses. After an event is simulated by inscribing data on the probe beam using an IM, a similar setup as what was used to create the pulses is also employed. Note that the use of optical elements that only modify the phase is intentional to make the setup reversible. This way, the event is not inscribed on the probe beam, avoiding its detection. Note that similar results can be obtained using temporal Fraunhofer diffraction rather than the Talbot effect [247]. Moreover, the previous work can be enhanced when using several CW lasers as the illumination source [248]. In this case, the cloaking can be performed over a particular frequency component by modifying the timing of the modulator. Hence, the cloaking can be made on a particular frequency channel, and data can be willingly cloaked or not with a supplementary degree of freedom, preventing the detection on a particular channel and allowing the switch to another.

Finally, it was demonstrated that a pulsed source could be used as the illumination source. In this case, the PMs have to be driven by a multiple of the repetition frequency of the source, and the cloaking can be used in the same way we have seen above [249], or for data preservation applications [248]. However in these cases, the combs generated for cloaking are not really EOCs since the source is already a comb, which falls behind the scope of this paper.

6. OUTLOOK AND DISCUSSION

Although EOCs have a lot of advantages and are used for various applications, electro-optic components could still be improved in their conception, which will enhance their characteristics. In particular, increasing the bandwidth of EOMs is a key point towards high linespacing and shorter pulse generation. Studies have recently shown that particular MZMs allowed a more than 70 GHz electro-optic bandwidth and could easily reach 100 GHz [250–252]. Moreover, it was reported that under proper design, a PM can show a response up to 500 GHz [253]. These enhancements of EOMs could pave the way to comb generation with linespacings that are, for the moment, only available when using microresonators.

Enhancements of EOMs could also be made by modifying or changing the electro-optic material used. Indeed, EOMs are nowadays mainly based on lithium niobate, which can be inconvenient to use for integrated systems due to the device lengths that are in the centimeter range, the relatively high driving voltages up to 10 V, and the difficulty to be integrated into CMOS chips. Nevertheless, recent developments have demonstrated CMOS compatible voltage [252]. In the same time, other materials with a higher electro-optic coefficient have been considered in recent years. Thus, the barrier of 100 Gb/s modulation data rate was reached by the use of silicon-organic hybrid (SOH) technology [254]. These modulators exploit the ultrafast Pockels effect of polymer materials deposited within a silicon photonic slot waveguide with a footprint of 500 μm, but they still require a high driving voltage reaching 22 V. More recently, replacing the silicon slot by a plasmonic slot, the authors of Ref. [255] have demonstrated a 40 Gb/s plasmonic PM of 29 μm length with a voltage lower than 7.5 V and

even a MZM at 54 Gb/s with a footprint as small as 10 μm [256]. Since then, a new record has been published for a bit rate as high as 116 Gb/s and a voltage as low as 6 V for a 35 μm footprint [257], and several optimizations are still in progress for such plasmonic modulators [258]. Several studies investigated other potential candidates such as barium titanate $BaTiO_3$ [259,260]. It was experimentally demonstrated that $BaTiO_3$ can exhibit an electro-optic coefficient 30 times higher than $LiNbO_3$ but also a modulation up to 65 GHz [259]. Another example of investigated material is silicon [261,262].

Other enhancements such as the bandwidth of EOCs could be approached by using new techniques. The use of on-chip nanostructures such as nanomechanical-photonic waveguides has showed that, under proper design, the use of nanomechanic effects can broaden the spectrum of an EOC in a different way than accumulating EOMs or spectral broadening [263].

Finally, new applications could be made with EOCs. We have seen in the spectroscopic part that only linear spectroscopy with EOCs has been performed. However, nonlinear spectroscopy has already been demonstrated using OFCs [264]. Since EOCs can possess high power per comb line, these combs could make perfect candidates for nonlinear spectroscopy, and a proof of principle was demonstrated in Ref. [265].

7. CONCLUSION

In this paper, we presented the basic principles up to the most recent advances in the generation of OFCs based on the electro-optic modulation of a CW laser. We showed that using only the electro-optic effect, several very different setups can be designed for frequency comb generation. Each of these setups possess particular characteristics that make the generated combs complementary among them, since all of these combs can be shaped due to the high number of degrees of freedom associated with electro-optic modulators. Indeed, when compared to other comb sources, combs produced by electro-optic modulation are rather different in their characteristics: several advantages of these combs, such as their tunable linespacing or their shape have been put into light, and several limitations, such as their bandwidth or their phase noise features, have also been studied. All of the particularities presented in this review make EOCs unique and suitable for lots of applications such as high resolution spectroscopy, optical imaging, distance measurements, and calibration of instruments. Finally, new setups for EOC generation are in constant development such as for reaching the MIR or for obtaining higher electro-optic bandwidths. These enhanced performances could open new opportunities for a variety of applications.

DISCLOSURES

The authors declare no conflicts of interest.

REFERENCES

1. T. H. Maiman, "Stimulated optical radiation in ruby," Nature **187**, 493–494 (1960).

2. L. E. Hargrove, R. L. Fork, and M. A. Pollack, "Locking of He-Ne laser modes induced by synchronous intracavity modulation," Appl. Phys. Lett. **5**, 4–5 (1964).

3. T. W. Hänsch, "Nobel lecture: passion for precision," Rev. Mod. Phys. **78**, 1297–1309 (2006).

4. J. L. Hall, "Nobel lecture: defining and measuring optical frequencies," Rev. Mod. Phys. **78**, 1279–1295 (2006).

5. T. Udem, R. Holzwarth, and T. W. Hänsch, "Optical frequency metrology," Nature **416**, 233–237 (2002).

6. T. Wilken, G. L. Curto, R. A. Probst, T. Steinmetz, A. Manescau, L. Pasquini, J. I. G. Hernández, R. Rebolo, T. W. Hänsch, T. Udem, and R. Holzwarth, "A spectrograph for exoplanet observations calibrated at the centimetre-per-second level," Nature **485**, 611–614 (2012).

7. A. Matveev, C. G. Parthey, K. Predehl, J. Alnis, A. Beyer, R. Holzwarth, T. Udem, T. Wilken, N. Kolachevsky, M. Abgrall, D. Rovera, C. Salomon, P. Laurent, G. Grosche, O. Terra, T. Legero, H. Schnatz, S. Weyers, B. Altschul, and T. W. Hänsch, "Precision measurement of the hydrogen $1S$–$2S$ frequency via a 920-km fiber link," Phys. Rev. Lett. **110**, 230801 (2013).

8. F. X. Kärtner, U. Morgner, T. Schibli, R. Ell, H. A. Haus, J. G. Fujimoto, and E. P. Ippen, *Few-Cycle Pulses Directly from a Laser* (Springer, 2004), pp. 73–136.

9. J. Reichert, R. Holzwarth, T. Udem, and T. Hänsch, "Measuring the frequency of light with mode-locked lasers," Opt. Commun. **172**, 59–68 (1999).

10. D. J. Jones, S. A. Diddams, J. K. Ranka, A. Stentz, R. S. Windeler, J. L. Hall, and S. T. Cundiff, "Carrier-envelope phase control of femtosecond mode-locked lasers and direct optical frequency synthesis," Science **288**, 635–639 (2000).

11. J. Reichert, M. Niering, R. Holzwarth, M. Weitz, T. Udem, and T. W. Hänsch, "Phase coherent vacuum-ultraviolet to radio frequency comparison with a mode-locked laser," Phys. Rev. Lett. **84**, 3232–3235 (2000).

12. D. E. Spence, P. N. Kean, and W. Sibbett, "60-fsec pulse generation from a self-mode-locked Ti:sapphire laser," Opt. Lett. **16**, 42–44 (1991).

13. S. T. Cundiff and J. Ye, "Colloquium: femtosecond optical frequency combs," Rev. Mod. Phys. **75**, 325–342 (2003).

14. V. J. Matsas, T. P. Newson, D. J. Richardson, and D. N. Payne, "Selfstarting passively mode-locked fibre ring soliton laser exploiting nonlinear polarisation rotation," Electron. Lett. **28**, 1391–1393 (1992).

15. K. Tamura, H. A. Haus, and E. P. Ippen, "Self-starting additive pulse mode-locked erbium fibre ring laser," Electron. Lett. **28**, 2226–2228 (1992).

16. S. Droste, G. Ycas, B. R. Washburn, I. Coddington, and N. R. Newbury, "Optical frequency comb generation based on erbium fiber lasers," Nanophotonics **5**, 196–213 (2016).

17. J. Ye and S. Cundiff, *Femtosecond Optical Frequency Comb: Principle, Operation and Applications* (Springer, 2006).

18. T. Udem, R. Holzwarth, and T. Hänsch, "Femtosecond optical frequency combs," Eur. Phys. J. Spec. Top. **172**, 69–79 (2009).

19. J. Kim and Y. Song, "Ultralow-noise mode-locked fiber lasers and frequency combs: principles, status, and applications," Adv. Opt. Photon. **8**, 465–540 (2016).

20. P. Del'Haye, A. Schliesser, O. Arcizet, T. Wilken, R. Holzwarth, and T. J. Kippenberg, "Optical frequency comb generation from a monolithic microresonator," Nature **450**, 1214–1217 (2007).

21. G. Lin, A. Coillet, and Y. K. Chembo, "Nonlinear photonics with high-Q whispering-gallery-mode resonators," Adv. Opt. Photon. **9**, 828–890 (2017).

22. A. Pasquazi, M. Peccianti, L. Razzari, D. J. Moss, S. Coen, M. Erkintalo, Y. K. Chembo, T. Hansson, S. Wabnitz, P. Del'Haye, X. Xue, A. M. Weiner, and R. Morandotti, "Micro-combs: a novel generation of optical sources," Phys. Rep. **729**, 1–81 (2018).

23. T. J. Kippenberg, A. L. Gaeta, M. Lipson, and M. L. Gorodetsky, "Dissipative Kerr solitons in optical microresonators," Science **361**, eaan8083 (2018).

24. G. Agrawal, *Nonlinear Fiber Optics, Optics and Photonics Series*, 6th ed. (Academic, 2019).

25. M. I. Kayes and M. Rochette, "Optical frequency comb generation with ultra-narrow spectral lines," Opt. Lett. **42**, 2718–2721 (2017).

26. E. Myslivets, B. P. Kuo, N. Alic, and S. Radic, "Generation of wideband frequency combs by continuous-wave seeding of multistage mixers with synthesized dispersion," Opt. Express **20**, 3331–3344 (2012).

27. A. Antikainen and G. P. Agrawal, "Dual-pump frequency comb generation in normally dispersive optical fibers," J. Opt. Soc. Am. B **32**, 1705–1711 (2015).

28. V. Durán, C. Schnébelin, and H. G. de Chatellus, "Coherent multi-heterodyne spectroscopy using acousto-optic frequency combs," Opt. Express **26**, 13800–13809 (2018).

29. T. Chen, W. Kong, H. Liu, and R. Shu, "Frequency-stepped pulse train generation in an amplified frequency-shifted loop for oxygen A-band spectroscopy," Opt. Express **26**, 34753–34762 (2018).

30. R. W. Boyd, *Nonlinear Optics*, 3rd ed. (Academic, 2008).

31. F. Pockels, "Ueber den Einfluss elastischer Deformationen, speciell einseitigen Druckes, auf das optische Verhalten krystallinischer Körper," Ann. Phys. **273**, 144–172 (1889).

32. A. Kundt, "Ueber das optische Verhalten des Quarzes im electrischen Felde," Ann. Phys. **254**, 228–233 (1883).

33. W. Röntgen, "Ueber die durch elektrische Kräfte erzeugte Aenderung der Doppelbrechung des Quarzes," Ber. Oberhess. Ges. Nat. Heilkd. Giessen Naturwiss. Abt. **22**, 49–64 (1883).

34. J. Kerr, "Xl. A new relation between electricity and light: dielectrified media birefringent," London Edinburgh Dublin Philos. Mag. J. Sci. **50**, 337–348 (1875).

35. L. Zehnder, "Ein neuer Interferenzrefractor," Z. Instrumentenkd. **11**, 275–285 (1891).

36. L. Mach, "Uber einer Interferenzrefractor," Z. Instrumentenkd. **12**, 89–93 (1892).

37. W. Steier, "A push-pull optical amplitude modulator," IEEE J. Quantum Electron. **3**, 664–667 (1967).

38. G. B. Arfken, H. J. Weber, and F. E. Harris, *Mathematical Methods for Physicists*, 7th ed. (Academic, 2013).

39. K. E. Iverson, *A Programming Language* (Wiley, 1962).

40. R. L. Graham, D. E. Knuth, and O. Patashnik, *Concrete Mathematics: a Foundation for Computer Science*, 2nd ed. (Addison-Wesley, 1994).

41. T. Sakamoto, T. Kawanishi, and M. Izutsu, "Widely wavelength-tunable ultra-flat frequency comb generation using conventional dual-drive Mach-Zehnder modulator," Electron. Lett. **43**, 1039–1040 (2007).

42. T. Sakamoto, T. Kawanishi, and M. Izutsu, "Asymptotic formalism for ultraflat optical frequency comb generation using a Mach–Zehnder modulator," Opt. Lett. **32**, 1515–1517 (2007).

43. T. Sakamoto, T. Kawanishi, and M. Tsuchiya, "10 GHz, 2.4 ps pulse generation using a single-stage dual-drive Mach–Zehnder modulator," Opt. Lett. **33**, 890–892 (2008).

44. N. Yokota, K. Abe, S. Mieda, and H. Yasaka, "Harmonic superposition for tailored optical frequency comb generation by a Mach–Zehnder modulator," Opt. Lett. **41**, 1026–1029 (2016).

45. K. Qu, S. Zhao, X. Li, Z. Zhu, D. Liang, and D. Liang, "Ultra-flat and broadband optical frequency comb generator via a single Mach–Zehnder modulator," IEEE Photon. Technol. Lett. **29**, 255–258 (2017).

46. L. Liu, X. Zhang, T. Xu, Z. Dai, S. Dai, and T. Liu, "Simple and seamless broadband optical frequency comb generation using an InAs/InP quantum dot laser," Opt. Lett. **42**, 1173–1176 (2017).

47. L. Liu, X. Zhang, T. Xu, Z. Dai, and T. Liu, "Simple optical frequency comb generation using a passively mode-locked quantum dot laser," Opt. Commun. **396**, 105–109 (2017).

48. M. Fujiwara, M. Teshima, J. Kani, H. Suzuki, N. Takachio, and K. Iwatsuki, "Optical carrier supply module using flattened optical multicarrier generation based on sinusoidal amplitude and phase hybrid modulation," J. Lightwave Technol. **21**, 2705–2714 (2003).

49. C.-B. Huang, S.-G. Park, D. E. Leaird, and A. M. Weiner, "Nonlinearly broadened phase-modulated continuous-wave laser frequency combs characterized using DPSK decoding," Opt. Express **16**, 2520–2527 (2008).

50. A. Ishizawa, T. Nishikawa, A. Mizutori, H. Takara, S. Aozasa, A. Mori, H. Nakano, A. Takada, and M. Koga, "Octave-spanning frequency comb generated by 250 fs pulse train emitted from 25 GHz externally phase-modulated laser diode for carrier-envelope-offset-locking," Electron. Lett. **46**, 1343–1344 (2010).

51. R. Wu, V. R. Supradeepa, C. M. Long, D. E. Leaird, and A. M. Weiner, "Generation of very flat optical frequency combs from continuous-wave lasers using cascaded intensity and phase modulators driven by tailored radio frequency waveforms," Opt. Lett. **35**, 3234–3236 (2010).

52. Y. Dou, H. Zhang, and M. Yao, "Generation of flat optical-frequency comb using cascaded intensity and phase modulators," IEEE Photon. Technol. Lett. **24**, 727–729 (2012).

53. V. Torres-Company and A. M. Weiner, "Optical frequency comb technology for ultra-broadband radio-frequency photonics," Laser Photon. Rev. **8**, 368–393 (2014).

54. A. Ishizawa, T. Nishikawa, A. Mizutori, H. Takara, H. Nakano, T. Sogawa, A. Takada, and M. Koga, "Generation of 120-fs laser pulses at 1-GHz repetition rate derived from continuous wave laser diode," Opt. Express **19**, 22402–22409 (2011).

55. R. Wu, V. Torres-Company, D. E. Leaird, and A. M. Weiner, "Supercontinuum-based 10-GHz flat-topped optical frequency comb generation," Opt. Express **21**, 6045–6052 (2013).

56. A. J. Metcalf, V. Torres-Company, D. E. Leaird, and A. M. Weiner, "High-power broadly tunable electrooptic frequency comb generator," IEEE J. Sel. Top. Quantum Electron. **19**, 231–236 (2013).

57. A. Aubourg, J. Lhermite, S. Hocquet, E. Cormier, and G. Santarelli, "Generation of picosecond laser pulses at 1030 nm with gigahertz range continuously tunable repetition rate," Opt. Lett. **40**, 5610–5613 (2015).

58. D. C. Cole, K. M. Beha, S. A. Diddams, and S. B. Papp, "Octave-spanning super-continuum generation via microwave frequency multiplication," J. Phys. Conf. Ser. **723**, 012035 (2016).

59. K. Kashiwagi, T. Kurokawa, Y. Okuyama, T. Mori, Y. Tanaka, Y. Yamamoto, and M. Hirano, "Direct generation of 12.5-GHz-spaced optical frequency comb with ultrabroad coverage in near-infrared region by cascaded fiber configuration," Opt. Express **24**, 8120–8131 (2016).

60. C. Chen, F. Zhang, and S. Pan, "Generation of seven-line optical frequency comb based on a single polarization modulator," IEEE Photon. Technol. Lett. **25**, 2164–2166 (2013).

61. T. Healy, F. C. G. Gunning, A. D. Ellis, and J. D. Bull, "Multi-wavelength source using low drive-voltage amplitude modulators for optical communications," Opt. Express **15**, 2981–2986 (2007).

62. C. He, S. Pan, R. Guo, Y. Zhao, and M. Pan, "Ultraflat optical frequency comb generated based on cascaded polarization modulators," Opt. Lett. **37**, 3834–3836 (2012).

63. Y. Yang, J. Ma, X. Xin, Q. Zhang, Y. Zhang, X. Yin, R. Zhang, and W. Liu, "Optical frequency comb generation using two cascaded polarization modulators," Photon. Netw. Commun. **32**, 126–132 (2016).

64. C. Chen, C. He, D. Zhu, R. Guo, F. Zhang, and S. Pan, "Generation of a flat optical frequency comb based on a cascaded polarization modulator and phase modulator," Opt. Lett. **38**, 3137–3139 (2013).

65. S. Pan and J. Yao, "Generation of a chirp-free optical pulse train with tunable pulse width based on a polarization modulator and an intensity modulator," Opt. Lett. **34**, 2186–2188 (2009).

66. F. Zhang, X. Ge, and S. Pan, "A two-stage optical frequency comb generator based on polarization modulators and a Mach–Zehnder interferometer," Opt. Commun. **354**, 94–102 (2015).

67. X. Zou, W. Pan, B. Luo, and L. Yan, "Generation of repetition-rate-quadrupled optical pulse trains using a PolM or a pair of PolMs," IEEE J. Quantum Electron. **48**, 3–7 (2012).

68. R. B. Chaudhuri and A. D. Barman, "Generation of an optical frequency comb based on two cascaded dual-parallel polarization modulators," Appl. Opt. **57**, 9164–9171 (2018).

69. T. Kobayashi, T. Sueta, Y. Cho, and Y. Matsuo, "High-repetition-rate optical pulse generator using a Fabry-Perot electro-optic modulator," Appl. Phys. Lett. **21**, 341–343 (1972).

70. M. Kourogi, K. Nakagawa, and M. Ohtsu, "Wide-span optical frequency comb generator for accurate optical frequency difference measurement," IEEE J. Quantum Electron. **29**, 2693–2701 (1993).

71. R. P. Kovacich, U. Sterr, and H. R. Telle, "Short-pulse properties of optical frequency comb generators," Appl. Opt. **39**, 4372–4376 (2000).

72. J. Kim, D. J. Richardson, and R. Slavík, "Cavity-induced phase noise suppression in a Fabry–Perot modulator-based optical frequency comb," Opt. Lett. **42**, 1536–1539 (2017).

73. K. Ho and J. M. Kahn, "Optical frequency comb generator using phase modulation in amplified circulating loop," IEEE Photon. Technol. Lett. **5**, 721–725 (1993).

74. P. Shen, N. J. Gomes, P. A. Davies, P. G. Huggard, and B. N. Ellison, "Analysis and demonstration of a fast tunable fiber-ring-based optical frequency comb generator," J. Lightwave Technol. **25**, 3257–3264 (2007).

75. M. Hirano and A. Morimoto, "Generation of flat optical frequency comb by fiber loop modulation," Opt. Rev. **18**, 13–18 (2011).

76. J. Zhang, N. Chi, J. Yu, Y. Shao, J. Zhu, B. Huang, and L. Tao, "Generation of coherent and frequency-lock multi-carriers using cascaded phase modulators and recirculating frequency shifter for Tb/s optical communication," Opt. Express **19**, 12891–12902 (2011).

77. J. Zhang, J. Yu, Z. Dong, Y. Shao, and N. Chi, "Generation of full C-band coherent and frequency-lock multi-carriers by using recirculating frequency shifter loops based on phase modulator with external injection," Opt. Express **19**, 26370–26381 (2011).

78. L. Ponnampalam, M. Fice, H. Shams, C. Renaud, and A. Seeds, "Optical comb for generation of a continuously tunable coherent THz signal from 122.5 GHz to > 2.7 THz," Opt. Lett. **43**, 2507–2510 (2018).

79. N. Dupuis, C. R. Doerr, L. Zhang, L. Chen, N. J. Sauer, P. Dong, L. L. Buhl, and D. Ahn, "InP-based comb generator for optical OFDM," J. Lightwave Technol. **30**, 466–472 (2012).

80. V. Corral, R. Guzmán, C. Gordón, X. J. M. Leijtens, and G. Carpintero, "Optical frequency comb generator based on a monolithically integrated passive mode-locked ring laser with a Mach–Zehnder interferometer," Opt. Lett. **41**, 1937–1940 (2016).

81. I. Demirtzioglou, C. Lacava, K. R. H. Bottrill, D. J. Thomson, G. T. Reed, D. J. Richardson, and P. Petropoulos, "Frequency comb generation in a silicon ring resonator modulator," Opt. Express **26**, 790–796 (2018).

82. M. Zhang, B. Buscaino, C. Wang, A. Shams-Ansari, C. Reimer, R. Zhu, J. M. Kahn, and M. Loncar, "Broadband electro-optic frequency comb generation in a lithium niobate microring resonator," Nature **568**, 373–377 (2019).

83. V. S. Ilchenko, A. A. Savchenkov, A. B. Matsko, and L. Maleki, "Whispering-gallery-mode electro-optic modulator and photonic microwave receiver," J. Opt. Soc. Am. B **20**, 333–342 (2003).

84. A. Rueda, F. Sedlmeir, M. Kumari, G. Leuchs, and H. G. L. Schwefel, "Resonant electro-optic frequency comb," Nature **568**, 378–381 (2019).

85. I. El Mansouri, J. Fatome, C. Finot, M. Lintz, and S. Pitois, "All-fibered high-quality stable 20- and 40-GHz picosecond pulse generators for 160-Gb/s OTDM applications," IEEE Photon. Technol. Lett. **23**, 1487–1489 (2011).

86. J. Fatome, K. Hammani, B. Kibler, and C. Finot, "80 GHz waveform generated by the optical Fourier synthesis of four spectral sidebands," Laser Phys. Lett. **13**, 015102 (2016).

87. T. Sakamoto and A. Chiba, "Multiple-frequency-spaced flat optical comb generation using a multiple-parallel phase modulator," Opt. Lett. **42**, 4462–4465 (2017).

88. J. Fatome, I. El-Mansouri, J.-L. Blanchet, S. Pitois, G. Millot, S. Trillo, and S. Wabnitz, "Even harmonic pulse train generation by cross-polarization-modulation seeded instability in optical fibers," J. Opt. Soc. Am. B **30**, 99–106 (2013).

89. B. Zheng, Q. Xie, and C. Shu, "Comb spacing multiplication enabled widely spaced flexible frequency comb generation," J. Lightwave Technol. **36**, 2651–2659 (2018).

90. Y. Dou, H. Zhang, and M. Yao, "Improvement of flatness of optical frequency comb based on nonlinear effect of intensity modulator," Opt. Lett. **36**, 2749–2751 (2011).

91. M. E. Plascak, R. Bustos Ramirez, K. Bagnell, and P. J. Delfyett, "Tunable broadband electro-optic comb generation using an optically filtered optoelectronic oscillator," IEEE Photon. Technol. Lett. **30**, 335–338 (2018).

92. T. Yamamoto, T. Komukai, K. Suzuki, and A. Takada, "Spectrally flattened phase-locked multi-carrier light generator with phase modulators and chirped fibre Bragg grating," Electron. Lett. **43**, 1040–1042 (2007).

93. T. Yamamoto, T. Komukai, K. Suzuki, and A. Takada, "Multicarrier light source with flattened spectrum using phase modulators and dispersion medium," J. Lightwave Technol. **27**, 4297–4305 (2009).

94. V. Torres-Company, J. Lancis, and P. Andrés, "Lossless equalization of frequency combs," Opt. Lett. **33**, 1822–1824 (2008).

95. Y. Xing, Q. Wang, L. Huo, and C. Lou, "Frequency chirp linearization for ultra-flat optical frequency comb generation based on group velocity dispersion," Opt. Lett. **38**, 2188–2190 (2013).

96. I. L. Gheorma and G. K. Gopalakrishnan, "Flat frequency comb generation with an integrated dual-parallel modulator," IEEE Photon. Technol. Lett. **19**, 1011–1013 (2007).

97. Q. Wang, L. Huo, Y. Xing, and B. Zhou, "Ultra-flat optical frequency comb generator using a single-driven dual-parallel Mach–Zehnder modulator," Opt. Lett. **39**, 3050–3053 (2014).

98. L. Shang, Y. Li, L. Ma, and J. Chen, "A flexible and ultra-flat optical frequency comb generator using a parallel Mach–Zehnder modulator with a single DC bias," Opt. Commun. **356**, 70–73 (2015).

99. J. Li, H. Ma, Z. Li, and X. Zhang, "Optical frequency comb generation based on dual-polarization IQ modulator shared by two polarization-orthogonal recirculating frequency shifting loops," IEEE Photon. J. **9**, 2745558 (2017).

100. T. Lin, S. Zhao, Z. Zhu, X. Li, and K. Qu, "Generation of flat optical frequency comb based on a DP-QPSK modulator," IEEE Photon. Technol. Lett. **29**, 146–149 (2017).

101. A. K. Mishra, R. Schmogrow, I. Tomkos, D. Hillerkuss, C. Koos, W. Freude, and J. Leuthold, "Flexible RF-based comb generator," IEEE Photon. Technol. Lett. **25**, 701–704 (2013).

102. S. Ozharar, F. Quinlan, I. Ozdur, S. Gee, and P. J. Delfyett, "Ultraflat optical comb generation by phase-only modulation of continuous-wave light," IEEE Photon. Technol. Lett. **20**, 36–38 (2008).

103. R. Wei, J. Yan, Y. Peng, X. Yao, M. Bai, and Z. Zheng, "Optical frequency comb generation based on electro-optical modulation with high-order harmonic of a sine RF signal," Opt. Commun. **291**, 269–273 (2013).

104. J. Zhang, J. Yu, N. Chi, Z. Dong, X. Li, Y. Shao, J. Yu, and L. Tao, "Flattened comb generation using only phase modulators driven by fundamental frequency sinusoidal sources with small frequency offset," Opt. Lett. **38**, 552–554 (2013).

105. Y. Bao, X. Yi, Z. Li, Q. Chen, J. Li, X. Fan, and X. Zhang, "A digitally generated ultrafine optical frequency comb for spectral measurements with 0.01-pm resolution and 0.7-μs response time," Light Sci. Appl. **4**, e300 (2015).

106. X. Yan, X. Zou, W. Pan, L. Yan, and J. Azaña, "Fully digital programmable optical frequency comb generation and application," Opt. Lett. **43**, 283–286 (2018).

107. M. A. Soto, M. Alem, M. A. Shoaie, A. Vedadi, C.-S. Brès, L. Thévenaz, and T. Schneider, "Optical sinc-shaped Nyquist pulses of exceptional quality," Nat. Commun. **4**, 2898 (2013).

108. S. Preußler, N. Wenzel, and T. Schneider, "Flexible Nyquist pulse sequence generation with variable bandwidth and repetition rate," IEEE Photon. J. **6**, 7901608 (2014).

109. S. Cordette, A. Vedadi, M. A. Shoaie, and C.-S. Brès, "Bandwidth and repetition rate programmable Nyquist sinc-shaped pulse train source based on intensity modulators and four-wave mixing," Opt. Lett. **39**, 6668–6671 (2014).

110. Y. Fang, J. Yu, J. Zhang, X. Li, N. Chi, and J. Xiao, "Frequency comb selection enabled flexible all optical Nyquist pulse generation," Opt. Commun. **349**, 60–64 (2015).

111. J. Wu, J. Zang, Y. Li, D. Kong, J. Qiu, S. Zhou, J. Shi, and J. Lin, "Investigation on Nyquist pulse generation using a single dual-parallel Mach-Zehnder modulator," Opt. Express **22**, 20463–20472 (2014).

112. N. Yokota, R. Igarashi, and H. Yasaka, "Optical Nyquist pulse generation by using a dual-electrode Mach–Zehnder modulator," Opt. Lett. **42**, 1856–1859 (2017).

113. E. A. Whittaker, M. Gehrtz, and G. C. Bjorklund, "Residual amplitude modulation in laser electro-optic phase modulation," J. Opt. Soc. Am. B **2**, 1320–1326 (1985).

114. N. C. Wong and J. L. Hall, "Servo control of amplitude modulation in frequency-modulation spectroscopy: demonstration of shot-noise-limited detection," J. Opt. Soc. Am. B **2**, 1527–1533 (1985).

115. J. Sathian and E. Jaatinen, "Intensity dependent residual amplitude modulation in electro-optic phase modulators," Appl. Opt. **51**, 3684–3691 (2012).

116. K. Kokeyama, K. Izumi, W. Z. Korth, N. Smith-Lefebvre, K. Arai, and R. X. Adhikari, "Residual amplitude modulation in interferometric gravitational wave detectors," J. Opt. Soc. Am. A **31**, 81–88 (2014).

117. W. Zhang, M. J. Martin, C. Benko, J. L. Hall, J. Ye, C. Hagemann, T. Legero, U. Sterr, F. Riehle, G. D. Cole, and M. Aspelmeyer, "Reduction of residual amplitude modulation to for frequency modulation and laser stabilization," Opt. Lett. **39**, 1980–1983 (2014).

118. J. Bi, Y. Zhi, L. Li, and L. Chen, "Suppressing residual amplitude modulation to the level in optical phase modulation," Appl. Opt. **58**, 690–694 (2019).

119. J. Chiles and S. Fathpour, "Mid-infrared integrated waveguide modulators based on silicon-on-lithium-niobate photonics," Optica **1**, 350–355 (2014).

120. R. Peng, K. Khaliji, N. Youngblood, R. Grassi, T. Low, and M. Li, "Midinfrared electro-optic modulation in few-layer black phosphorus," Nano Lett. **17**, 6315–6320 (2017).

121. K. Kashiwagi, S. Okubo, and H. Inaba, "High repetition rate visible frequency comb generation from electro-optic modulation in the 1550 nm region," in *Conference on Lasers and Electro-Optics* (Optical Society of America, 2019), paper JW2A.97.

122. G. Xu, V. Pêcheur, J. Fatome, M. Chauvet, and B. Kibler, "Optical cavity-less 40-GHz picosecond pulse generator in the visible wavelength range," in *Conference on Lasers and Electro-Optics Europe and European Quantum Electronics Conference* (Optical Society of America, 2019), paper cd_12_5.

123. A. J. Metcalf, C. D. Fredrick, R. C. Terrien, S. B. Papp, and S. A. Diddams, "30 GHz electro-optic frequency comb spanning 300 THz in the near infrared and visible," Opt. Lett. **44**, 2673–2676 (2019).

124. E. Obrzud, V. Brasch, T. Voumard, A. Stroganov, M. Geiselmann, F. Wildi, F. Pepe, S. Lecomte, and T. Herr, "Visible blue-to-red 10 GHz frequency comb via on-chip triple-sum-frequency generation," Opt. Lett. **44**, 5290–5293 (2019).

125. A. Parriaux, K. Hammani, and G. Millot, "Two-micron all-fibered dual-comb spectrometer based on electro-optic modulators and wavelength conversion," Commun. Phys. **1**, 17 (2018).

126. M. Yan, P.-L. Luo, K. Iwakuni, G. Millot, T. W. Hänsch, and N. Picqué, "Mid-infrared dual-comb spectroscopy with electro-optic modulators," Light Sci. Appl. **6**, e17076 (2017).

127. B. Jerez, P. Martín-Mateos, F. Walla, C. de Dios, and P. Acedo, "Flexible electro-optic, single-crystal difference frequency generation architecture for

ultrafast mid-infrared dual-comb spectroscopy," ACS Photon. **5**, 2348–2353 (2018).

128. P.-L. Luo, E.-C. Horng, and Y.-C. Guan, "Fast molecular fingerprinting with coherent, rapidly tunable dual-comb spectrometer near 3 μm," Phys. Chem. Chem. Phys. **21**, 18400–18405 (2019).

129. S. Xiao, L. Hollberg, N. R. Newbury, and S. A. Diddams, "Toward a low-jitter 10 GHz pulsed source with an optical frequency comb generator," Opt. Express **16**, 8498–8508 (2008).

130. A. J. Metcalf, F. Quinlan, T. M. Fortier, S. A. Diddams, and A. M. Weiner, "Broadly tunable, low timing jitter, high repetition rate optoelectronic comb generator," Electron. Lett. **51**, 1596–1598 (2015).

131. Z. Tong, A. O. J. Wiberg, E. Myslivets, B. P. P. Kuo, N. Alic, and S. Radic, "Spectral linewidth preservation in parametric frequency combs seeded by dual pumps," Opt. Express **20**, 17610–17619 (2012).

132. K. Beha, D. C. Cole, P. Del'Haye, A. Coillet, S. A. Diddams, and S. B. Papp, "Electronic synthesis of light," Optica **4**, 406–411 (2017).

133. D. R. Carlson, D. D. Hickstein, W. Zhang, A. J. Metcalf, F. Quinlan, S. A. Diddams, and S. B. Papp, "Ultrafast electro-optic light with subcycle control," Science **361**, 1358–1363 (2018).

134. A. Ishizawa, T. Nishikawa, A. Mizutori, H. Takara, A. Takada, T. Sogawa, and M. Koga, "Phase-noise characteristics of a 25-GHz-spaced optical frequency comb based on a phase- and intensity-modulated laser," Opt. Express **21**, 29186–29194 (2013).

135. L. Lundberg, M. Mazur, A. Fülöp, V. Torres-Company, M. Karlsson, and P. A. Andrekson, "Phase correlation between lines of electro-optical frequency combs," in *Conference on Lasers and Electro-Optics (CLEO)* (Optical Society of America, 2018), paper JW2A.149.

136. R. T. Watts, S. G. Murdoch, and L. P. Barry, "Phase noise reduction of an optical frequency comb using a feed-forward heterodyne detection scheme," IEEE Photon. J. **8**, 1–7 (2016).

137. A. Ishizawa, T. Nishikawa, T. Goto, K. Hitachi, T. Sogawa, and H. Gotoh, "Ultralow-phase-noise millimetre-wave signal generator assisted with an electro-optics-modulator-based optical frequency comb," Sci. Rep. **6**, 24621 (2016).

138. N. Kuse, T. R. Schibli, and M. E. Fermann, "Low noise electro-optic comb generation by fully stabilizing to a mode-locked fiber comb," Opt. Express **24**, 16884–16893 (2016).

139. N. Ismail, C. C. Kores, D. Geskus, and M. Pollnau, "Fabry-Pérot resonator: spectral line shapes, generic and related Airy distributions, linewidths, finesses, and performance at low or frequency-dependent reflectivity," Opt. Express **24**, 16366–16389 (2016).

140. R. W. P. Drever, J. L. Hall, F. V. Kowalski, J. Hough, G. M. Ford, A. J. Munley, and H. Ward, "Laser phase and frequency stabilization using an optical resonator," Appl. Phys. B **31**, 97–105 (1983).

141. T. Kobayashi, H. Yao, K. Amano, Y. Fukushima, A. Morimoto, and T. Sueta, "Optical pulse compression using high-frequency electrooptic phase modulation," IEEE J. Quantum Electron. **24**, 382–387 (1988).

142. M. A. Prantil, E. Cormier, J. W. Dawson, D. J. Gibson, M. J. Messerly, and C. P. J. Barty, "Widely tunable 11 GHz femtosecond fiber laser based on a nonmode-locked source," Opt. Lett. **38**, 3216–3218 (2013).

143. K. R. Tamura, H. Kuhota, and M. Nakazawa, "Fundamentals of stable continuum generation at high repetition rates," IEEE J. Quantum Electron. **36**, 773–779 (2000).

144. I. Morohashi, T. Sakamoto, H. Sotobayashi, T. Kawanishi, I. Hosako, and M. Tsuchiya, "Widely repetition-tunable 200 fs pulse source using a Mach–Zehnder-modulator-based flat comb generator and dispersion-flattened dispersion-decreasing fiber," Opt. Lett. **33**, 1192–1194 (2008).

145. I. Morohashi, T. Sakamoto, H. Sotobayashi, T. Kawanishi, and I. Hosako, "Broadband wavelength-tunable ultrashort pulse source using a Mach–Zehnder modulator and dispersion-flattened dispersion-decreasing fiber," Opt. Lett. **34**, 2297–2299 (2009).

146. V. Ataie, E. Temprana, L. Liu, E. Myslivets, B. P. Kuo, N. Alic, and S. Radic, "Ultrahigh count coherent WDM channels transmission using optical parametric comb-based frequency synthesizer," J. Lightwave Technol. **33**, 694–699 (2015).

147. I. Morohashi, T. Sakamoto, N. Sekine, A. Kasamatsu, and I. Hosako, "Ultrashort optical pulse source using Mach-Zehnder-modulator-based flat comb generator," Nano Commun. Network **10**, 79–84 (2016), Special Issue on Terahertz Communications.

148. T. Kurokawa, T. Shioda, M. Koriba, M. Ito, K. Kashiwagi, T. Serizawa, and Y. Tanaka, "Generation of broadband frequency-variable laser comb allowing full-frequency sweep in the near-infrared region," Opt. Commun. **438**, 13–17 (2019).

149. T. Yang, J. Dong, S. Liao, D. Huang, and X. Zhang, "Comparison analysis of optical frequency comb generation with nonlinear effects in highly nonlinear fibers," Opt. Express **21**, 8508–8520 (2013).

150. S. Yu, F. Bao, and H. Hu, "Broadband optical frequency comb generation with flexible frequency spacing and center wavelength," IEEE Photon. J. **10**, 7202107 (2018).

151. E. Obrzud, M. Rainer, A. Harutyunyan, B. Chazelas, M. Cecconi, A. Ghedina, E. Molinari, S. Kundermann, S. Lecomte, F. Pepe, F. Wildi, F. Bouchy, and T. Herr, "Broadband near-infrared astronomical spectrometer calibration and on-sky validation with an electro-optic laser frequency comb," Opt. Express **26**, 34830–34841 (2018).

152. N. J. Doran and D. Wood, "Nonlinear-optical loop mirror," Opt. Lett. **13**, 56–58 (1988).

153. M. E. Fermann, F. Haberl, M. Hofer, and H. Hochreiter, "Nonlinear amplifying loop mirror," Opt. Lett. **15**, 752–754 (1990).

154. S. Yang and X. Bao, "Generating a high-extinction-ratio pulse from a phase-modulated optical signal with a dispersion-imbalanced nonlinear loop mirror," Opt. Lett. **31**, 1032–1034 (2006).

155. V. Ataie, E. Myslivets, B. P. Kuo, N. Alic, and S. Radic, "Spectrally equalized frequency comb generation in multistage parametric mixer with nonlinear pulse shaping," J. Lightwave Technol. **32**, 840–846 (2014).

156. E. Obrzud, V. Brasch, S. Lecomte, F. Wildi, F. Bouchy, F. Pepe, and T. Herr, "All-fiber electro-optic frequency comb for near-infrared astronomical spectrograph calibration," in *Conference on Lasers and Electro-Optics (CLEO)* (Optical Society of America, 2019), paper AF2K.2.

157. D. R. Carlson, D. D. Hickstein, S. A. Diddams, and S. B. Papp, "High-speed ultra-broadband dual-comb spectroscopy using electro-optics," in *Conference on Lasers and Electro-Optics (CLEO)* (Optical Society of America, 2018), paper SW4L.2.

158. A. J. Metcalf, T. Anderson, C. F. Bender, S. Blakeslee, W. Brand, D. R. Carlson, W. D. Cochran, S. A. Diddams, M. Endl, C. Fredrick, S. Halverson, D. D. Hickstein, F. Hearty, J. Jennings, S. Kanodia, K. F. Kaplan, E. Levi, E. Lubar, S. Mahadevan, A. Monson, J. P. Ninan, C. Nitroy, S. Osterman, S. B. Papp, F. Quinlan, L. Ramsey, P. Robertson, A. Roy, C. Schwab, S. Sigurdsson, K. Srinivasan, G. Stefansson, D. A. Sterner, R. Terrien, A. Wolszczan, J. T. Wright,

and G. Ycas, "Stellar spectroscopy in the near-infrared with a laser frequency comb," Optica **6**, 233–239 (2019).

159. V. R. Supradeepa and A. M. Weiner, "Bandwidth scaling and spectral flatness enhancement of optical frequency combs from phase-modulated continuous-wave lasers using cascaded four-wave mixing," Opt. Lett. **37**, 3066–3068 (2012).

160. V. R. Supradeepa, C. M. Long, R. Wu, F. Ferdous, E. Hamidi, D. E. Leaird, and A. M. Weiner, "Comb-based radiofrequency photonic filters with rapid tunability and high selectivity," Nat. Photonics **6**, 186–194 (2012).

161. Y. Liu, A. J. Metcalf, V. T. Company, R. Wu, L. Fan, L. T. Varghese, M. Qi, and A. M. Weiner, "Bandwidth scaling of a phase-modulated continuous-wave comb through four-wave mixing in a silicon nano-waveguide," Opt. Lett. **39**, 6478–6481 (2014).

162. C. Finot, B. Kibler, L. Provost, and S. Wabnitz, "Beneficial impact of wave-breaking for coherent continuum formation in normally dispersive nonlinear fibers," J. Opt. Soc. Am. B **25**, 1938–1948 (2008).

163. G. Millot, S. Pitois, M. Yan, T. Hovhannisyan, A. Bendahmane, T. W. Hänsch, and N. Picqué, "Frequency-agile dual-comb spectroscopy," Nat. Photonics **10**, 27–30 (2016).

164. V. Durán, P. A. Andrekson, and V. Torres-Company, "Electro-optic dual-comb interferometry over 40 nm bandwidth," Opt. Lett. **41**, 4190–4193 (2016).

165. A. Parriaux, M. Conforti, A. Bendahmane, J. Fatome, C. Finot, S. Trillo, N. Picqué, and G. Millot, "Spectral broadening of picosecond pulses forming dispersive shock waves in optical fibers," Opt. Lett. **42**, 3044–3047 (2017).

166. J. Kang, P. Feng, B. Li, C. Zhang, X. Wei, E. Y. Lam, K. K. Tsia, and K. K. Y. Wong, "Video-rate centimeter-range optical coherence tomography based on dual optical frequency combs by electro-optic modulators," Opt. Express **26**, 24928–24939 (2018).

167. P. Feng, J. Kang, S. Tan, Y.-X. Ren, C. Zhang, and K. K. Y. Wong, "Dual-comb spectrally encoded confocal microscopy by electro-optic modulators," Opt. Lett. **44**, 2919–2922 (2019).

168. N. B. Hébert, V. Michaud-Belleau, J. D. Anstie, J.-D. Deschênes, A. N. Luiten, and J. Genest, "Self-heterodyne interference spectroscopy using a comb generated by pseudo-random modulation," Opt. Express **23**, 27806–27818 (2015).

169. N. B. Hébert, V. Michaud-Belleau, C. Perrella, G.-W. Truong, J. D. Anstie, T. M. Stace, J. Genest, and A. N. Luiten, "Real-time dynamic atomic spectroscopy using electro-optic frequency combs," Phys. Rev. Appl. **6**, 044012 (2016).

170. D. A. Long, A. J. Fleisher, D. F. Plusquellic, and J. T. Hodges, "Multiplexed sub-Doppler spectroscopy with an optical frequency comb," Phys. Rev. A **94**, 061801 (2016).

171. D. A. Long, A. J. Fleisher, D. F. Plusquellic, and J. T. Hodges, "Electromagnetically induced transparency in vacuum and buffer gas potassium cells probed via electro-optic frequency combs," Opt. Lett. **42**, 4430–4433 (2017).

172. N. Wilson, N. B. Hébert, C. Perrella, P. Light, J. Genest, S. Pustelny, and A. Luiten, "Simultaneous observation of nonlinear magneto-optical rotation in the temporal and spectral domains with an electro-optic frequency comb," Phys. Rev. Appl. **10**, 034012 (2018).

173. S. Schiller, "Spectrometry with frequency combs," Opt. Lett. **27**, 766–768 (2002).

174. I. Coddington, N. Newbury, and W. Swann, "Dual-comb spectroscopy," Optica **3**, 414–426 (2016).

175. I. Coddington, W. C. Swann, and N. R. Newbury, "Coherent multiheterodyne spectroscopy using stabilized optical frequency combs," Phys. Rev. Lett. **100**, 013902 (2008).

176. T. Ideguchi, A. Poisson, G. Guelachvili, N. Picqué, and T. W. Hänsch, "Adaptive real-time dual-comb spectroscopy," Nat. Commun. **5**, 3375 (2014).

177. D. A. Long, A. J. Fleisher, K. O. Douglass, S. E. Maxwell, K. Bielska, J. T. Hodges, and D. F. Plusquellic, "Multiheterodyne spectroscopy with optical frequency combs generated from a continuous-wave laser," Opt. Lett. **39**, 2688–2690 (2014).

178. P. Guay, J. Genest, and A. J. Fleisher, "Precision spectroscopy of CN using a free-running, all-fiber dual electro-optic frequency comb system," Opt. Lett. **43**, 1407–1410 (2018).

179. A. J. Fleisher, D. A. Long, and J. T. Hodges, "Quantitative modeling of complex molecular response in coherent cavity-enhanced dual-comb spectroscopy," J. Mol. Spectrosc. **352**, 26–35 (2018).

180. P. Martin-Mateos, M. Ruiz-Llata, J. Posada-Roman, and P. Acedo, "Dual-comb architecture for fast spectroscopic measurements and spectral characterization," IEEE Photon. Technol. Lett. **27**, 1309–1312 (2015).

181. A. J. Fleisher, D. A. Long, Z. D. Reed, J. T. Hodges, and D. F. Plusquellic, "Coherent cavity-enhanced dual-comb spectroscopy," Opt. Express **24**, 10424–10434 (2016).

182. P. Martin-Mateos, B. Jerez, P. Largo-Izquierdo, and P. Acedo, "Frequency accurate coherent electro-optic dual-comb spectroscopy in real-time," Opt. Express **26**, 9700–9713 (2018).

183. P. Martin-Mateos, B. Jerez, and P. Acedo, "Dual electro-optic optical frequency combs for multiheterodyne molecular dispersion spectroscopy," Opt. Express **23**, 21149–21158 (2015).

184. K. Fdil, V. Michaud-Belleau, N. B. Hébert, P. Guay, A. J. Fleisher, J.-D. Deschênes, and J. Genest, "Dual electro-optic frequency comb spectroscopy using pseudo-random modulation," Opt. Lett. **44**, 4415–4418 (2019).

185. http://www.cfa.harvard.edu/hitran/.

186. A. Parriaux, K. Hammani, and G. Millot, "Electro-optic dual-comb spectrometer in the thulium amplification band for gas sensing applications," Opt. Lett. **44**, 4335–4338 (2019).

187. A. Ishizawa, T. Nishikawa, M. Yan, G. Millot, H. Gotoh, T. W. Hänsch, and N. Picqué, "Optical frequency combs of multi-GHz line-spacing for real-time multi-heterodyne spectroscopy," in *Conference on Lasers and Electro-Optics (CLEO)* (2015), pp. 1–2.

188. T. Nishikawa, A. Ishizawa, M. Yan, H. Gotoh, T. Hänsch, and N. Picqué, "Broadband dual-comb spectroscopy with cascaded-electro-optic-modulator-based frequency combs," in *Conference on Lasers and Electro-Optics (CLEO)* (Optical Society of America, 2015), paper SW3G.2.

189. T. Nishikawa, A. Oohara, S. Uda, A. Ishizawa, K. Hitachi, N. Picqué, and T. Hänsch, "Automatic interpolation of 25 GHz mode spacing in dual EOM comb spectroscopy," in *Conference on Lasers and Electro-Optics (CLEO)* (Optical Society of America, 2019), paper SF1I.3.

190. V. Durán, S. Tainta, and V. Torres-Company, "Ultrafast electrooptic dual-comb interferometry," Opt. Express **23**, 30557–30569 (2015).

191. S. Wang, X. Fan, B. Xu, and Z. He, "Dense electro-optic frequency comb generated by two-stage modulation for dual-comb spectroscopy," Opt. Lett. **42**, 3984–3987 (2017).

192. B. Xu, X. Fan, S. Wang, and Z. He, "Broadband and high-resolution electro-optic dual-comb interferometer with frequency agility," Opt. Express **27**, 9266–9275 (2019).

193. S. Wang, X. Fan, B. Xu, B. Wang, J. Du, and Z. He, "Hybrid dual-comb interferometer with easily established mutual coherence and a very high refresh rate," Opt. Lett. **43**, 3441–3444 (2018).

194. N. B. Hébert, S. Boudreau, J. Genest, and J.-D. Deschênes, "Coherent dual-comb interferometry with quasi-integer-ratio repetition rates," Opt. Express **22**, 29152–29160 (2014).

195. S. Wang, X. Fan, B. Xu, and Z. He, "Fast MHz spectral-resolution dual-comb spectroscopy with electro-optic modulators," Opt. Lett. **44**, 65–68 (2019).

196. M. I. Kayes and M. Rochette, "Fourier transform spectroscopy by repetition rate sweeping of a single electro-optic frequency comb," Opt. Lett. **43**, 967–970 (2018).

197. D. R. Carlson, D. D. Hickstein, D. C. Cole, S. A. Diddams, and S. B. Papp, "Dual-comb interferometry via repetition rate switching of a single frequency comb," Opt. Lett. **43**, 3614–3617 (2018).

198. A. Shams-Ansari, M. Yu, Z. Chen, C. Reimer, M. Zhang, N. Picqué, and M. Loncar, "Microring electro-optic frequency comb sources for dual-comb spectroscopy," in *Conference on Lasers and Electro-Optics(CLEO)* (Optical Society of America, 2019), paper JTh5B.8.

199. B. Jerez, F. Walla, A. Betancur, P. Martín-Mateos, C. de Dios, and P. Acedo, "Electro-optic THz dual-comb architecture for high-resolution, absolute spectroscopy," Opt. Lett. **44**, 415–418 (2019).

200. S.-J. Lee, B. Widiyatmoko, M. Kourogi, and M. Ohtsu, "Ultrahigh scanning speed optical coherence tomography using optical frequency comb generators," Jpn. J. Appl. Phys. **40**, L878–L880 (2001).

201. Z. Zhu and G. Wu, "Dual-comb ranging," Engineering **4**, 772–778 (2018).

202. O. P. Lay, S. Dubovitsky, R. D. Peters, J. P. Burger, S.-W. Ahn, W. H. Steier, H. R. Fetterman, and Y. Chang, "MSTAR: a submicrometer absolute metrology system," Opt. Lett. **28**, 890–892 (2003).

203. R. Yang, F. Pollinger, K. Meiners-Hagen, J. Tan, and H. Bosse, "Heterodyne multi-wavelength absolute interferometry based on a cavity-enhanced electro-optic frequency comb pair," Opt. Lett. **39**, 5834–5837 (2014).

204. J. Posada-Roman, J. Garcia-Souto, D. Poiana, and P. Acedo, "Fast interrogation of fiber Bragg gratings with electro-optical dual optical frequency combs," Sensors **16**, 2007 (2016).

205. E. L. Teleanu, V. Durán, and V. Torres-Company, "Electro-optic dual-comb interferometer for high-speed vibrometry," Opt. Express **25**, 16427–16436 (2017).

206. J. E. Posada-Roman, H. Angelina, B. Jerez, M. Ruiz-Llata, and P. Acedo, "Laser range finder approach based on a fieldable electro-optic dual optical frequency comb: a proof of concept," Appl. Opt. **56**, 6087–6093 (2017).

207. B. Xue, Z. Wang, H. Zhang, K. Zhang, Y. Chen, M. He, B. Lin, and H. Wu, "Absolute distance measurement by self-heterodyne EO comb interferometry," IEEE Photon. Technol. Lett. **30**, 861–864 (2018).

208. H. Wu, T. Zhao, Z. Wang, K. Zhang, B. Xue, J. Li, M. He, and X. Qu, "Long distance measurement up to 1.2 km by electro-optic dual-comb interferometry," Appl. Phys. Lett. **111**, 251901 (2017).

209. M. I. Kayes and M. Rochette, "Precise distance measurement by a single electro-optic frequency comb," IEEE Photon. Technol. Lett. **31**, 775–778 (2019).

210. X. Zhao, X. Qu, F. Zhang, Y. Zhao, and G. Tang, "Absolute distance measurement by multi-heterodyne interferometry using an electro-optic triple comb," Opt. Lett. **43**, 807–810 (2018).

211. C. Weimann, A. Messner, T. Baumgartner, S. Wolf, F. Hoeller, W. Freude, and C. Koos, "Fast high-precision distance metrology using a pair of modulator-generated dual-color frequency combs," Opt. Express **26**, 34305–34335 (2018).

212. F. Ferdous, D. E. Leaird, C.-B. Huang, and A. M. Weiner, "Dual-comb electric-field cross-correlation technique for optical arbitrary waveform characterization," Opt. Lett. **34**, 3875–3877 (2009).

213. O. E. Bonilla-Manrique, P. Martín-Mateos, B. Jerez, M. Ruiz-Llata, and P. Acedo, "High-resolution optical thickness measurement based on electro-optic dual-optical frequency comb sources," IEEE J. Sel. Top. Quantum Electron. **23**, 140–146 (2017).

214. M. T. Murphy, T. Udem, R. Holzwarth, A. Sizmann, L. Pasquini, C. Araujo, H. Dekker, S. D'Odorico, M. Fischer, T. Hänsch, and A. Manescau, "High-precision wavelength calibration of astronomical spectrographs with laser frequency combs," Mon. Not. R. Astron. Soc. **380**, 839–847 (2007).

215. T. Wilken, C. Lovis, A. Manescau, T. Steinmetz, L. Pasquini, G. Lo Curto, T. Hänsch, R. Holzwarth, and T. Udem, "High-precision calibration of spectrographs," Mon. Not. R. Astron. Soc. Lett. **405**, L16–L20 (2010).

216. M. Mayor and D. Queloz, "A Jupiter-mass companion to a solar-type star," Nature **378**, 355–359 (1995).

217. T. Steinmetz, T. Wilken, C. Araujo-Hauck, R. Holzwarth, T. W. Hänsch, L. Pasquini, A. Manescau, S. D'Odorico, M. T. Murphy, T. Kentischer, W. Schmidt, and T. Udem, "Laser frequency combs for astronomical observations," Science **321**, 1335–1337 (2008).

218. R. A. McCracken, J. M. Charsley, and D. T. Reid, "A decade of astrocombs: recent advances in frequency combs for astronomy [Invited]," Opt. Express **25**, 15058–15078 (2017).

219. X. Bonfils, X. Delfosse, S. Udry, T. Forveille, M. Mayor, C. Perrier, F. Bouchy, M. Gillon, C. Lovis, F. Pepe, D. Queloz, N. C. Santos, D. Ségransan, and J.-L. Bertaux, "The HARPS search for southern extra-solar planets - XXXI. The M-dwarf sample," Astron. Astrophys. **549**, A109 (2013).

220. X. Yi, K. Vahala, J. Li, S. Diddams, G. Ycas, P. Plavchan, S. Leifer, J. Sandhu, G. Vasisht, P. Chen, P. Gao, J. Gagne, E. Furlan, M. Bottom, E. C. Martin, M. P. Fitzgerald, G. Doppmann, and C. Beichman, "Demonstration of a near-IR line-referenced electro-optical laser frequency comb for precision radial velocity measurements in astronomy," Nat. Commun. **7**, 10436 (2016).

221. B. Dai, Z. Gao, X. Wang, H. Chen, N. Kataoka, and N. Wada, "Generation of versatile waveforms from CW light using a dual-drive Mach-Zehnder modulator and employing chromatic dispersion," J. Lightwave Technol. **31**, 145–151 (2013).

222. A. M. Weiner, "Ultrafast optical pulse shaping: a tutorial review," Opt. Commun. **284**, 3669–3692 (2011), Special Issue on Optical Pulse Shaping, Arbitrary Waveform Generation, and Pulse Characterization.

223. Z. Jiang, D. S. Seo, D. E. Leaird, and A. M. Weiner, "Spectral line-by-line pulse shaping," Opt. Lett. **30**, 1557–1559 (2005).

224. C.-B. Huang, Z. Jiang, D. Leaird, J. Caraquitena, and A. Weiner, "Spectral line-by-line shaping for optical and microwave arbitrary waveform generations," Laser Photon. Rev. **2**, 227–248 (2008).

225. Z. Jiang, D. E. Leaird, and A. M. Weiner, "Optical processing based on spectral line-by-line pulse shaping on a phase-modulated CW laser," IEEE J. Quantum Electron. **42**, 657–665 (2006).

226. Z. Jiang, C.-B. Huang, D. E. Leaird, and A. M. Weiner, "Optical arbitrary waveform processing of more than 100 spectral comb lines," Nat. Photonics **1**, 463–467 (2007).

227. Z. Jiang, D. E. Leaird, C. Huang, H. Miao, M. Kourogi, K. Imai, and A. M. Weiner, "Spectral line-by-line pulse shaping on an optical frequency comb generator," IEEE J. Quantum Electron. **43**, 1163–1174 (2007).

228. V. Torres-Company, A. J. Metcalf, D. E. Leaird, and A. M. Weiner, "Multichannel radio-frequency arbitrary waveform generation based on multi-wavelength comb switching and 2-D line-by-line pulse shaping," IEEE Photon. Technol. Lett. **24**, 891–893 (2012).

229. C. Finot, "40-GHz photonic waveform generator by linear shaping of four spectral sidebands," Opt. Lett. **40**, 1422–1425 (2015).

230. D. Miyamoto, K. Mandai, T. Kurokawa, S. Takeda, T. Shioda, and H. Tsuda, "Waveform-controllable optical pulse generation using an optical pulse synthesizer," IEEE Photon. Technol. Lett. **18**, 721–723 (2006).

231. A. J. Metcalf, H.-J. Kim, D. E. Leaird, J. A. Jaramillo-Villegas, K. A. McKinzie, V. Lal, A. Hosseini, G. E. Hoefler, F. Kish, and A. M. Weiner, "Integrated line-by-line optical pulse shaper for high-fidelity and rapidly reconfigurable RF-filtering," Opt. Express **24**, 23925–23940 (2016).

232. B. Frisquet, B. Kibler, and G. Millot, "Collision of Akhmediev breathers in non-linear fiber optics," Phys. Rev. X **3**, 041032 (2013).

233. B. Kibler, A. Chabchoub, A. Gelash, N. Akhmediev, and V. E. Zakharov, "Superregular breathers in optics and hydrodynamics: omnipresent modulation instability beyond simple periodicity," Phys. Rev. X **5**, 041026 (2015).

234. G. Xu, A. Gelash, A. Chabchoub, V. Zakharov, and B. Kibler, "Breather wave molecules," Phys. Rev. Lett. **122**, 084101 (2019).

235. B. Frisquet, A. Chabchoub, J. Fatome, C. Finot, B. Kibler, and G. Millot, "Two-stage linear-nonlinear shaping of an optical frequency comb as rogue nonlinear-Schrödinger-equation-solution generator," Phys. Rev. A **89**, 023821 (2014).

236. F. Baronio, B. Frisquet, S. Chen, G. Millot, S. Wabnitz, and B. Kibler, "Observation of a group of dark rogue waves in a telecommunication optical fiber," Phys. Rev. A **97**, 013852 (2018).

237. K. Hammani, B. Kibler, C. Finot, P. Morin, J. Fatome, J. M. Dudley, and G. Millot, "Peregrine soliton generation and breakup in standard telecommunications fiber," Opt. Lett. **36**, 112–114 (2011).

238. F. Audo, B. Kibler, J. Fatome, and C. Finot, "Experimental observation of the emergence of Peregrine-like events in focusing dam break flows," Opt. Lett. **43**, 2864–2867 (2018).

239. G. Xu, K. Hammani, A. Chabchoub, J. M. Dudley, B. Kibler, and C. Finot, "Phase evolution of Peregrine-like breathers in optics and hydrodynamics," Phys. Rev. E **99**, 012207 (2019).

240. B. Kibler, J. Fatome, C. Finot, G. Millot, F. Dias, G. Genty, N. Akhmediev, and J. M. Dudley, "The Peregrine soliton in nonlinear fibre optics," Nat. Phys. **6**, 790–795 (2010).

241. K. Hammani, B. Kibler, J. Fatome, S. Boscolo, G. Genty, J. M. Dudley, G. Millot, and C. Finot, "Nonlinear spectral shaping and optical rogue events in fiber-based systems," Opt. Fiber Technol. **18**, 248–256 (2012), Special Issue on Fiber Supercontinuum Sources and Their Applications.

242. B. Kibler, J. Fatome, C. Finot, G. Millot, G. Genty, B. Wetzel, N. Akhmediev, F. Dias, and J. M. Dudley, "Observation of Kuznetsov-Ma soliton dynamics in optical fibre," Sci. Rep. **2**, 463 (2012).

243. L. Lundberg, M. Karlsson, A. Lorences-Riesgo, M. Mazur, V. Torres-Company, J. Schröder, and P. Andrekson, "Frequency comb-based WDM transmission systems enabling joint signal processing," Appl. Sci. **8**, 718 (2018).

244. X. Zou, B. Lu, W. Pan, L. Yan, A. Stöhr, and J. Yao, "Photonics for microwave measurements," Laser Photon. Rev. **10**, 711–734 (2016).

245. I. Morohashi, I. Katayama, M. Kirigaya, Y. Irimajiri, N. Sekine, and I. Hosako, "High precision frequency measurement of terahertz waves using optical combs from a Mach–Zehnder-modulator-based flat comb generator," Opt. Lett. **44**, 487–490 (2019).

246. J. M. Lukens, D. E. Leaird, and A. M. Weiner, "A temporal cloak at telecommunication data rate," Nature **498**, 205–208 (2013).

247. F. Zhou, J. Dong, S. Yan, and T. Yang, "Temporal cloak with large fractional hiding window at telecommunication data rate," Opt. Commun. **388**, 77–83 (2017).

248. J. M. Lukens, A. J. Metcalf, D. E. Leaird, and A. M. Weiner, "Temporal cloaking for data suppression and retrieval," Optica **1**, 372–375 (2014).

249. L. R. Cortés, M. Seghilani, R. Maram, and J. Azaña, "Full-field broadband invisibility through reversible wave frequency-spectrum control," Optica **5**, 779–786 (2018).

250. P. O. Weigel, J. Zhao, K. Fang, H. Al-Rubaye, D. Trotter, D. Hood, J. Mudrick, C. Dallo, A. T. Pomerene, A. L. Starbuck, C. T. DeRose, A. L. Lentine, G. Rebeiz, and S. Mookherjea, "Bonded thin film lithium niobate modulator on a silicon photonics platform exceeding 100 GHz 3-dB electrical modulation bandwidth," Opt. Express **26**, 23728–23739 (2018).

251. M. He, M. Xu, Y. Ren, J. Jian, Z. Ruan, Y. Xu, S. Gao, S. Sun, X. Wen, L. Zhou, L. Liu, C. Guo, H. Chen, S. Yu, L. Liu, and X. Cai, "High-performance hybrid silicon and lithium niobate Mach–Zehnder modulators for 100 Gbit/s^{-1} and beyond," Nat. Photonics **13**, 359–364 (2019).

252. C. Wang, M. Zhang, X. Chen, M. Bertrand, A. Shams-Ansari, S. Chandrasekhar, P. Winzer, and M. Lončar, "Integrated lithium niobate electro-optic modulators operating at CMOS-compatible voltages," Nature **562**, 101–104 (2018).

253. A. J. Mercante, S. Shi, P. Yao, L. Xie, R. M. Weikle, and D. W. Prather, "Thin film lithium niobate electro-optic modulator with terahertz operating bandwidth," Opt. Express **26**, 14810–14816 (2018).

254. L. Alloatti, R. Palmer, S. Diebold, K. P. Pahl, B. Chen, R. Dinu, M. Fournier, J.-M. Fedeli, T. Zwick, W. Freude, C. Koos, and J. Leuthold, "100 GHz silicon-organic hybrid modulator," Light Sci. Appl. **3**, e173 (2014).

255. A. Melikyan, L. Alloatti, A. Muslija, D. Hillerkuss, P. C. Schindler, J. Li, R. Palmer, D. Korn, S. Muehlbrandt, D. V. Thourhout, B. Chen, R. Dinu, M. Sommer, C. Koos, M. Kohl, W. Freude, and J. Leuthold, "High-speed plasmonic phase modulators," Nat. Photonics **8**, 229–233 (2014).

256. C. Haffner, W. Heni, Y. Fedoryshyn, J. Niegemann, A. Melikyan, D. L. Elder, B. Baeuerle, Y. Salamin, A. Josten, U. Koch, C. Hoessbacher, F. Ducry, L. Juchli, A. Emboras, D. Hillerkuss, M. Kohl, L. R. Dalton, C. Hafner, and J. Leuthold, "All-plasmonic Mach–Zehnder modulator enabling optical high-speed communication at the microscale," Nat. Photonics **9**, 525–528 (2015).

257. M. Ayata, Y. Fedoryshyn, W. Heni, B. Baeuerle, A. Josten, M. Zahner, U. Koch, Y. Salamin, C. Hoessbacher, C. Haffner, D. L. Elder, L. R. Dalton, and J. Leuthold, "High-speed plasmonic modulator in a single metal layer," Science **358**, 630–632 (2017).

258. B. Baeuerle, W. Heni, C. Hoessbacher, Y. Fedoryshyn, U. Koch, A. Josten, T. Watanabe, C. Uhl, H. Hettrich, D. L. Elder, L. R. Dalton, M. Möller, and J. Leuthold, "120 GBd plasmonic Mach-Zehnder modulator with a novel differential electrode design operated at a peak-to-peak drive voltage of 178 mV," Opt. Express **27**, 16823–16832 (2019).

259. S. Abel, F. Eltes, J. E. Ortmann, A. Messner, P. Castera, T. Wagner, D. Urbonas, A. Rosa, A. M. Gutierrez, D. Tulli, P. Ma, B. Baeuerle, A. Josten, W. Heni, D. Caimi, L. Czornomaz, A. A. Demkov, J. Leuthold, P. Sanchis, and J. Fompeyrine, "Large Pockels effect in micro- and nanostructured barium titanate integrated on silicon," Nat. Mater. **18**, 42–47 (2018).

260. F. Eltes, C. Mai, D. Caimi, M. Kroh, Y. Popoff, G. Winzer, D. Petousi, S. Lischke, J. E. Ortmann, L. Czornomaz, L. Zimmermann, J. Fompeyrine, and S. Abel, "A BaTiO$_3$-based electro-optic Pockels modulator monolithically integrated on an advanced silicon photonics platform," J. Lightwave Technol. **37**, 1456–1462 (2019).

261. M. Li, L. Wang, X. Li, X. Xiao, and S. Yu, "Silicon intensity Mach–Zehnder modulator for single lane 100 Gb/s applications," Photon. Res. **6**, 109–116 (2018).

262. H. Sepehrian, J. Lin, L. A. Rusch, and W. Shi, "Silicon photonic IQ modulators for 400 Gb/s and beyond," J. Lightwave Technol. **37**, 3078–3086 (2019).

263. L. Fan, C.-L. Zou, N. Zhu, and H. X. Tang, "Spectrotemporal shaping of itinerant photons via distributed nanomechanics," Nat. Photonics **13**, 323–327 (2019).

264. T. Ideguchi, S. Holzner, B. Bernhardt, G. Guelachvili, N. Picqué, and T. W. Hänsch, "Coherent Raman spectro-imaging with laser frequency combs," Nature **502**, 355–358 (2013).

265. D. Carlson, D. Hickstein, S. A. Diddams, and S. B. Papp, "An ultrafast electro-optic dual comb for linear and nonlinear spectroscopy," in *Light, Energy and the Environment 2018 (E2, FTS, HISE, SOLAR, SSL)* (Optical Society of America, 2018), paper FT4B.2.

Alexandre Parriaux received a master's degree in 2017 from the École Normale Supérieure de Lyon and at the University of Burgundy (UB). Shortly after, he started a Ph.D. at the UB entitled "Frequency comb generation and applications." His research activities include the study of nonlinear optical phenomena in optical fibers, frequency conversion techniques, and frequency comb generation with electro-optic modulators for spectroscopic applications.
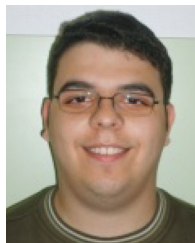
Kamal Hammani received a Ph.D. in physics from the University of Burgundy (UB) in 2011. In 2012, he went as a postdoctoral research fellow at the Optoelectronics Research Center (University of Southampton) in the United Kingdom (2012–2013). Since September 2013, he has been an Assistant Professor at the University of Burgundy. His research covers nonlinear optics, optical communication, optical fibers, and nanophotonics for applications in opto-electronics in near- and mid-infrared. He has published more than 30 articles in international peer-reviewed journals.

Guy Millot received a Ph.D. in physics from the University of Burgundy (UB) in 1986. In 1987, he carried out postdoctoral research at Massachusetts Institute of Technology (MIT) on time-resolved infrared double resonance experiments. He was an Assistant Professor at UB between 1988 and 1994, where he carried out research on laser Raman spectroscopy applied to combustion media. In 1994, he was promoted to a full professor position and began working on the theme of optical solitons and modulation instabilities; he has created a cutting-edge laboratory for nonlinear and fiber optics and has achieved several important scientific breakthroughs. His main current research interests are focused on optical rogue waves, nonlinear spatiotemporal dynamics in multimode fibers, and dual-comb spectroscopy. He is the author and coauthor of over 210 papers in peer-review journals. His research has been highly valued by three prestigious awards: nominations at the Institut Universitaire de France (IUF) in 2000 and 2019, and the Silver Medal from the CNRS in 2004. He was elected as a Fellow of the The Optical Society of America.